CENTRO DE INVESTIGACIONES EN ÓPTICA, A.C.

"SERS SUBSTRATES WITH GOLD NANOPARTICLES FUNCTIONALIZED TO DETECT SPECIFIC ANALYTES".

Doctorado en Ciencias (Óptica)

Student:
M.O. Leonardo Pérez Mayen

Adviser:
Dr. Elder de la Rosa Cruz

Agosto de 2016
León, Guanajuato, México

"Centro de Investigaciones en Óptica A.C."

SERS Substrates with Gold Nanoparticles Functionalized To Detect Specific Analytes

by

Leonardo Pérez Mayen

Chairperson of the Supervisory Committee:

Dr. Elder de la Rosa Cruz
Nanophotonics And Advanced Materials Research Group

ABSTRACT

This thesis presents results on the SERS substrates research in the experimental point of view. The characteristics needed in the nanoparticles, its geometric implications, the absorption of light related with surface plasmon and the spatial distribution. It also shows a proposal in order to obtain multipurpose substrate and specific functionalization by use of bobbin albumin for Glucose detection.

Table of Contents

Acknowledgments

The author wishes to express sincere appreciation to Dr. De La Rosa and Dr. Oliva for their assistance in the preparation of this manuscript. In addition, special thanks to Dr. L. Díaz, Dr. C. Frausto, Dr. E. Camus and Dr. J. Gonzalez for the support given for this thesis.

Special thanks to M. C. Albor, Dr. S. Calixto, J. L. Flores, Dr. P. Salas, and all CIO workers that contributed during my phD project and CONACyT, for the scholarship and the founds given for the research.

Also, to my family, friends and colleagues which contributed to my growing those years.

Introduction

Raman spectroscopy is a valuable tool in various research fields, like biology[1–4], genetics [1,4–9], toxicology[10], and others chemical applications[1,10–20]. This spectroscopy technique provides structural information from various samples often without the need for extensive sample preparation[4]. However, this is a feeble phenomenon that scatter the photons in inelastic way and approximately 1 in 10^6–10^{10} photons are scattered inelastically[8,10,21]. In 1974 Fleischmann et al., first reported on the Surface Enhanced Raman Scattering (SERS) phenomenon in pyridine which gave an enhanced Raman scattering signal at roughened silver electrodes[22]. This opened up a new possibilities to the researchers and later on it was found to be arising due to the electromagnetic enhancement originating from the interaction between the excited radiation with the surface electrons on the rough metal surface which was named as plasmon[13]. The best enhancement factor (EF) obtained for the pyridine system was $5x10^5$, using substrates made by metal electrochemical attack[17]that enables the use of Raman spectroscopy in many research fields like: biology, forensic science, toxic agent detection, pharmaceutics, art and material science[4, 8,9,23]. This particular area of research became more demanding and SERS is being studied rigorously by

various research groups. The next promising approach to enhance the SERS is to make use of novel metal nanoparticles as an object of electromagnetic enhancement which aids greatly in order to enhance Raman signals by several approaches[24,20,15,25,26]. Two main approximations were developed which dealt with these metal nanoparticles.

The first approximation is based on liquid solutions [3,26,27] using novel metal nanoparticle solutions which are blended with the analytes solution. In this case the interaction between the electromagnetic field and the analytes with the metal nanoparticles allows the detection by SERS[9,15,26,27,28]. Colloidal gold and silver were appropriate solutions in order to get a good enhancement in the Raman signal[29,30]. When colloidal nanoparticles used as the Raman enhancement media, EF between 10^4 and 10^8 is achieved in liquid measurements, whereas if the particle aggregates are used, an average enhancement of 10^{10} is obtained for the scattering volume sample[5,16]. This enhancement factors opened up the possibilities for the single molecule detection even though, the reproducibility of the liquid measurements with high enhancement factors is difficult to achieve.

The second one, SERS substrate based on novel metal nanoparticles,[4,13, 16,31,32,33] in which the geometrical conditions of the nanoparticles and its

distribution can promote electromagnetic field confinement enable enhancement factors up to 10^{10} for SERS [2,9,11,16,24,26,34]. When the SERS substrates achieve EF up to 10^8 they becomes a powerful tool to identify even a single molecule [1,4–6,11,14,18,35–37]. Because SERS substrates can be applied for detection of low molecular concentration, they have found special interest in research. Several research groups are working on the development of the SERS substrates for sensing unknown molecules and specific analytes[1,4,6,8,9,11,19,20,23,25,28,33,38–44].

The method for construction of SERS substrates is a widely explored topic of investigation. This thesis deals with the experimental techniques supported by theoretical and applied research on SERS substrates in order to propose a methodology to fabricate SERS substrates with good enhancement factors up to 10^8. In addition it also explores its applications in chemical detection and biology which is achieved by using three main goals as discussed below.

First, to obtain the protocol for depositing nanoparticles on silicon substrate, glass and/or polymer with the homogeneous distribution and reproducibility by chemical (self-assembly)[20,45,46] and physical (Langmuir-Blodgett) methods[47,48].

Second, to get the protocol for the conjugation/functionalization of nanoparticles with functional groups such as, amines, carboxyls, peptides, thiols, etc. in addition with primary and secondary antigens, to ensure the selectivity of the molecule of interest.

Third, understand the Raman response (SERS or SERRS) from substrates under study using different concentrations of analytes, particularly for a single molecule.

These objectives are discussed in detail in the first chapter which states all considerations required to have good SERS substrate. The substrate which fulfills all the conditions to obtain the high Raman signal either for random or specific analytes, is considered to be a good SERS substrate[4,9,16,23,24,26,29,32–34,36,41,49]. The second chapter deals with the discussion on the first and second objectives whereas the third chapter deals with the third objective. The third chapter also discusses the results obtained during this project of thesis.

Chapter 1

Theoretical and experimental considerations needed for SERS substrates.

Overview

This chapter presents an overview of the state of the art referent to SERS substrates using novel mental nanoparticles. The bests approaches of the SERS substrates are analyzed for getting the best ideas and physics concepts involved on the electromagnetic fields related with Raman enhancement. The geometric requirements of the particles and the conditions for have the best enhancement factor. Also the size, material and shape of the metal nanoparticles are studied. A proposal of architecture for SERS substrates is presented for two cases a multipurpose SERS substrate and selective SERS substrates.

1.1 Raman Scattering

When, an incident electromagnetic wave induces a dipole moment during the light material interaction. The strength of the induced dipole moment, **P**, is given by

$$\mathbf{P} = \boldsymbol{\alpha}\,\mathbf{E} \quad (\mathbf{1})\,\mathbf{.}$$

Where $\boldsymbol{\alpha}$ is the polarizability and **E** is the strength of electric field of the incident electromagnetic wave. The polarizability is a material property that depends on the molecular structure and nature of the bonds. For the incident electromagnetic wave, the electric field may be expressed as

$$\mathbf{E} = \mathbf{E_0}\cos(\mathbf{2\pi\nu_0 t}) \quad (\mathbf{2})\,\mathbf{,}$$

Where $\boldsymbol{\nu_0}$ is the frequency (Hz) of the incident electromagnetic wave ($\nu_0 = {}^{c}/_{\lambda}$) Substituting Equqtion (2) into (1) yields the time-dependent induced dipole moment,

$$\mathbf{P} = \boldsymbol{\alpha}\,\mathbf{E_0}\cos(\mathbf{2\pi\nu_0 t}) \quad (\mathbf{3}).$$

Because the ability to perturb the local electron cloud of a molecular structure depends on the relative location of the individual atoms, it follows that the polarizability is a function of the instantaneous position of constituent atoms. For any molecular bond, the individual atoms are confined to specific vibrational modes, in which the vibrational energy levels

are quantized in a manner similar to electronic energies. The vibrational energy of a particular mode is given by

$$\boldsymbol{E_{vib} = \left(j + \frac{1}{2}\right) h\nu_{vib}} \quad \textbf{(4).}$$

Where j is the vibrational quantum number (j = 0,1,2…), ν_{vib} is the frequency of the vibrational mode, and h is the Planck constant. The physical displacement dQ of the atoms about their equilibrium position due to the particular vibrational mode may be expressed as

$$\boldsymbol{dQ = Q_0 \cos(2\pi\nu_{vib} t)} \quad \textbf{(5),}$$

where $\boldsymbol{Q_0}$ is the maximum displacement about the equilibrium position. Considering small displacements, the polarizability may be approximated by a Taylor series expansion, namely,

$$\boldsymbol{\alpha = \alpha_0 + \frac{\partial \alpha}{\partial Q} dQ} \quad \textbf{(6),}$$

where $\boldsymbol{\alpha_0}$ is the polarizability of the molecular mode at equilibrium position. Based on the vibrational displacement of equation (5), the polarizability may be given as

$$\boldsymbol{\alpha = \alpha_0 + \frac{\partial \alpha}{\partial Q} Q_0 \cos(2\pi\nu_{vib} t)} \quad \textbf{(7).}$$

Finally, Equation. (7) may be substituted into Equation. (3), which yields

$$\boldsymbol{P = \alpha E_0 \cos(2\pi\nu_0 t) + \frac{\partial \alpha}{\partial Q} Q_0 E_0 \cos(2\pi\nu_0 t)\cos(2\pi\nu_{vib} t)} \quad \textbf{(8),}$$

Using a trigonometric identity, the above relation may be recast as

$$\mathbf{P} = \boldsymbol{\alpha}\,\mathbf{E_0}\cos(2\pi\boldsymbol{\nu_0}\mathbf{t}) + \left(\frac{\partial\alpha}{\partial Q}\frac{\mathbf{Q_0E_0}}{2}\right)\{\cos[2\pi(\boldsymbol{\nu_0}-\boldsymbol{\nu_{vib}})\mathbf{t}] + \cos[2\pi(\boldsymbol{\nu_0}+\boldsymbol{\nu_{vib}})\mathbf{t}]\} \quad \mathbf{(9).}$$

Examination of the above equation reveals that induced dipole moments are created at three distinct frequencies, namely $\boldsymbol{\nu_0}$, $(\boldsymbol{\nu_0}-\boldsymbol{\nu_{vib}})$ and $(\boldsymbol{\nu_0}+\boldsymbol{\nu_{vib}})$, which results in scattered radiation at these same three frequencies. The first scattered frequency corresponds to the incident frequency, hence is elastic scattering (Mie or Rayleigh), while the latter two frequencies are shifted to lower or higher frequencies and are therefore inelastic processes. The scattered light in these latter two cases is referred to as Raman scattering, with the down-shifted frequency (longer wavelength) referred to as Stokes scattering, and the up-shifted frequency (shorter wavelength) referred to as anti-Stokes scattering.

1.2 Surface enhanced Raman Scattering (SERS)

The electromagnetic enhancement can be viewed as essentially a redistribution of the electromagnetic (EM) field around the SERS substrate, resulting in strongly localized regions of high field intensities, so-called hot-spots[50]. The effect is mediated through resonance of the light with the surface plasmon of the metal[51], with the enhancement falling off with distance from the substrate[52]. Roughly speaking, plasmons are collective excitations of the surface conduction electrons that propagate along the metal surface[53]. At certain frequencies of incident light these electrons become highly polarizable, giving rise to large EM fields[54]. The details of plasmon resonance are complicated and a variety of terms exist to describe different aspects of plasmons depending on the research emphasis; such terms include surface plasmon polaritons[55], radiative and non-radiative plasmons[53], localized and propagating plasmons[56]. Here we present only some of the most basic theory needed to outline the SERS effect. It should be noted that in the context of this thesis, all plasmon-related effects can be understood as electromagnetic effects, and the relation to the free electrons of the metal is only secondary. In this sense, all characteristics of plasmons is contained within the dielectric function (and its wavelength dependence) and the geometry of a specific problem.

In terms of the basic properties of the metal, it is suitable for use in SERS if its refractive index has:

- A negative real part of the dielectric function (preferably large and negative);and
- A small imaginary part of the dielectric function.

The metals that fulfill this best are the alkali and noble metals (Cu, Ag, and Au). On this thesis we choose to work with gold by their intrinsic properties.

1.2.1 Plasmon resonances and wavelength dependence in SERS

In simple terms, the plasmon resonances of a metal can be considered in terms of certain electromagnetic modes that exist for a material body described by a local dielectric function and a given geometry[57–59]. When the electromagnetic modes of a substrate are resonant with the incident light from an external source, enhancement occurs. Put another way, the optical response of the plasmon results in a redistribution of the energy around the object[36,52,57], such that some regions are locally enhanced. This can be seen in the absorption spectra of a SERS substrate. It should be noted, however, that we can not simply use the absorption spectrum as an accurate indicator of the SERS enhancement of a given substrate at a given wavelength. First, the Raman effect involves enhancement of both the incident and radiative photons (at different energies), so the final enhancement depends on the convolution of these individual enhancements[52,56,57,60]. In addition, for resonant molecules, pre-resonance effects may mean that SERS enhancements occur well before the resonances shown by the absorption profile[57,61–63].

1.3 SERS substrates approximations

Several ides and physics concepts have been developed for novel metal nanoparticle substrates applied to SERS. The first SERS substrates made at 1974 were based on electrochemical attack on metal. Using this kind of substrates the maximum enhancement factor was $5x10^5$ (using a of $1X10^{-2}$ M Pyridine, on silver electrode) at these time the researchers observed that on the surface of the metal the waves of light form evanescence electromagnetic fields [17,22]. In order to have a homogenous Electromagnetic field the roughness of the surface metal should be homogeneous.

During the 1990's decade the main approaches to get SERS substrates was the use of novel metal specially silver, deposited on substrates by methods as Vapor-Deposited Films, Electrochemically Roughened Electrodes, foil Roughened with Nitric Acid, Films Produced from the Tollens reaction and Photo deposited Films on TiO_2. The limits of detection (LOD) of this approximation were 0.6 to 50 x 10^{-8} M ±.02 of trans-1, 2-bis (4-pyridyl) ethane[64].

During the 2000's, some of the first approaches to SERS substrates were improved and new approaches started to be applied for diverse analytes as: Bacillus anthracis biomarker, Glucose in a serum protein mixture and

Bacillus subtilis spores[65]. The use of nanoparticles started to be more common in order to obtain SERS substrates and the methods and techniques involved nanoparticles to obtain SERS substrates starting to appear.

The most important methods refereed by authors on 2000's decade are: electron beam lithography(EBL) [41,55,66–74], nanosphere-lithography and photo-lithography(NSL) [26,49,66,66,75–84], the template method[24,34,66,66,80–82,85–91], the hybrid method[36,37,82,92–95], and vapor deposition method(OAD) [10,65,75,78,82,91,96–98]. A comparative study of these methods was presented by Ralph A. Tripp et all, they made a table which compares the advantages and disadvantages of the methods mentioned as the most relevant on the 2000's decade, the maximums EF for these methods for fabricated SERS substrates were for the lithography using silicon oxide nanoparticles as a mask.

Fabrication Method	EBL	NSL[47]	Template method	Hybrid Method	OAD
Enhancement Factor	–	10^7–10^9	10^6–10^7 [50,52,53]	10^6–10^8 [59]	>10^8 [64]
Substrate Area (cm^2)	Typically < 0.001 x 0.001	~1 x 1	> 2.5 x 2.5	> 2.5 x 5.0	> 2.5 x 7.5
Uniformity (%)	–	–	< 15 %[50]	–	< 10 %[64]
Reproducibility	<20 %[38]	–	–	–	< 15 %[64]
Shelf time (days)	–	–	–	> 40 (for Au)[60,61]	~ 7 (for Ag)
Fabrication Steps	3	3	3	> 2	1–2
Cost	Expensive	Inexpensive	Inexpensive	Inexpensive	Moderate

Figure 1. Comparison of different SERS substrate fabrication techniques that could potentially generate uniform and large area SERS substrates[82] (image taken by the article).

On 2009 Xiu-Mei Lin, et all[99], establish on a review the features of an ideal SERS substrate:

-1. The substrate should have high SERS activity and therefore provide high sensitivity. By controlling the size (more than 50 nm) and interparticle spacing (less than 10 nm) of nanoparticles, one can tune the LSPR frequency of the substrate to match the incident laser frequency and the effective coupling between nanoparticles can be induced to maximize the enhancement.

2. The substrate should be uniform so that the deviation in enhancement over the whole surface can be less than 20%, which requires a relatively ordered arrangement of the nanoparticles on the substrate.

3. The substrate should have good stability and reproducibility. Even after a long shelf time, the enhancement effect can still be maintained. The deviation in the enhancement should be less than 20% for different batches of substrates prepared by the same method.

4. The substrate should be clean enough so that it can be applied to study not only strong adsorbates but also some weak adsorbates or even unknown samples.-

During the decade from 2000 to 2010, other methodologies to achieve the best SERS substrate started to be developed based on the use of metal nanoparticles made by wet chemical process. The two more promising were the self assembly and the Langmuir Blodgett Trough.

Self assembly, in a general sense, might be defined as the spontaneous formation of complex hierarchical structures from pre-designed building blocks[100], typically involving multiple energy scales and multiple degrees of freedom. Consists on use some molecule that has affinity for two materials one is attached to the metallic nanoparticles and other linked to the base substrate[37,73,97,100–105]. This technique can be used to form homogeneous layers on substrates and choosing different lengths on the molecule chains the space between nanoparticles can be controlled as needed[37,73,81,87,89,106].

Langmuir Blodgett Trough (LB), The LB technique was originally used to prepare a large area film of Amphiphile molecules on solid substrates[46,107–112]. By dissolving an Amphiphile molecule in a volatile solvent immiscible with water, and dispersing the solution on the surface of the water phase, a monolayer of the molecule will form at the interface after the evaporation of the solvent. By changing the position of the movable barrier in the LB trough, one can change the density of the monolayer film. The film can then

be deposited on the substrate by the dipping and pulling method. Similarly, to prepare a nanoparticle film, the nanoparticles should first be modified with hydrophobic molecules and dispersed into highly volatile chloroform or hexane, which is immiscible with water. By dispersion of the solution into the water phase, a layer of randomly distributed nanoparticles will be left at the interface after the evaporation of the solvent. As a result of compression of the layer by moving the barrier, an ordered layer of nanoparticles will be formed on the surface of the water and transfer to the substrate forming a SERS substrate[98–108].

Based on the information found in the literature, Self assembly (SA) and the Langmuir Blodgett Trough, can be used to form a large area, of SERS substrates. Also the cost of these methods is lower compared to electron beam lithography (EBL), nanosphere-lithography and photo-lithography (NSL), the template method, the hybrid method, and vapor deposition method (OAD). Therefore the two methods chosen to be applied an improved in this thesis project were Self assembly and the Langmuir Blodgett Trough. The theoretical studies that have been done about the nanoparticles and the plasmon on nanoparticles and substrates are discussed in the next section.

1.4 Spatial and geometric conditions for SERS substrates

SERS substrates can be divided into two fundamental classes: random and engineered substrates. Random substrates, such as fractal nanoparticle agglomerates, can support localized dipole modes, which lead to high SERS signal enhancements[74]. When dipole modes are resonant with the wavelength at precise locations of the spots of giant |E| field enhancement this region are called "hot spots"[109–112]. Two strategies have emerged which can generate hot spots at the tip of a sharp feature on a nanoparticle by taking advantage of "the lightening rod effect" (antenna effect), phenomenon that occurred at sharp points [5,27,54,59,72,99,114,127–133] or in the "gap region" between two closely spaced nanoparticles because of the coupling of plasmon modes[2,26,57,79–81,92,126,134,135]. The reproducibility of their enhancement factors is difficult to control in completely random structures so the engineered substrates are the best approach in order to achieve the hot spots.

For "the lightening rod effect" several shapes of novel metal nanoparticles have been simulated, on them properties of electromagnetic field confinement for several shapes even as: nanospheres (maximum EF 10^2)[131], nano-triangles (maximum EF 10^6)[72], nanorods (maximum EF 10^5)[136],

nanowires (maximum EF 10^6)[137], nanocubes (maximum EF 10^{6-8})[130] and nanostars (maximum EF 10^{8-10})[11].

The “gap region”, the optimums distance between nanoparticles has been found to be from 1 to 2 nm. (EF 10^{12})[41,138]. Some studies about the dependence of the distance among particles shows that the limit for good SERS (EF 10^6) is approximately 30 nm[14].

In SERS one particular case is presented when the nanoparticles, excitation and molecule have the same wavelength of resonance. This particular case can achieve EF up to 10^{12} on the hot spots[62,115,119] and receive the name of Surface Enhanced Resonance Raman scattering (SERRS). This Raman enhancement is only presented on some cases and requires that the analyte matches in resonance modes with the SERS substrate.

Based on the deep review of the literature the shape chosen for the nanoparticles using for this project was nanostars made of gold. These nanoparticles can be used in LB and SA by tailoring their surface and the substrate.

1.5 Proposed architecture to get the best substrate for SERS

Based on the theoretical criteria found in the literature, in order to construct SERS substrate is necessary follow the next architecture, use gold nanostars, and linked them by a molecule preferably no more than 3 nm in length, that posses one functional group able to link the substrate and in the other side one that link the nanoparticles, on figure 2, this architecture is schematic depicted. The nanoparticles should have also a gap between them in the range of 30 to 1 nanometer (according the literature enough distance to have SERS) and the same distance from nanoparticles to the analyte given by a molecule that link the analyte to the nanoparticle, or made the space between them in order to have SERS. In the cartoon the electromagnetic field around the particles is illustrated as a yellow oval, the color is shown darker in the gap of the gold nanostars to illustrate the region that can form a “hot spot”. It is important to mention if the nanoparticles and analyte present a bonding from a chemical reaction some of the peaks of the Raman spectrum will be lost. This process can decrease the signal or blank it. If the bonds form a new link if the new link has freedom for electronic oscillations a new peak can appear and will be in correspondence to the new link formed.

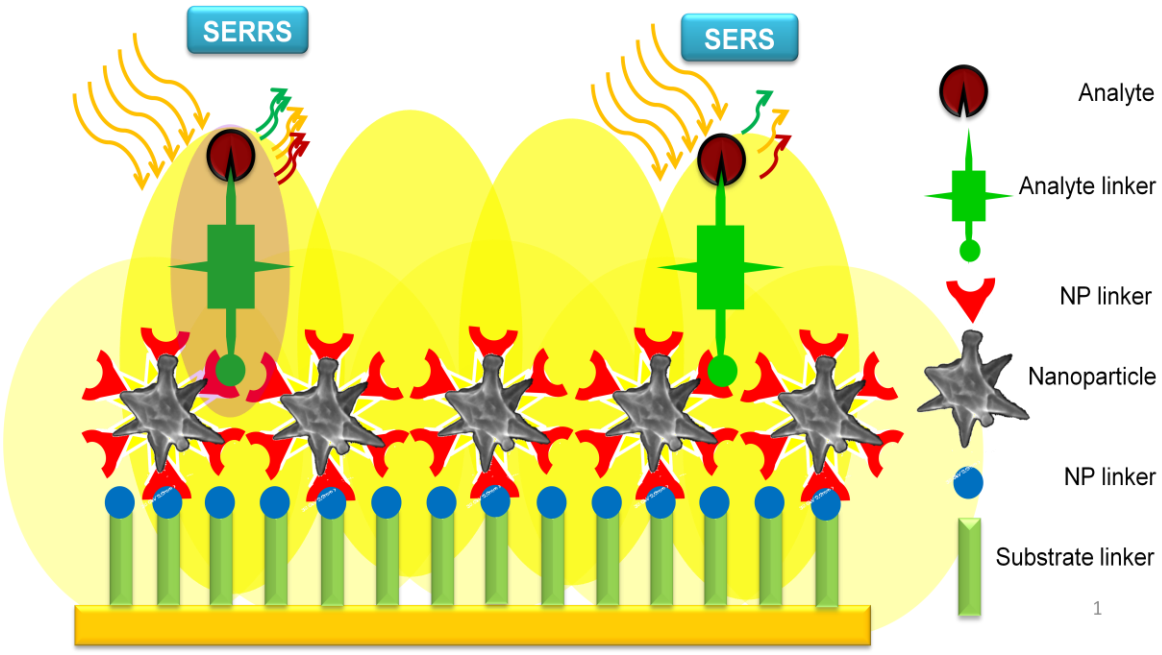

Figure 2. Architecture for SERS substrates, this cartoon show how should be the best architecture for a SERS and SERRS substrate describing all the parts in that is compound.

From the 1.1 title, two techniques, Langmuir Blodgett Trough and Self assembly were found promising for elaboration of SERS substrates. Each one have particularly features.

Langmuir Blodgett Trough, can produce compact nanoparticle, only separated between them by the molecules attached to their surface. The main problem of LB technique is the hydrophobic nature of the layers formed yet, it, is the best method for well ordered and homogenous distribution. On this project this method was applied for non selective substrates. This means that SERS substrates made by LB, will be designed

as multipurpose SERS substrates. Oriented to organic analytes, molecules that can be dispersed or dissolved on non aqueous organic solvents. As is show on Figure 3, the architecture proposed consist on hydrophobic gold nanostars, the hydrophobicity is generated by a molecule that in one extreme has a head or a functional group (yellow circle) that is linked to the gold nanostar and in the other extreme has an organic chain. The silicon substrate is cover by a molecule that links to it which has an unsaturated hydrocarbon. The silicon reacts whit unsaturated carbon molecules forming the Si-C bond, this kind of molecules and their bond are stronger. Linear alkene molecules with these characteristics are highly hydrophobic [139–141], and provide a homogeneous hydrophobic capping. The hydrophobic nanoparticles will be attached to the hydrophobic substrate by Van Der Waals Forces [20,37,42,142–145].

The length of the molecules used to make the hydrophobicity need to be around 1 nm, in order to have the best enhancement when the particles get closer together than the capping molecule. The hydrophobic organic chain on the nanoparticles and substrate helps to link, by Van Der Waals forces, analytes that are easily dissolved or dispersed on organic solvents. Enabling the substrate to have a large quantities analytes near the “hot spots” increases considerably the Raman scattered photons from the analytes.

Figure 3, show how the analytes can interact with the architecture proposed for the SERS substrates. Analytes can be placed among the particles, on the particles or diffuse to the bottom of the particles. The understanding the relationship between the size of the analytes their interaction with the SERS substrate and how it affects the enchantment is discussed in chapter 3.

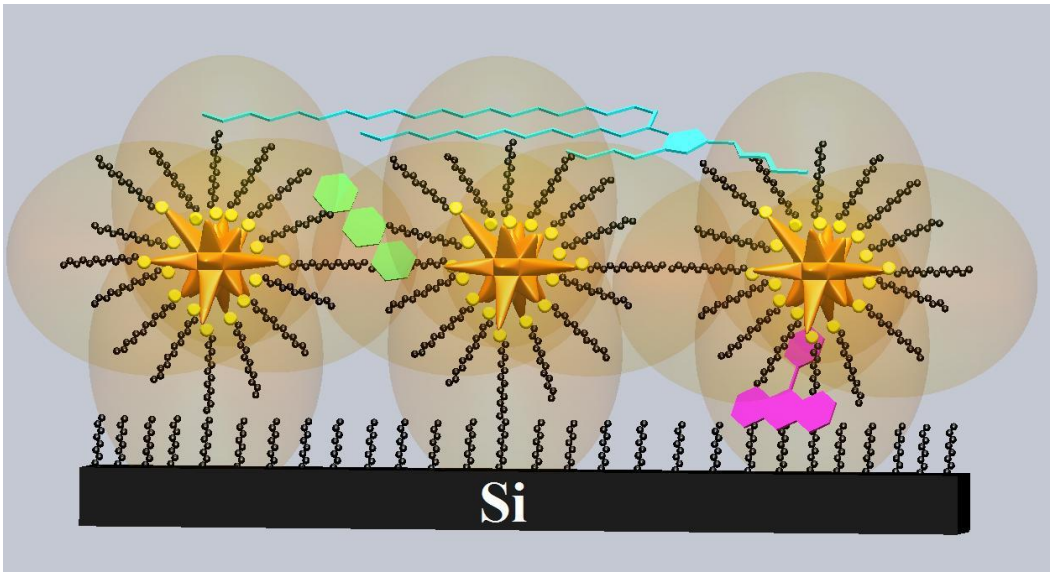

Figure 3. Architecture proposed for the multipurpose SERS substrate made by LB, the green blue and pink artifacts are examples of how the analytes can be attached on the substrate.

Self assembly, has been chosen in this project in order to built SERS substrates for applications in biology or in which water interactions with the analyte is needed. figure 4, shows the Architecture proposed for this project. The silicon used for the LB is changed for glass slides. Glass slides can react whit silicon alkoxides, some of them have a functional group that can be linked and form bond with the nanoparticles, for example NH_2[137–139]. Silicon alkoxides bonds to silicon slides by SiO bonds. Star nanoparticles for this architecture need to be modified, decreasing the length of the sharp peaks, in order to increase the binding probability of the particles to the exposed functional groups of silicon alkoxides. Figure 4, shows a purple transparent sphere that represents the selective shell on the particles that are linked to the substrate. This shell should be added after the deposition of the particles. This method enables the use of the substrate for any selectivity needed. Analytes, represented by hexagonal orange artifacts will link to the selective shell surrounding the nanoparticles. It is important that the thickness of the shell never excess 30 nm to have an EF up to 10^6 as reported in SERS.

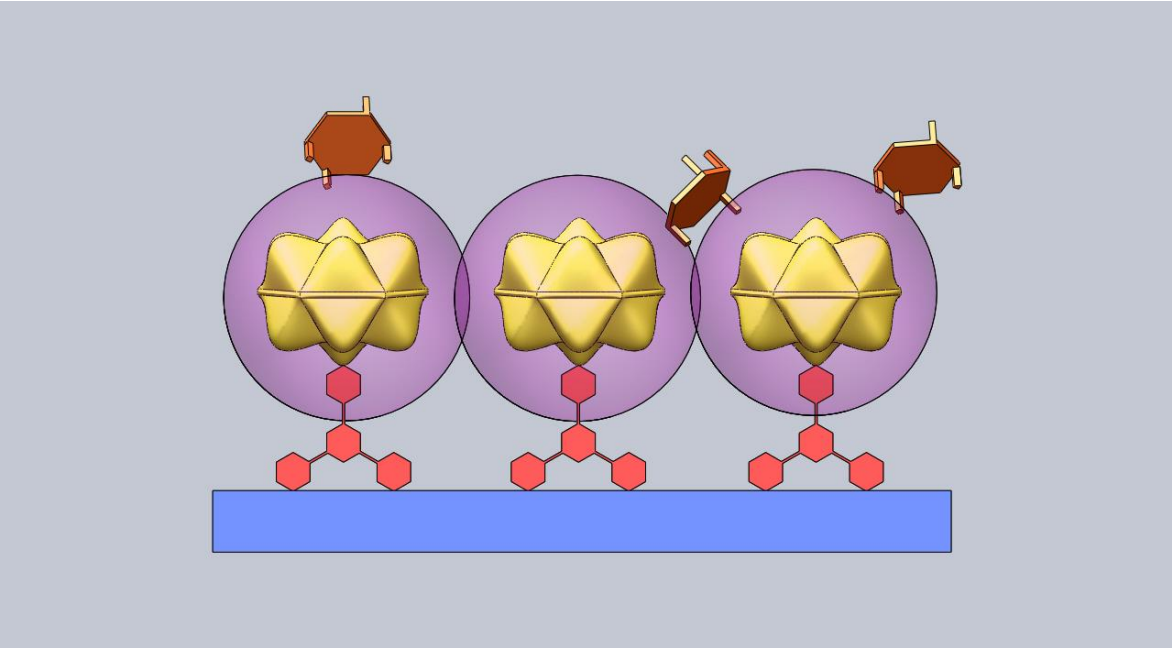

Figure 4. Architecture proposed for the selective SERS substrate made by Self assembly.

Chapter 2

Experimental development of the architectures proposed for SERS substrates[*].

Overview

This chapter deals with the experimental construction of the architecture model proposed for SERS substrates. Presents the design of multipurpose substrates using star-like gold nanoparticles synthesized using a wet chemical method and makes them hydrophobic using 1-dodecanethiol linked on their surface and deposited by LB. This molecule allowed us to obtain a spacing of ~2.6 nm between gold stars, which promoted the generation of hot spot points for SERS detection. In order to test the enhancement, substrates fabricated with the configuration: Si/Au film/Au nanoparticles were prepared.

Selective substrates designs using self assembly were implemented by gold nanoparticles previously linked to the substrate using 3-aminopropyl triethoxysilane (APTES) in order to obtain the selective conjugation they were coated with Albumin using the configuration: glass/Au

[*] Some contents of the chapter 2 are reproduced from Ref. [156,174] with permission from the Royal Society of Chemistry. http://www.rsc.org/journals-books-databases/journal-authors-reviewers/licences-copyright-permissions/#reuse-permission-requests.

nanoparticles/Albumin. All substrates were characterized by the techniques required.

2.1 SERS substrates prepared by Langmuir Blodgett Trough (LB)

2.1.1 Synthesis of gold nanoparticles for LB

The gold nanoparticles were synthesized using silver nanoparticles as seeds, which were fabricated previously using the Turkevich method[140–142] which involved a solution of $AgNO_3$ (0.0006M). Those silver seeds present a maximum absorption peak at 394 nm. The procedure of synthesis for star-like gold nanoparticles was as follows: 100 µl of $HAuCl_4$ (0.1M) and 250 µl (0.004M) of $AgNO_3$ are added in 10 ml of CTAB (0.001M) under moderate stirring. After this, 50 µl of seeds are added and maintained under stirring for 5 minutes. The stirring speed is decreased and 250 µl of ascorbic acid (0.08M) were added and the solution turned to a brown coloration if seen by reflection and blue coloration is seen through transmission after finishing the synthesis. The nanoparticles were washed 3 times with distilled water while being centrifuged. The centrifugation time should not exceed 5 minutes at 4500 rpm, in order to prevent permanent conglomeration of gold nanoparticles. Morphology of those gold nanoparticles was analyzed on a Field Emission Scanning Electron Microscope (FE-SEM) Model 7800F from JEOL, using electron acceleration energy between 1 and 5 KeV.

Gold nanoparticles were functionalized using the Amphiphile molecule 1-dodecanethiol (with approximate length of 1.3 nm) in order to disperse hydrophobic nanoparticles on the surface of the water bath of the LB equipment and to be linked on the hydrophobic substrate. In this case, 15 ml of gold nanoparticles dispersed in water were mixed with acetone and hexane using a volume ratio of 10:4:4. Then, 50 µl of 1-dodecanethiol were added and kept under strong stirring during 1 hr at room temperature. Finally the nanoparticles were washed and dispersed in chloroform.

2.1.2 Preparation of Substrates to LB

The substrates used in our experiments were (001) pieces of silicon (Si). Those substrates were washed with soap, ethanol and distilled water. Afterwards, the surface of the substrates were treated with 98% hydrofluoric acid for 15 min in order to remove the thin layer of SiO_2 formed by the O_2 interaction over the silicon wafer and then immersed in a solution of 1-octadecene (1 nm length) during 30 min at 50 °C to form Si-C bonding. This way, the substrate surface was functionalized providing a hydrophobic surface were gold nanoparticles can be attached. Some substrates were covered with a 20 nm gold film of using physical vapor deposition (PVD) at a base pressure of $5x10^{-6}$ mbar after treatment with

hydrofluoric acid. Those substrates with gold were made hydrophobic by immersing them into a solution of 50 µl of 1-dodecanethiol dissolved in 50 ml of hexane, later they were washed with hexane. Au nanoparticles were deposited on the substrates with/without gold film using the Langmuir-Blodgett method, taking into account the following considerations: the number of nanoparticles per ml obtained with the molarity of $HAuCl_4$ used, that in turn, is related with the average nanoparticle size; and the necessary amount of nanoparticles to fill the LB area under compression. Thus, the required quantity to spread was 500 µl of gold nanoparticles solution for each substrate experiment. After the preparation of substrates, 10 µl of a solution of Rhodamine B were dropped for SERS measurement on 4mm x 4mm substrate area. Six different samples[†] (R1-R6) with different molar concentrations of RhB dissolved in ethanol were prepared for this study. Complete description of molar composition of each sample is described in Table 1. All substrates under study were analyzed in a SEM FEI-Novananosem 200 using acceleration energy between 20 to 30KeV.

[†] Not only six samples were done during the project during this thesis several samples and tests were done, the six samples shows on the document are the most representatives. R1 to R6 are the samples reported on the scientific article "SERS substrates fabricated with star-like gold nanoparticles for Zeptomol detection of Analytes".

Table 1. Main parameters of detection for Raman measurements

A	B	C	D	E	F	G	H
Sample	Number of Moles on substrate	Number of molecules on substrate	Sample Area (μm^2)	Molecules/μm^2	Molecules/ spot area (189μm^2)	moles/spot area	Error (±%)
R1	$1.03x10^{-05}$	$6.21x10^{+18}$	$1.60x10^{+06}$	$3.88x10^{+12}$	$7.33x10^{+14}$	$1.22x10^{-09}$	**0.0703**
R2	$1.03x10^{-11}$	$6.21x10^{+12}$	$1.60x10^{+06}$	$3.88x10^{+06}$	$7.33x10^{+08}$	$1.22x10^{-15}$	**0.826**
R3	$1.03x10^{-12}$	$6.21x10^{+11}$	$1.60x10^{+06}$	$3.88x10^{+05}$	$7.33x10^{+07}$	$1.22x10^{-16}$	**1.066**
R4	$1.03x10^{-14}$	$6.21x10^{+09}$	$1.60x10^{+06}$	$3.88x10^{+03}$	$7.33x10^{+05}$	$1.22x10^{-18}$	**1.546**
R5	$1.03x10^{-16}$	$6.21x10^{+07}$	$1.60x10^{+06}$	$3.88x10^{+01}$	$7.33x10^{+03}$	$1.22x10^{-20}$	**2.026**
R6	$1.03x10^{-18}$	$6.21x10^{+05}$	$1.60x10^{+06}$	$3.88x10^{-01}$	$7.33x10^{+01}$	$1.22x10^{-22}$	**2.506**

2.1.3 Optical Characterization of LB substrates

The absorption spectrum of gold nanoparticles between 400nm to 1000 nm was obtained from a Perkin Elmer lamba 900 spectrometer using a quartz cuvette of 1 cm thickness. The IR spectra [Fourier transform infrared (FTIR)] of the samples were recorded in the range of 2700–3100 cm^{-1} on an ABA (MB300) spectrometer using the KBr pellet method[153]. Raman measurements in the range of 100-1800 cm^{-1} were carried out using a Raman Spectrometer R-S Renishaw (1000 B) which has a laser at 830 nm. The power used for all measurements was 0.01 mW and the spot area was around 189μm^2 it was calculated by measure the spot on the camera (diameter of ~ 15.5μm) of the Raman. It agree with the literature

that states for a 50X objective lens with NA 0.75 maximum diameter of 20 μm[154] the total time integration were 30 seconds.

2.1.4 Results and Discussion of LB substrates

The hydrophobic gold nanoparticles were dispersed onto a water surface of the Langmuir-Blodgett trough, see figure 5 a,b, at this stage the surface pressure was zero and the nanoparticles were randomly distributed. The next step is compressing the nanoparticles at a constant speed of 1mm/min, see figure 5c. At this stage the gold nanoparticles received a pressure in the range of 15-35 mN/m. The compressed nanoparticles moved toward the silicon substrate (interacting with the functionalized Si surface) while the tip holding the substrate was lifted progressively with controlled speed, as shown in 5d.

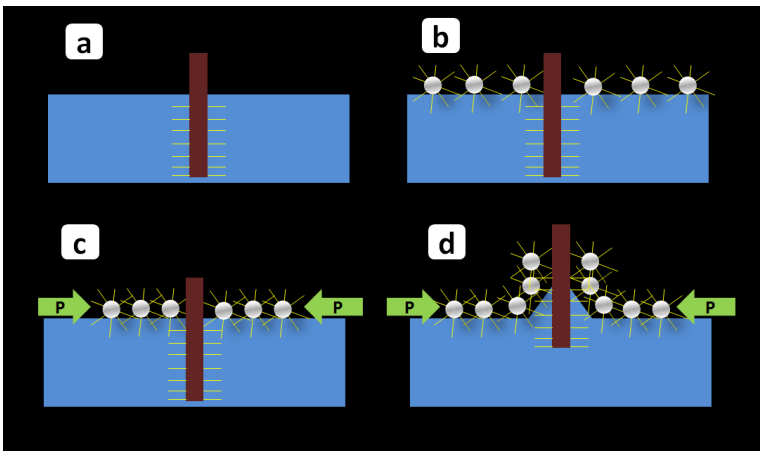

Figure 5. Exemplification of the Langmuir-Blodgett deposition.

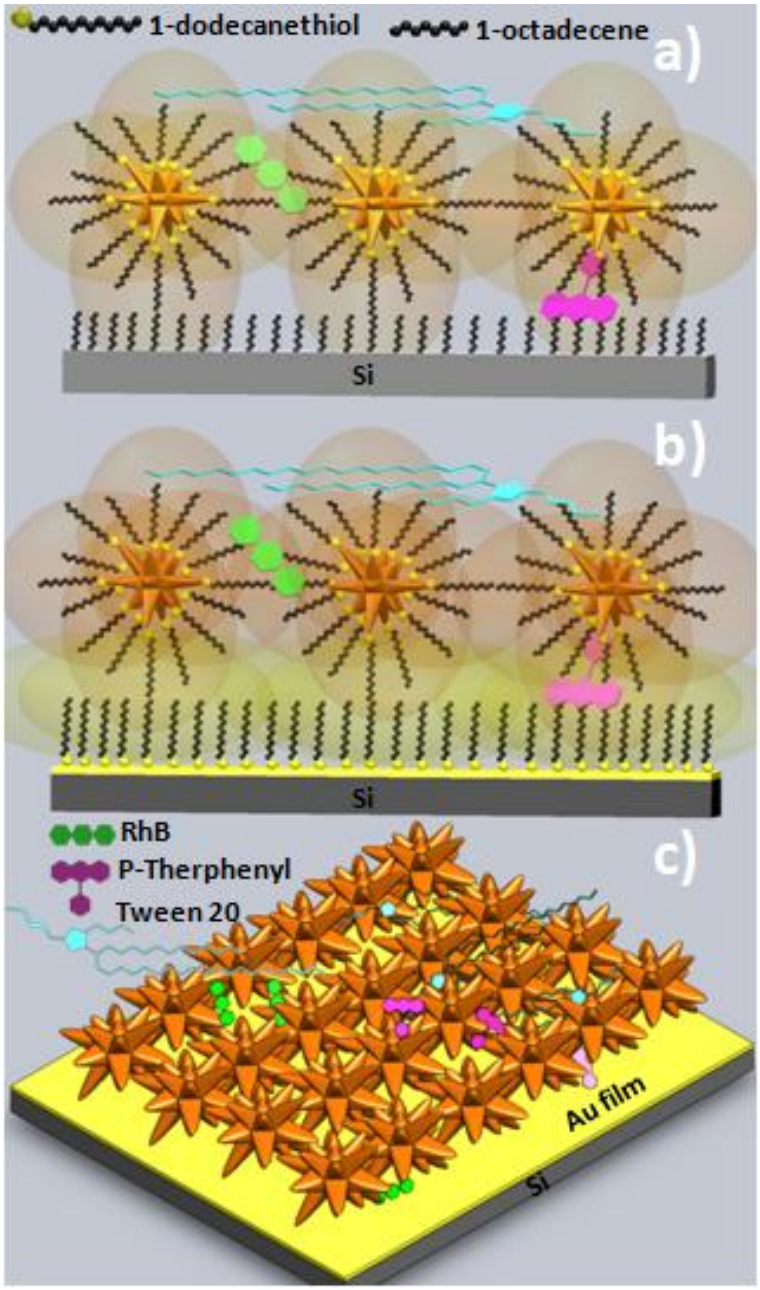

Figure 6. Schematics of each SERS substrate fabricated in this work: a) Si/Au nanoparticles, b) Si/Au film/Au nanoparticles, c) is a top view of different analytes deposited on our SERS substrates.

Functionalization of nanoparticles is a critical parameter for the distribution and their linking to the Si substrate as well as for the detection of the analyte, figure 6a shows a diagram to illustrate different bonds between the Si substrate and the gold nanoparticles functionalized with 1-dodecanethiol. Basically, 1-octadecene (1 nm length) is attached to the silicon substrates by Si-C bonds, this in turn, is linked due to by Van Der Waals forces to the paraffin part of the 1-dodecanethiol molecules located on the surface of gold nanoparticles, which are in turn linked to the gold star-like nanoparticles by their sulfhydryl groups (-SH).

In the case of SERS substrates with a gold film, (see figure 6b) only 1-dodecanethiol is used to separate the nanoparticles from the gold film, and it is attached to the Au film by its SH extreme. The presence of 1-dodecanethiol molecules on the surface of gold nanoparticles and on gold coated substrates is particularly useful in our case because the approximate length of the 1-dodecanethiol chain is 1.3 nm, therefore the minimum distance between two adjacent gold nanoparticles or between nanoparticles and gold coated silicon substrates should be 2.6 nm, which favors the generation of “hotspots”, see figure 6b. When the Au film is not on the Si substrate, the separation distance between the gold nanoparticles and the Si substrate is about 2.3 nm, see figure 6a.

The numbers of hotspots is directly related with the single molecules detection capacity of, since it has been reported that hotspots are points with a electric field enhancement factor of 10^{14} [52,155].

When rhodamine B molecules were deposited on the substrate, they spread out on the substrate by diffusion and can be situated among adjacent gold nanoparticles, between the gold nanoparticles and the Au thin film or on top of gold nanoparticles, see figures 6b, c. This enables us to increase our limit of detection in comparison with reference 118, where the analyte is necessarily located between the gold nanoparticles and the Au film.

The presence of the 1-octadecene on the surface of silicon substrates and 1-dodecanethiol on the surface of gold nanoparticles is confirmed by the FTIR spectra of figures 7a, b. It is observed that the peaks at 908 cm-1 and 721 cm^{-1} related to 1-octadecene appear in the FTIR spectra of the Si Substrate. In addition, the peaks located at 2915 cm^{-1} and 2848 cm^{-1} corresponding to 1-dodecanethiol are also present on the surface of functionalized gold nanoparticles.

There are variations in the distribution of gold nanoparticles on the silicon substrates depending of the pressure used during the LB deposition. Figure 8a, b show SEM images of typical Si substrates with gold nanoparticles deposited under a pressure of 15mN/m and 35 mN / m respectively.

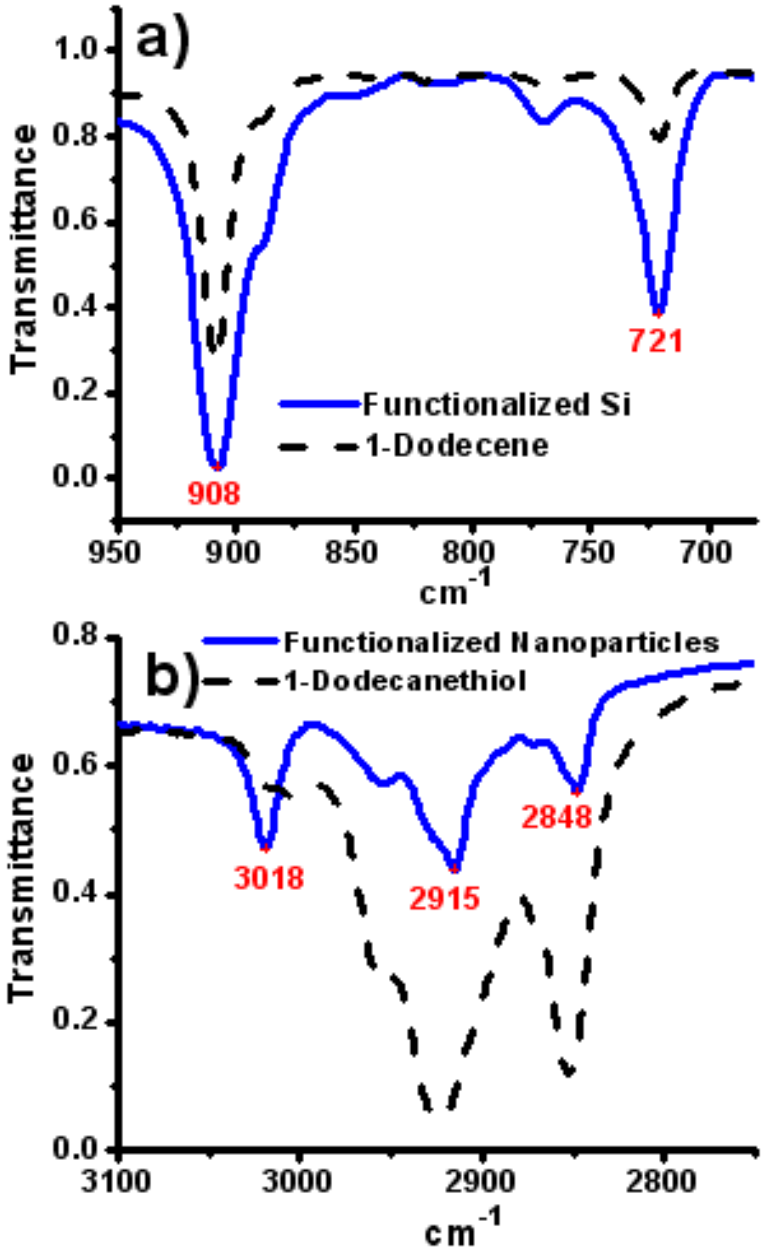

Figure 7. FTIR spectra of: a) 1-dodecene molecule and Si Substrate Functionalized and b) 1-dodecanethiol molecule and Au Nanoparticles functionalized with 1-dodecanethiol.

The distance of separation among nanoparticles in figure 8a is larger in comparison of that corresponding to figure 8b, which is to be expected because the pressure used was higher on the substrate of figure 8b. The morphology of our gold nanoparticles is important because they are star-like with several tips, see figure 8c. Those tips are particularly important for the enhancement of the electric field necessary in the Raman detection. The average size of those nanoparticles is 138 nm (from tip to tip). Figure 8d shows an image of the Si substrate with gold nanoparticles distributed on a gold film (pressure used 35 mN/m). It is remarkable the homogeneity of the distribution of nanoparticles in this film, which is important for Raman detection because this substrate allowed Raman detection up to 10^{-22} moles/spot size as explained later. According to the AFM measurements (not shown here), the roughness of this film is between 45-60 nm, which is in good agreement with half of the average diameter of 138 nm for gold nanoparticles. This is expected because the AFM cantilever should fall at half of the diameter (valley point) during AFM measurements (in points where two tips of two different stars are in contact). The maximum plasmatic absorption of Au nanoparticles dispersed in water and Au NPs on a silicon substrate covered with a gold film (Si/Au Film/Au NPs) are located at 653 nm and 750 nm respectively, see inset of figure 8d. As observed,

there was a shift of approximately 100 nm of the maximum plasmonic peak and a broadening of the plasmonic band on the substrates with gold film. Such broadening allowed us to use the 830 nm for Raman detection, since this wavelength is in resonance with the plasmonic band obtained in Si substrates with the gold film.

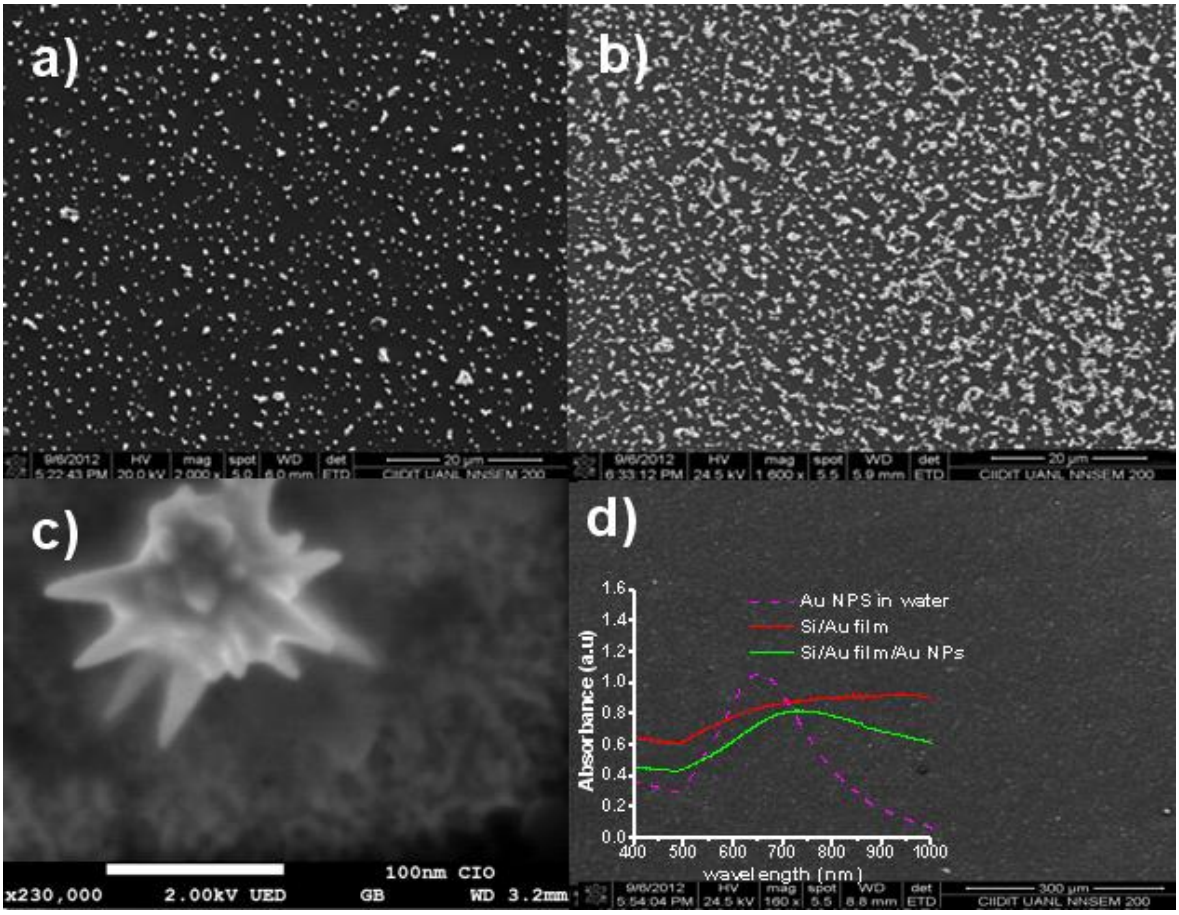

Figure 8. a) and b) are SEM images of the Au NPs distributed on the substrate for the values of pressure 15mN/m and 35 mN/m respectively. c) SEM image of Au NPs and d) SEM image of compacted Au nanoparticles on the Si Substrate.

2.2 SERS substrates prepared by Self assembly (SA)

2.2.1 Synthesis of gold nanoparticles for SA

All chemicals used for the synthesis and functionalization of nanoparticles were acquired from Sigma Aldrich and used without any further treatment. The gold nanoparticles were synthesized using silver nitrate as anisotropic low doping avoiding the use of silver seeds to reduce the length of the peaks. The procedure of synthesis for star-like gold nanoparticles was as follows: 100 μl of $HAuCl_4$ (0.1M) and 250 μl (0.004M) of $AgNO_3$ were added in 10 ml of CTAB (0.001M) under moderate stirring. Then, the stirring speed was decreased and 250 μl of ascorbic acid (0.08M) was added. A blue coloration is observed through transmission after finishing the synthesis. Those nanoparticles were washed 3 times with three-distilled water. The centrifugation time did not exceed 5 minutes at 4500 rpm in order to avoid a permanent conglomeration of the gold nanoparticles. Morphology of those gold nanoparticles was analyzed on a field emission scanning electron microscope (FE-SEM) model 7800F from JEOL, using electron acceleration energy between 1 and 5 KeV.

2.2.2 Preparation of Substrates by Self Assembly

Glass substrates from corning were washed thoroughly during 30 min under sonication using the following solvents: distilled water, ethanol and isopropyl alcohol. Later, those substrates were immersed in a solution of sulfuric acid (0.1M) during 10 min to remove any organic residues and to functionalize the surface of glass with OHs. After this, the glass substrates were immersed in a solution of anhydrous ethanol with 5 vol% of [(3-Aminopropyl) triethoxysilane (APTES) during 6 hours. During this time, the hydrolysis was achieved and the APTES was linked to the glass surface through radicals OHs. Subsequently, the substrates were washed several times with anhydrous ethanol. subsequently, the gold nanoparticles are attached to the glass substrates by immersing the substrate in the solution of gold nanoparticles for 2 hours. In the case of the sample with albumin, it was deposited after the gold nanoparticles using the spin coating method. In this case, a solution of Bovine Albumin (Immunicor Gamma USA) in distilled water (11 vol. %) was deposited at 4000 rpm during 1 min and then dried at 60 °C for 3 hours. After the preparation of substrates, 10 µl of a solution containing Glucose was dropped for SERS measurement on 4mm

x 4mm substrate area. Six different SERS substrates[‡] (M1-M6) with different molar Glucose concentrations were prepared in distilled water for this study. Only samples M5 and M6 contained Albumin. A complete description of the molar composition of each sample is described in Table 2. An additional sample named M5NA was prepared using the same molar concentration of Glucose as for M5, but this one was not coated with Albumin.

Table 2. main parameters of detection for Raman measurements.

A	B	C	D	E	F	G	H	I
Sample	**Molarity (mol/L)**	**Number of moles on substrate**	**Number of molecules on substrate**	**Sample area (μm^2)**	**Molecules (μm^2)**	**Molecules per spot area (189 μm^2)**	**Moles per spot area**	**Total error (±%)**
M1	**1.00E+00**	**1.00E-05**	**6.02E+18**	**$1.60x10^{+06}$**	**3.76E+12**	**7.11E+14**	**1.18E-09**	**0.76**
M2	**1.00E-03**	**1.00E-08**	**6.02E+15**	**$1.60x10^{+06}$**	**3.76E+09**	**7.11E+11**	**1.18E-12**	**0.88**
M3	**1.00E-05**	**1.00E-10**	**6.02E+13**	**$1.60x10^{+06}$**	**3.76E+07**	**7.11E+09**	**1.18E-14**	**0.96**
M4	**1.00E-07**	**1.00E-12**	**6.02E+11**	**$1.60x10^{+06}$**	**3.76E+05**	**7.11E+07**	**1.18E-16**	**1.04**
M5	**1.00E-09**	**1.00E-14**	**6.02E+09**	**$1.60x10^{+06}$**	**3.76E+03**	**7.11E+05**	**1.18E-18**	**1.12**
M6	**1.00E-11**	**1.00E-16**	**6.02E+07**	**$1.60x10^{+06}$**	**3.76E+01**	**7.11E+03**	**1.18E-20**	**1.20**

[‡] Not only six samples were done during the project during this thesis several samples and tests were done, the six samples shows on the document are the most representatives. M1 to M6 are the samples reported on the scientific article "Nanomolar detection of Glucose using SERS substrates fabricated with Albumin coated gold nanoparticles"

2.2.3 Optical Characterization of Self assembly substrates

The absorption spectra of gold nanoparticles ranging from 400-1000 nm were obtained from a Perkin Elmer lamba 900 spectrometer and using a quartz cuvette of 1 cm of thickness. The IR spectra [Fourier transform infrared (FTIR)] of samples were recorded in the range of 2700–3100 cm^{-1} on an ABA (MB300) spectrometer using the ATR method. Raman measurements in the range of 100-1800 cm^{-1} were carried out using a Raman Spectrometer R-S Renishaw (1000 B) which has incorporated a laser of 785 nm. The power used for all measurements was 2.4 mW and the spot area is around 180μm^2 it was calculated by measure the spot on the camera (diameter of ~ 15 μm) of the Raman. It agree with the literature that states for a 50X objective lens with NA 0.75 maximum diameter of 20 μm[154] the total time integration were 30 seconds.

2.2.4 Results and Discussion of SA substrates

The architecture of the SERS substrate and the morphology of nanoparticles are central in order to produce Raman enhancement and in order to reduce limit of detection. It has been published that star-like gold nanoparticles are useful in order to get a Raman enhancement factor up to 10^{12}, [156,11] while those with spherical nanoparticles are able to produce a

maximum EF of 10^8,[11] therefore, star-like nanoparticles were used in this work.

A SEM image of gold nanoparticles used in order to fabricate our SERS substrates is shown in Figure 9a. Those nanoparticles have sharp tips and their average size was 117 nm (from tip to tip). The particles have smaller peaks than the particles used on the LB methodology to promote the linked to the substrate. Figure 9b shows an image of gold nanoparticles deposited on a glass substrate. As seen in the image, the distribution of the nanoparticles is not uniform on the substrate, the particle cluster and some empty spaces appear among different conglomerations of particles, enabling the plasmon interaction between them by electromagnetic coupling[36]. When Albumin is deposited by spin coating, the gold nanoparticles look completely coated by this compound and clustering is still present, see figure 9c. A zoom of the Albumin coated nanoparticles is presented in figure 9d, the average size of the core (AuNPs)/shell (Albumin) particles is 132 nm. This means an increase of 15 nm after the Albumin deposition, and this increase should correspond to the thickness of the Albumin shell.

Figure 10 shows a diagram to illustrate different bonds between the glass substrate and the Albumin coated gold nanoparticles. Basically, APTES molecule (0.6 nm length) is attached to the glass substrates by Si-OH

bonds, this in turn, is linked to the gold nanoparticles by an amine (NH_2) termination (see figure 10a). The gold nanoparticles are bonded to the Albumin due to the formation of peptide bonds ($COOH\text{-}NH_2$), see figure 10c.

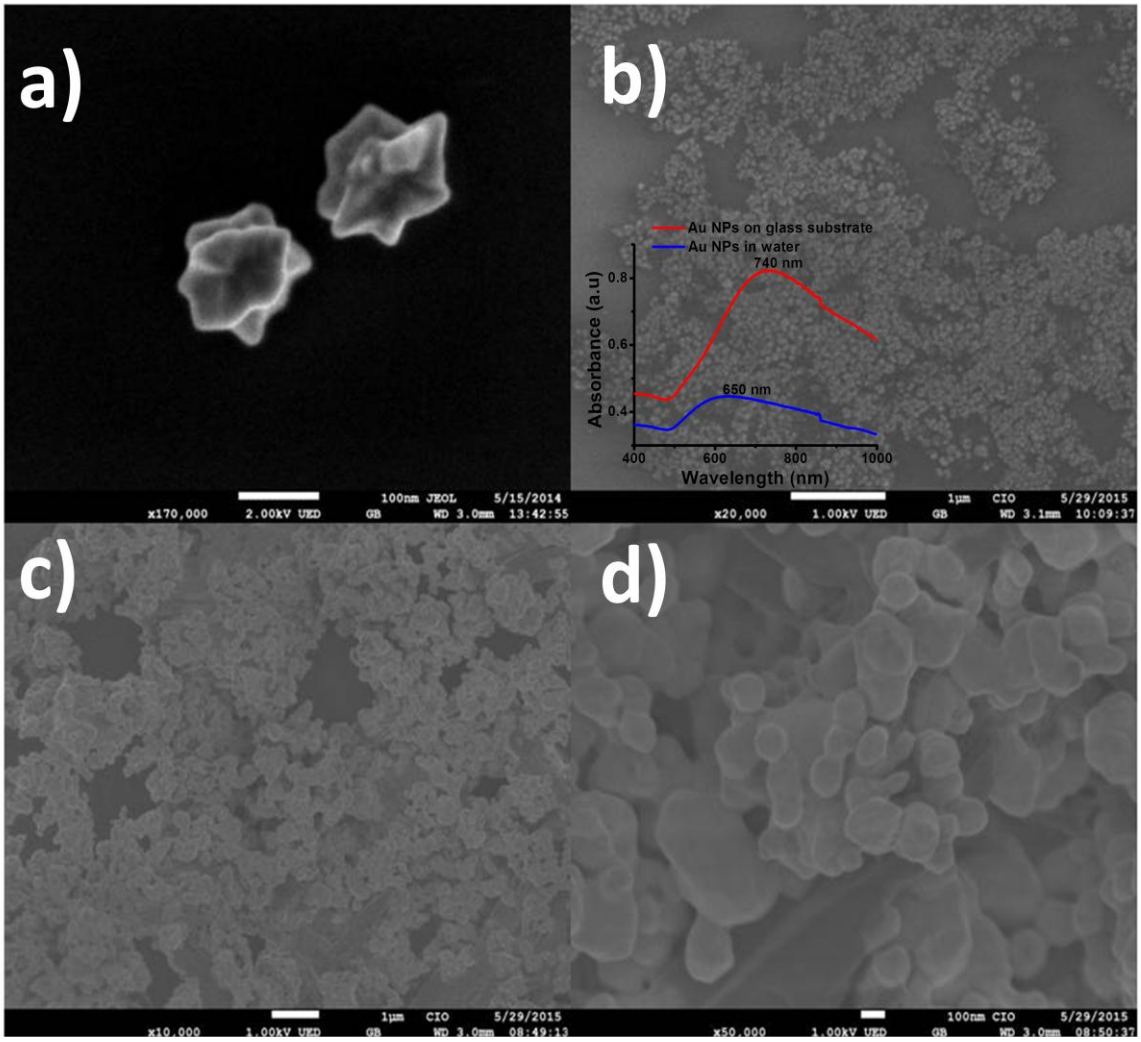

Figure 9. SEM images of: a) Star-like Gold nanoparticles, b) Gold nanoparticles on glass substrate, c) Albumin coated gold nanoparticles on glass, and d) Zoom of the substrate with Albumin coated gold nanoparticles. Inset in figure 1b shows the absorption spectra of gold nanoparticles dispersed in water and deposited on glass.

The formation of this bond is related with the limit of detection in our SERS substrates as explained later. The presence of gold nanoparticles was detected by absorbance measurements, inset in figure 9b shows the plasmon resonance of gold nanoparticles dispersed in water, which corresponds to the particles on the substrate. A red shift from 650 nm to 740 nm is observed for the plasmon resonance when the nanoparticles are deposited on the substrate, owing their conglomeration after deposition as observed in Figure 9b. In fact, this red shift was convenient because the plasmon resonance of gold nanoparticles is in near resonance with the laser wavelength used for Raman measurements (785 nm).

The measurement of Glucose in biological systems is an important interest in medicine and biology[3,151,149,157]. For this reason we have chosen Glucose as an analyte of interest. The early determination of Glucose content in human blood can help to prevent the development of diabetes in patients and its side effects[158,159,160]. As an effort to detect Glucose at very low levels, several types of sensors have been developed[3,151,157,161-34] in order to get the range of Glucose in human blood (4.4mM-6.6mM)[162,163]. On the other hand, Raman spectroscopy has emerged as an alternative to detect molecules of biological interest such as aminoacids, sugars, lipids etc[7-8]. In particular,

surface Raman enhanced spectroscopy (SERS) has been used because it can enhance the inelastic light scattering by a factor of at least 10^4,[5-35].

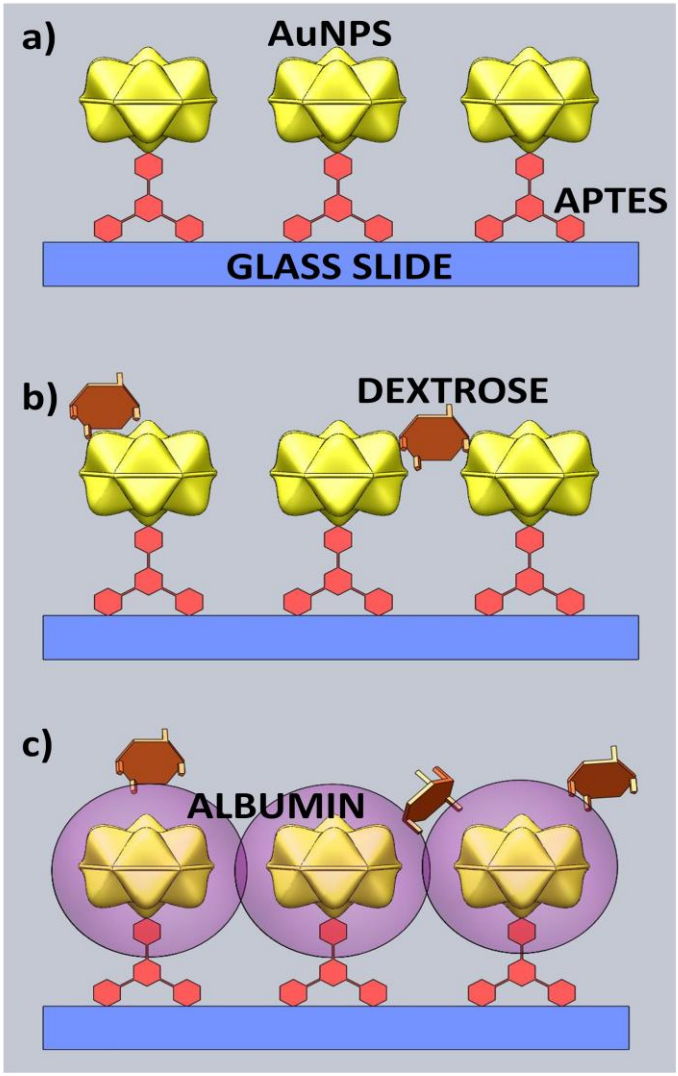

Figure 10. Schematics of each SERS substrate fabricated in this work: a) Glass/Au NPs, b) Glass/Au nanoparticles/Glucose, and c) Glass/Au NPs/Albumin/Glucose.

It is well-known that the detection of Glucose is difficult because of the anomeric effect. It is a chemical phenomenon where the chemical structure of the molecule is changing continuously when it is dispersed in liquids, this effect is present specially in sugars[164,165]. If this effect is reduced or completely eliminated, the detection of Glucose would be easier given that the molecule would be more stable. A possible approach in order to chemically stabilize the Glucose molecule would be bonding it to another molecule such as Albumin, this last molecule can be a good option since it can form glycated Albumin (peptide bonds) after interacting with the Glucose molecule[166,167]. The performance of our SERS substrates was studied without and with Albumin, in order to determine the detection limit and the effect of gold nanoparticles in our system under this phenomenon. We added a droplet of Glucose (10 µl) dispersed in water on our SERS substrates, after this, the Glucose molecules spread out on the substrate by diffusion and was positioned among adjacent gold nanoparticles or above them, see figure 10b. They cannot be located between the gold nanoparticles and the substrate since the molecule length of APTES (0.6 nm) is smaller than that of Glucose (0.87 nm).

We confirm our results of interaction between Albumin and Glucose with FTIR measurements. Figure 11 depicts the FTIR spectra of Albumin, Glucose and a mixture of Albumin + Glucose. The bands located in the range of 1550 cm^{-1}-1660 cm^{-1} and associated to the amide groups I and II of Albumin can clear be seen in figure 11b. The intensity of such bands decreased dramatically when Albumin was mixed with Glucose, as observed by comparing figures 11a and 11b. It is also noticeable that the peaks of Albumin located at 1405 cm^{-1} and 1653 cm^{-1} are completely attenuated while the main peaks of Glucose located at 915 cm^{-1}, 1073 cm^{-1}, 1126 cm^{-1} are enhanced. According to the literature, the peaks located at 1405 cm^{-1} and 1653 cm^{-1} corresponds to the amide groups (named I and II) of Albumin [168,169]. The simultaneous enhancement and attenuation of some peaks indicates that the Albumin and Glucose molecules are interacting by forming new bonds. According to the literature, Glucose can form peptide bonds (COOH-NH_2) with Albumin through the interaction of amide groups fof Albumin (NH_2) with COOH groups of Glucose[170-37]. Those peptide bonds are also named glycated Albumin[167] and are important for the stabilization of the Glucose molecule as mentioned earlier.

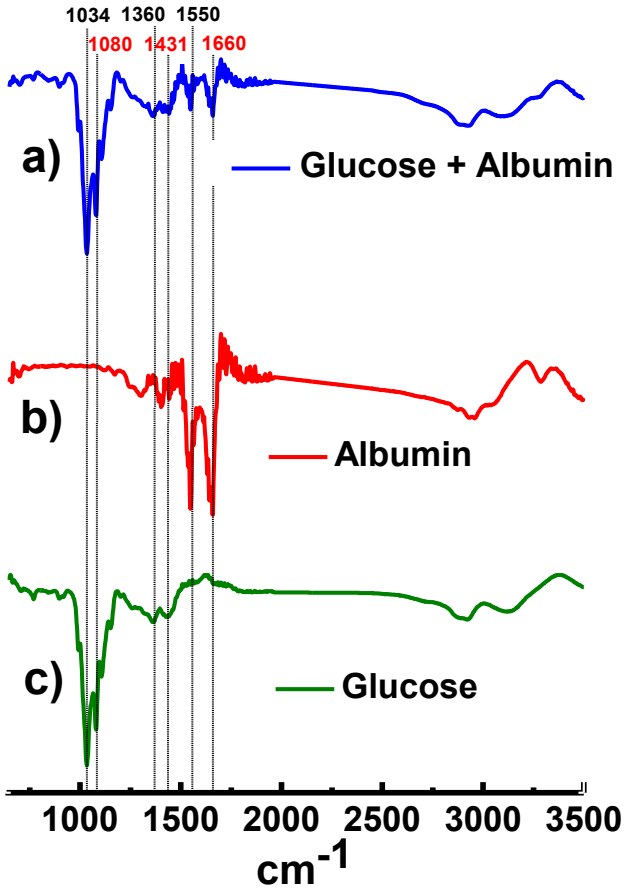

Figure 11. FTIR Spectra of solutions of Glucose (1M), Albumin (11 vol.%) and a mixture of Glucose (1M)+Albumin (11 vol.%).

Chapter 3

SERS substrates response characterization[§].

Overview

This chapter shows the SERS results achieved by the multipurpose SERS substrates and self assembly SERS substrates.

The gold nanoparticles which were deposited using the Langmuir Blodgett trough technique on silicon substrates or on gold coated silicon substrates permitted the zeptomol detection of Rhodamine B (total moles per laser spot area). The Raman enhancement factor (EF) reached for this level of detection was 10^{12}, and was obtained on the SERS substrate fabricated with the configuration: Si/Au film/Au nanoparticles. Raman spectra of the molecules TWEEN 20 and P-terphenyl were also measured in order to elucidate the effect of the molecule's length on the enhancement factor. According to those results, our SERS substrates without the gold film are useful for a minimum detection level of ~10^{-14} moles of analytes with sizes equal to or less than 1.3 nm and ~10^{-18} moles of analytes with gold film (total moles per sample).

---

§ Some contents of the chapter 3 are reproduced from Ref. [156,174] with permission from the Royal Society of Chemistry. http://www.rsc.org/journals-books-databases/journal-authors-reviewers/licences-copyright-permissions/#reuse-permission-requests.

The self assembly SERS substrates were used for Glucose detection as low as 10^{-7} M which represents an enhancement factor (EF) of 10^9, as a result of the hot spot formed by the spike termination and appropriate distribution of gold nanoparticles. An improvement of two orders of magnitude was obtained by coating gold nanoparticles with Albumin with the configuration: glass/Au nanoparticles/Albumin. In this case the lowest detection was 10^{-9} M for an EF of 10^{11}. The Albumin molecule allowed us to enhance the Raman signal because of the formation of peptide bonds (COOH-NH_2) generated due to the interaction of Glucose with Albumin, and to the appropriate separation distance between the Glucose molecules and gold nanoparticles. The presence of such peptide conjugates was confirmed by FTIR spectra. Thus, our results suggest that our SERS substrates can be useful for the detection of very low Glucose concentration, which is important for the diagnosis of diabetes.

3.1 Results obtained for SERS substrates prepared by Langmuir Blodgett Trough (LB)

3.1.1 SERS results for Rhodamine B

The data obtained from Raman measurements requires a careful treatment to avoid peaks unrelated to the analyte subject to analysis (in this case RhB) and to eliminate Raman peaks related to the Silicon substrates, Au film and Au NPs. The background corresponding to the three elements just mentioned above were subtracted from Raman measurements in order to guarantee that the observed Raman peaks correspond only to Rhodamine B. in order to determine the limit of Raman detection for the conditions of measurement and type of substrate established in this work, several molar solutions were prepared by diluting RhB in ethanol, later 10 µl of each solution were deposited on the substrates. From here, the amounts of RhB deposited on each substrate were calculated, see column B in table 1, chapter 2.

It is possible to obtain the Raman signal for a concentration of $1.03x10^{-5}$ moles when RhB is deposited on a Si substrate only, see figure 12a, but it is not possible when we have less than $1.031x10^{-11}$ moles on the Si substrates, a peak at about 940 cm^{-1} related with the Si substrate is visualized (see Raman spectra for Si in Figure 12a).

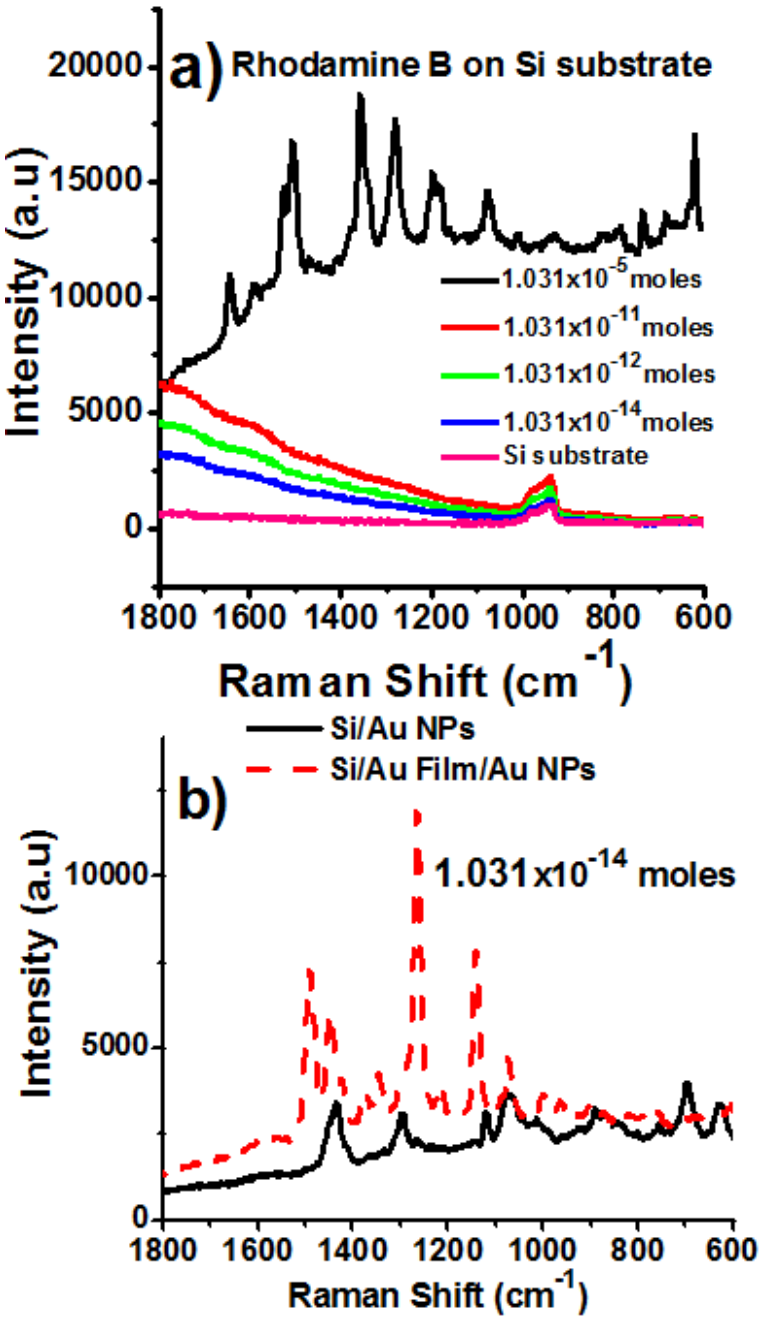

Figure 12. Raman spectra of (a) R1–R4 samples on Si substrate and (b) R4 with/without Au film.

This demonstrates that the silicon substrate is not good enough for Raman detection at very low concentrations. In order to improve Raman detection, Au NPs were deposited by LB to the Silicon substrates. In figure 12b a black line, shows an example of Raman enhancement for sample R4 with 10^{-14} moles of RhB; it is clearly observed that Raman peaks appeared in the configuration Si/Au NPs. In order to have an idea about the improvement of Raman detection due to the presence of gold nanoparticles, the Raman enhancement factor (EF) was calculated using the formula: $EF= (I_{SERS}*N_{REF})/(I_{REF}*N_{SERS})$ where I_{SERS} is the enhanced Raman intensity of the adsorbed RhB molecules on the substrate, I_{REF} is the spontaneous Raman scattering intensity from the RhB molecules under the laser spot, which are on the Si substrate (without Au NPs), N_{REF} represents the number of RhB molecules excited by the laser without Raman enhancement effect and N_{SERS} is the number of molecules uniformly covering the SERS substrate in the laser spot area[16,171]. Thus, it is possible to state that the EF improved from 0 (Si substrate without Au NPs) to 10^9 when the nanoparticles were added, see figure 12b. This value of EF is in perfect agreement with the value reported from numerical simulations[11,44]. The surprising enhancement of the Raman signal is caused by the tips located in our gold nanoparticles. From boundary element methods (BEM) it has been found

that there are plasmon oscillations confined within the tips (localized plasmons), which give rise to an enhancement of the electric field, that in turn, is associated to the optical response[11,44,147]. In order to increase the enhancement of the Raman signal again for the concentration of RhB molecules in sample R4 (10^{-14} moles), an extra layer of gold was deposited on the Si substrate with the configuration: Si/Au Film/Au NPs. As a result of this additional layer, new Raman peaks appeared and their intensity increased with Au NPs, see Figure 12b (red line). The additional improvement is produced by the overlapping of the plasmonic absorption of the gold nanoparticles and that of the substrate with the Au film (Si/Au Film/Au NPs), see inset in figure 6d chapter 2. This is the result of the increase in the dipolar oscillations related to the electric field enhancement in the tips when both, the Au film and the Au NPs are interacting at the same time with the laser at 830 nm. The limit of Raman detection without the presence of the Au film was determined as 1.03×10^{-14} moles (total moles per sample). If the concentration is further decreased, it is not possible to detect Raman peaks only with the presence of Au NPs. Table 1 chapter 2, summarizes the values of the main parameters to have an idea about the level of detection in this work. Column C presents the number of molecules deposited on the SERS substrates with an area of 4 mm x 4 mm

($16x10^6 \mu m^2$), this column was calculated taking into account 1 mol of molecules, column D shows the area of the samples R1-R6, Column E resulted for dividing column C by column D, column F was calculated multiplying column E by 189 μm^2 (laser spot area), column G resulted from the operation: (column B/$16x10^6 \mu m^2$)*189 μm^2, and finally column H shows the total error of each parameter in columns B-G corresponding to each sample. This table also shows that detection of ~10^{-18} moles distributed on the substrate is possible, this is equivalent to detect just 1 molecule in each 3 μm^2 or $1.22x10^{-22}$ moles on an area of 189 μm^2, this level of zeptomol detection was achieved just with the simultaneous presence of an Au film and Au NPs, see column E for sample R6. Figure 13a shows the Raman spectra for different molar concentrations on the SERS substrate, the Raman spectrum for the sample R1 with $1.031x10^{-5}$ moles of RhB is shown for reference. As observed, all Raman peaks presented in samples R2-R6 have good agreement with those shown for R1, see vertical lines on that plot. All of those peaks also coincide with those reported in the literature[172]. Figure 13b shows the Raman spectra for samples R3-R6.

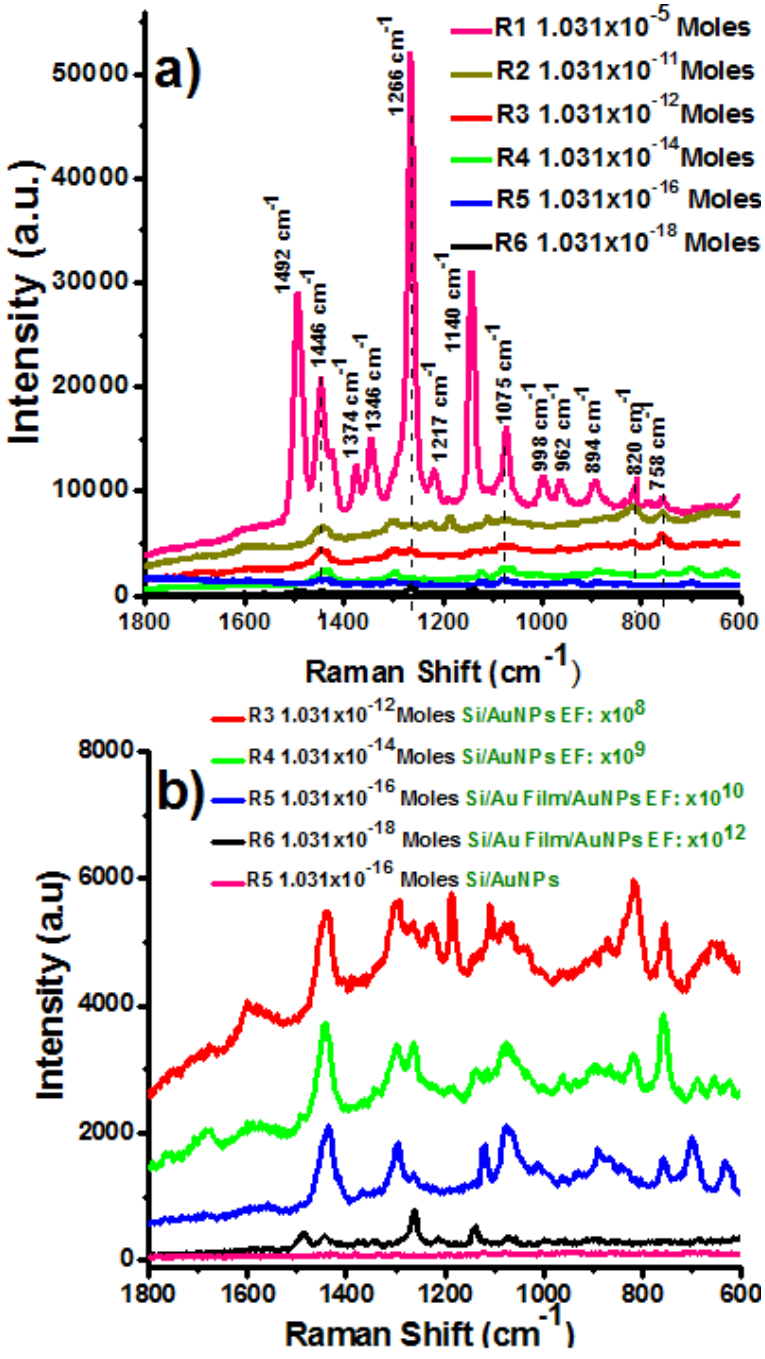

Figure 13. Raman spectra of a) samples R1-R6 and b) samples R3-R6

Raman spectra are accompanied with the corresponding Enhancement factors; the Au film permits EF of 10^{10} and 10^{12} for samples R5 and R6 respectively, which is in agreement with literature for zeptomol detection[11,136]. As mentioned before, our design for the SERS substrate does not need to attach the analyte between the gold nanoparticles and the Au film. When this occurs, some intrinsic Raman peaks related to the analyte disappear because it forms bonds with the gold nanoparticles or Au films as shown in ref. [11,136]. In our case, the Raman spectra show intrinsic vibrational modes corresponding to Rhodamine B, since it is not being bound with gold nanoparticles or the Au film, this in turn, allows us to increase our level of detection. The Raman spectra of samples R3 ($1.03x10^{-12}$ moles) and R4 ($1.03x10^{-14}$ moles) were possible to observe without Au film and their EF were 10^8 and 10^9 respectively. The Raman signal of the sample R5 ($1.03x10^{-16}$ moles) was not observed without Au film suggesting that such film effectively improves Raman detection and EF by the mechanisms explained above.

3.1.2 SERS results for The effect of the molecule's length

The effect of the molecule's length on the Raman enhancement using our SERS substrates was also studied without a gold film. Figures 14a-c show the Raman spectra for SERS substrates which contained $1x10^{-5}$ moles (total moles per sample) of P-therphenyl, RhB and TWEEN 20 respectively. Those ones will be used as references to be compared with the Raman spectra obtained from substrates with lower amount of moles for the same substances as depicted in figures 14d-f. The insets in figures 14d-f show the structure of the molecules. As observed, all peaks appearing in the plots 14d-f are matching those on figures 14a-c. Moreover, the minimum amount of moles of P-therphenyl and RhB which were possible to detect using the configuration Si/Au NPs/molecules (without Au film) was $1.031x10^{-14}$ moles (total moles per sample) and the EF for the Raman signal obtained from these substrates with P-therphenyl and RhB was 10^9 (the same for both cases).

The Raman enhancement factor (EF) was calculated using the formula: $EF=(I_{SERS}*N_{REF})/(I_{REF}*N_{SERS})$ where I_{SERS} is the enhanced Raman intensity of the adsorbed molecules on the substrate, I_{REF} is the spontaneous Raman scattering intensity from the molecules under the laser spot, which are on the Si substrate (without Au NPs), N_{REF} represents the number of molecules

excited by the laser without Raman enhancement effect and N_{SERS} is the number of molecules uniformly covering the SERS substrate in the laser spot area[16,171].

The EF in the case of the molecule TWEEN 20 was 10^7, and the minimum amount of moles detected was $1.03x10^{-9}$ moles. The size of that molecule and its position on the SERS substrate could be related directly to the reduction of two orders of magnitude in EF compared to that for P-therphenyl. The TWEEN 20 molecule is bigger compared to RhB and P-therphenyl, making difficult its diffusion and can not be introduced between adjacent gold nanoparticles, it can remain only on gold nanoparticles, see figure 6a chapter 2. In contrast, the P-therphenyl is smaller and can be diffused easily on SERS substrates, being located in the same positions as RhB, in consequence, a higher EF is expected for this molecule. It has been reported that hotspots responsible of the Raman enhancement are regularly located between tips of gold nanostars separated at about 2 nm[41,138]. Thus, if we want to produce Raman enhancement for certain molecules, their size of them should be small enough to fit inside the hotspot. Based on this assumption, it is expected that large molecules such as TWEEN 20 with an approximate length of 6 nm should not fit inside the 2.6 nm between adjacent gold nanoparticles.

As a result, the amount of molecules detected would be lower compared to the one corresponding to RhB or P-therphenyl with a length of 1.3 nm and 0.7 nm, respectively. Therefore, the probability to fit them inside a hotspot is higher than that for TWEEN 20. In consequence, the detection of lower amounts of those molecules was possible ($1.03x10^{-14}$ moles for p-therphenyl and RhB).

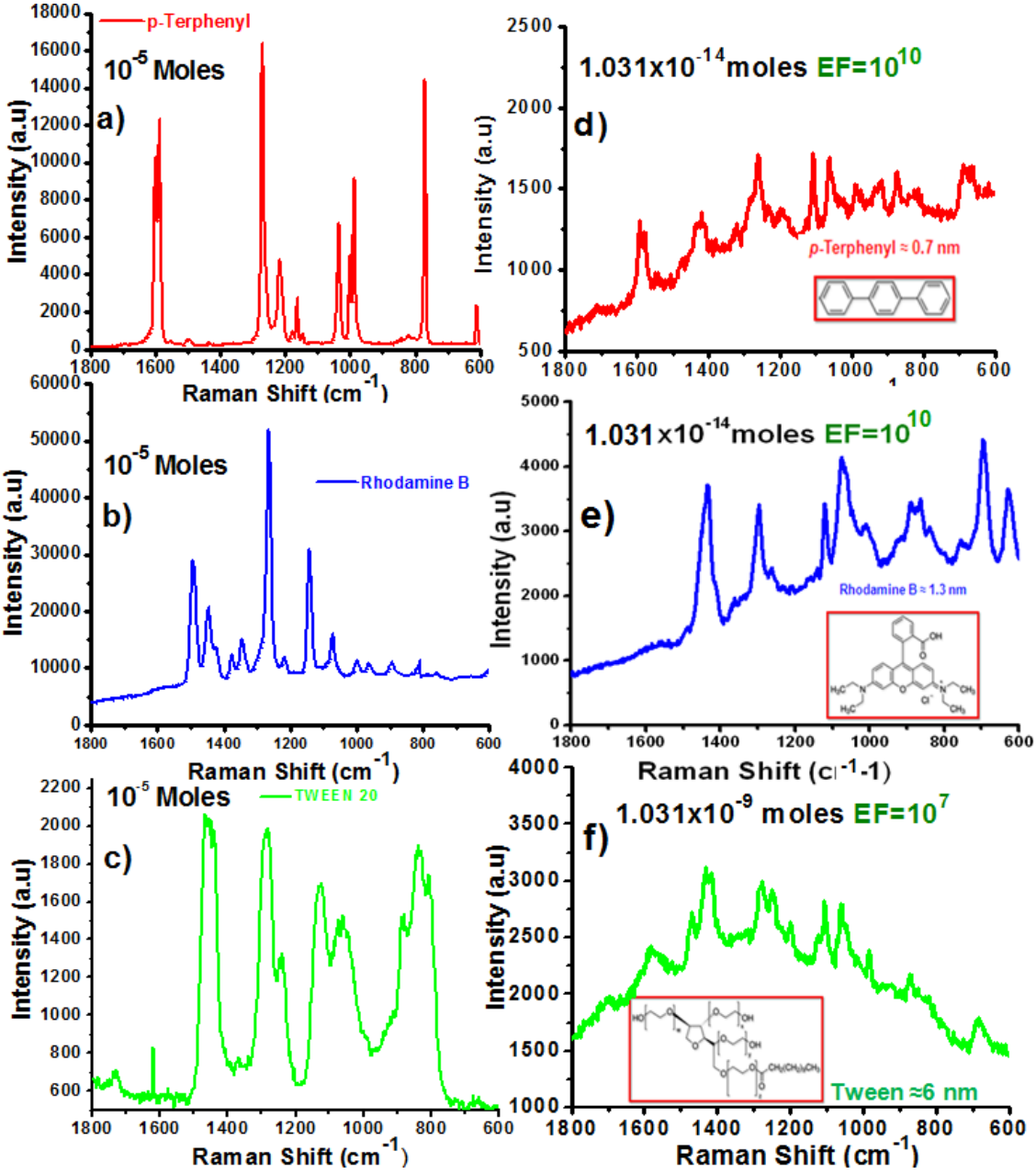

Figure 14. (a), (b) and (c) show the Raman spectra for 10−5 moles of p-terphenyl, RhB and TWEEN 20 respectively. (d), (e) and (f) show the Raman spectra for p-terphenyl, RhB and TWEEN 20 respectively using the configuration: Si substrate/Au NPs/molecule. Insets in figures (d), (e) and (f) show the molecular structures of p-terphenyl, RhB and TWEEN 20 respectively.

3.2 Results obtained in SERS substrates prepared by self assembly (SA)

3.2.1 SERS results for Glucose

The Raman spectra were obtained for samples M1-M4 and M5NA as depicted in figure 15a. As observed, some peaks of Glucose located at 1073 cm^{-1} and 1126 cm^{-1} which are associated to C-C, C-O and C-O-H bonds[23] are still visible for sample M4 with a molar concentration of 10^{-7} and no peaks are observed for a concentration of 10^{-9}M. This suggests that 10^{-7} M is the detection limit for our SERS substrates with only gold nanoparticles and no Albumin. A summary of each type of bond related with the Raman peaks of Glucose is presented in table 3, those ones were obtained from references 7, [162], [163], and [164].

Table 3. Summary of main bonds for identification of Glucose.

Raman Peaks at: (cm^{-1})	650	770	841	915	1073	1126	1334	1405	1653
Glucose (solid)	**651**	**773**	**843**	**916**	**1075**	**1121**	**1332**	**---**	**----**
Glucose in Water (Our samples)	**650**	**770**	**841**	**915**	**1073**	**1126**	**1334**	**---**	**----**
Albumin	**--**	**--**	**--**	**--**	**--**	**1126**	**1334**	**1405**	**1653**
Bond	**C-C**	**C-H**	**C-C C_1-H_1**	**C-C C-H C-0**	**C-C C-O C-O-H**	**COH**	**O-C-H C-O-H C-C-H**	**CH_2 and CH_2OH deformations**	**H-bonded C=O stretch Amide(I): -NH_2**

It is observed that all peaks in our Raman spectra are in agreement with literature. To the best of our knowledge, this is the first time that a detection of 10^{-7} M is reached using the SERS effect without nanoparticles functionalization. This is three orders of magnitude more sensitive than the detection limit of 0.1 mM reported before in the literature for electro chemical metods[173,157] and one order of magnitude better in comparison to the report of Al-Ogaidi et al. where a minimum level of detection of 16 μM using gold nanostar@silica core-shell nanoparticles was reported [15].

We associate this improvement in the detection to the fact that the Glucose molecules attached to the gold nanoparticles are directly in contact with the tips of gold nanostars. We can also have two effects which can improve the Raman scattering in our system: the first one is the enhancement owing to dipolar fields of the particle plasmon resonance, while the second one is a purely geometric factor identified in literature as the lightning rod factor[27,59]. Thus, higher EFs are possible with gold nanostars in comparison to spherical nanoparticles [156,11].

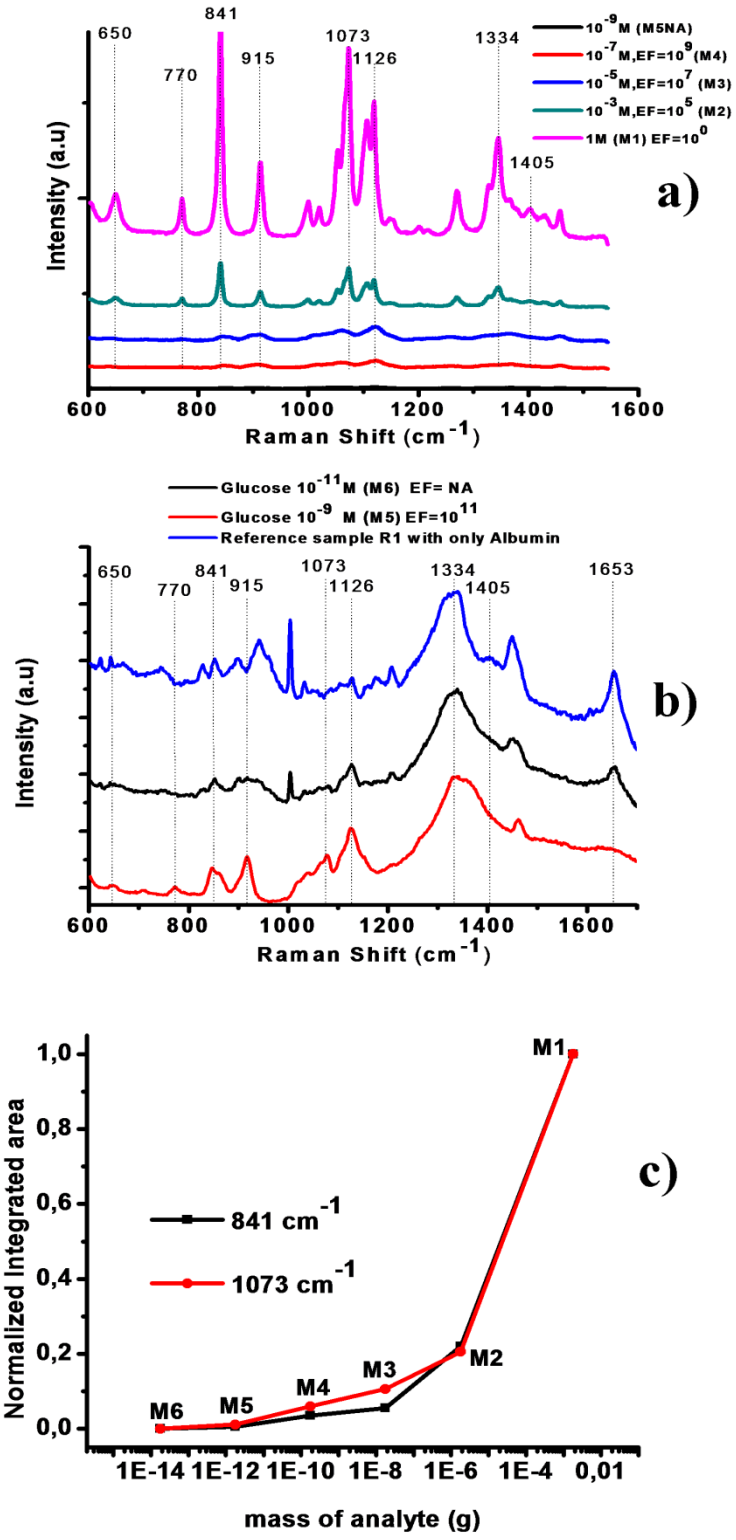

Figure 15. Raman spectra of: a) Samples M1-M4 and M5NA without Albumin, and b) M5, M6 and that of the reference substrate R1 (glass/Au NPs/Albumin). c) shows the normalized integrated area for the Raman lines at 841 cm-1 and 1073 cm-1 versus the mass of analyte for each sample M1-M6

Moreover, the Glucose molecule can diffuse among the clustered gold nanoparticles[23], increasing the probability for Glucose molecules to be located between several gold nanostars at the same time and this could promote the SERS effect, since it has been reported that hotspots responsible of the Raman enhancement are regularly located between tips of gold nanostars separated at about 2 nm[11,6,44]. The numbers of hotspots is directly related to the detection capacity single molecule, given that it has been reported that hotspots are points with a factor of enhanced electric field E^2 up to 10^{14} [16, 16, 43]. In our case, A Glucose molecule can fit into the hotspot perfectly because its length (0.87 nm) is small enough to fit inside the hotspot (2 nm).

In order to have an idea about the improvement of Raman signal detection produced by the presence of gold nanoparticles, the Raman enhancement factor was calculated using the formula: $EF= (I_{SERS}*N_{REF})/(I_{REF}*N_{SERS})$ where I_{SERS} is the enhanced Raman intensity of the adsorbed Glucose molecules on the substrate, I_{REF} is the spontaneous Raman scattering intensity from the Glucose molecules under the laser spot, which are on the glass substrate (without Au NPs), N_{REF} is the number of Glucose molecules excited by the laser without Raman enhancement effect and N_{SERS} is the

number of molecules covering uniformly the SERS substrate and within the laser spot[16,24].

The enhancement factors for M2, M3 and M4 were 10^5, 10^7 and 10^9. Therefore, the EF improved from 1 (substrate without Au NPs and with a concentration of 1M) to a maximum of 10^9 when the gold nanoparticles are added, see figure 15a. Table 2 chapter 2, summarizes the values of the main parameters in order to have an idea about the level of detection reported in this work. Columns B and C show the molar concentration and the number of moles of Glucose deposited on the substrates. Column D presents the number of molecules deposited on the SERS substrates with an area of 4 mm x 4 mm ($16x10^6$ μm^2), this column was calculated taking into account that 1 mol, column E shows the area of the samples M1-M6, Column F resulted by dividing column D with column E, column G was calculated multiplying column F by 180 μm^2 (laser spot area), column H resulted from the operation: (column C/$16x10^6$ μm^2)*180 μm^2, and finally column I shows the total error of each parameter in columns B-H corresponding to each sample. This table indicates that that we can detect as low as 1 picomole on our SERS substrates (sample M4) even though the anomeric effect is present. We can detect as low as 1.18 $x10^{-16}$ moles or

$7.11x10^7$ molecules per spot area, see column H for M4, taking into account the laser spot area (180 μm^2).

As confirmed above, it is not possible to detect any Raman signal of Glucose for concentrations below 10^{-7} M only with the presence of Au NPs. We overcame this problem by adding Albumin to our substrate with gold nanoparticles, figure 10d chapter 2 illustrate the Albumin coated nanoparticles. As mentioned before (chapter 2), the detection of Glucose is difficult due to the anomeric effect. If this effect is reduced or completely stopped, the detection of Glucose would be easier. An alternative to chemically stabilize the Glucose molecule would be by bonding them to another molecule such as Albumin, this last molecule can be a good option since it can form glycated Albumin (peptide bonds) after interacting with Glucose,[166,167]. After this, Glucose detection for concentrations as low as 10^{-9}M would be possible. Figure 15b shows the Raman spectra of sample M5 with a Glucose concentration of 10^{-9} M and the reference substrate with only Albumin (named R1: Glass/Au NPs/Albumin (11 vol.%)). It is clearly observed in sample M5 some peaks which do not appear in the reference sample R1 or they are broader, they are located at: 841 cm^{-1}, 915 cm^{-1}, 1073 cm^{-1}, 1126 cm^{-1} and 1334 cm^{-1}. Such peaks are in agreement with

those observed in the Glucose molecule (see Raman spectrum for sample M1 in figure 15a).

The EF of sample M5 was 10^{11}, which is two orders of magnitude higher than for M4 without Albumin. It is also noticeable that the peaks of Albumin located at 1405 cm^{-1} and 1653 cm^{-1} are completely attenuated while the main peaks of Glucose located at 915 cm^{-1}, 1073 cm^{-1}, 1126 cm^{-1} are enhanced. According to literature, the peaks located at 1405 cm^{-1} and 1653 cm^{-1} corresponds to the amide groups (named I and II) of Albumin [168,169]. The simultaneous enhancement and attenuation of some peaks indicates that the Albumin and Glucose molecules are interacting to form new bonds. According to literature, the Glucose can form peptide bonds (COOH-NH2) with Albumin through the interaction of amide groups from Albumin (NH2) with COOH groups from Glucose[170-37]. Those peptide bonds are also named glycated Albumin[167] and are important for the stabilization of the Glucose molecule as mentioned above. After this interaction, the Raman signal of C-O bonds of Glucose located in the range of 890 cm^{-1}-1150 cm^{-1} can be enhanced with the SERS effect. This is confirmed with sample M5 with a concentration of 10^{-9} M of Glucose which presents some characteristic peaks (915 cm^{-1}, 1073 cm^{-1} and 1126 cm^{-1}) in that range. Thus, an attenuation of bands corresponding to amide I and II groups (NH_2)

at 1405 cm^{-1} and 1653 cm^{-1} demonstrates the formation of peptide bonds, which in turn, favor the enhancement of Raman peaks associated to Glucose (compare Raman spectra of samples R1 and M5 in figure 15b). If the concentration is decreased even more, for example a concentration of 10^{-11}M, it is observed that its Raman spectra is very similar to that of the reference sample with Albumin only, samples R1 and M6 in figure 15b. In this case, the peak at 1653 cm^{-1} appears again and all peaks observed in the range of 890 cm^{-1}-1150 cm^{-1} do not appear anymore, suggesting that the interaction between Albumin and Glucose at very low concentrations is not strong enough in order to observe a SERS signal. To better visualize the limit of detection in our system, we have plotted a curve of normalized integrated area versus the mass of analyte deposited on the substrate[49-51] by using the peaks at 841cm^{-1} and 1073cm^{-1}, see figure 15c. It is observed that the integrated area decreases as the concentration of Glucose decreases. The sample M5 which had a Glucose mass of of 1.8 x 10^{-12} g corresponding to 10^{-9} M, still presented some weak peaks at 841cm^{-1} and 1073cm^{-1}. For lower molarities of Glucose such as that for sample M6 (10^{-11} M) which had a analyte mass of 1.8 x 10^{-14} g, the raman signal was not observed and the observed integrated area was zero. This means that the limit of detection is 10^{-9} M in our system with Albumin.

Chapter 4

Conclusions[**]

In conclusion, the molecule 1-dodecanethiol was helpful to produce a spacing of ~2.6 nm between adjacent gold nanoparticles, this promotes the generation of hotspots (see appendix A.3). We expect to have a higher amount of hotspots on SERS substrates with gold film compared to those ones without the gold films because additional hotspots can be produced between the Au film and the tips of gold stars. Therefore, the level of detection of analytes increases several orders of magnitude. Zeptomol detection of RhB, that is, the detection of a single molecule of RhB in 3 μm^2 or $1.22x10^{-22}$ moles on 189 μm^2 (laser spot area) was achieved using a SERS substrate with the configuration: Si/Au film/Au nanoparticles. Such a level of detection was produced by the enhancement of the electric field in hotspots produced between gold nano stars and due to the plasmonic coupling between the Au nanoparticles and the gold film. For this architecture the average EF is 10^{12} with a reproducible error of ±12.45% (see appendix A.2).

[**] Some contents of the chapter 4 are reproduced from Ref. [156,174] with permission from the Royal Society of Chemistry. http://www.rsc.org/journals-books-databases/journal-authors-reviewers/licences-copyright-permissions/#reuse-permission-requests.

Furthermore, the SERS substrate with the gold film enables us to detect a concentration of 10^{-9} moles for large molecules such as TWEEN 20 (~6nm), even though it could not fit into the hotspots formed between adjacent Au nanostars (interparticle distance 2.6 nm). If the size of the molecule is equal or below 1.3 nm, it is possible to detect up to $13.28x10^{-14}$ moles using a SERS substrate without gold film as demonstrated for RhB and P-therphenyl. Those results suggest that our SERS substrates have high potential to detect concentrations as low as 10^{-18} moles for molecule lengths less than 2.6 nm. Finally, the characteristics and design of our SERS substrates open the possibility to detect molecules of medical and biological interest. This work demonstrated the fabrication of SERS substrates for ultralow concentration detection of Glucose, as a result of the hot spots formed by the spike termination of Au NPs and the appropriate distribution of gold nanoparticles. Glucose Detection for concentrations as low as 10^{-7} M was demonstrated with substrates prepared with star-like gold nanoparticle in order to decrease even more the detection limit we coated our gold nanoparticles with Albumin, this compound interacts with the Glucose by forming peptide bonds, which in turn, allow us to detect Glucose for concentrations as low as 10^{-9} M by enhancing the Raman peaks

corresponding to the C-O bonds. For this architecture the average EF is 10^{11} with a reproducible error of ±20.9% (see appendix A.2).

To the best of our knowledge, this is the lowest detection limit reported with SERS to 13th May 2016. Hence, our results can pave the way for the development of new types of biosensors for the detection of Glucose in any living organism.

R e f e r e n c e s

1. Kneipp, J., Kneipp, H. & Kneipp, K. SERS--a single-molecule and nanoscale tool for bioanalytics. *Chem. Soc. Rev.* **37,** 1052–1060 (2008).
2. Singh, A. K. *et al.* Development of a long-range surface-enhanced raman spectroscopy ruler. *J. Am. Chem. Soc.* **134,** 8662–8669 (2012).
3. Kim, N.-Y. *et al.* Rapid, sensitive, and reusable detection of Glucose by a robust radiofrequency integrated passive device biosensor chip. *Sci. Rep.* **5,** 7807–7807 (2015).
4. Hering, K. *et al.* SERS: a versatile tool in chemical and biochemical diagnostics. *Anal. Bioanal. Chem.* **390,** 113–124 (2008).
5. Israelsen, N. D., Hanson, C. & Vargis, E. Nanoparticle Properties and Synthesis Effects on Surface-Enhanced Raman Scattering Enhancement Factor : An Introduction. *Sci. world J.* **2015,** 1–12 (2015).
6. Kneipp, K., Kneipp, H., Itzkan, I., Dasari, R. R. & Feld, M. S. Surface-enhanced Raman scattering and biophysics. *J. Phys. Condens. Matter* **14,** R597–R624 (2002).
7. Ellis, D. I., Cowcher, D. P., Ashton, L., O'Hagan, S. & Goodacre, R. Illuminating disease and enlightening biomedicine: Raman spectroscopy as a diagnostic tool. *Analyst* **138,** 3871–3884 (2013).
8. Bantz, K. C. *et al.* Recent progress in SERS biosensing. *Phys. Chem. Chem. Phys.* **13,** 11551–11567 (2011).
9. Harper, M. M., McKeating, K. S. & Faulds, K. Recent developments and future directions in SERS for bioanalysis. *Phys. Chem. Chem. Phys.* **15,** 5312 (2013).
10. McCreery, R. L. *Raman Spectroscopy for Chemical Analysis. A Ser. Monogr. Anal. Chemisry its Appl.* **157,** (A JOHN WILEY & SONS, INC., PUBLICATION, 2000).
11. Rodríguez-Lorenzo, L. *et al.* Zeptomol Detection Through Controlled Ultrasensitive Surface-Enhanced Raman Scattering. *J. Am. Chem. Soc.* **131,** 4616–4618 (2009).
12. Massarini, E. *et al.* Sensors and Actuators B : Chemical Methodologies for assessment of limit of detection and limit of identification using surface-enhanced Raman spectroscopy. *Sensors Actuators B. Chem.* **207,** 437–446 (2015).
13. Creighton, J. A. Contributions to the early development of surface-enhanced Raman spectroscopy. 175–183 (2010).

doi:10.1098/rsnr.2009.0061
14. Kukushkin, V. I., Van'kov, A. B. & Kukushkin, I. V. Long-range manifestation of surface-enhanced Raman scattering. *JETP Lett.* **98,** 64–69 (2013).
15. Al-ogaidi, I. *et al.* Analytica Chimica Acta A gold @ silica core – shell nanoparticle-based surface-enhanced Raman scattering biosensor for label-free Glucose detection. *Anal. Chim. Acta* **811,** 76–80 (2014).
16. Ru, E. C. Le, Blackie, E., Meyer, M. & Etchegoin, P. G. Surface Enhanced Raman Scattering Enhancement Factors : A Comprehensive Study. *J. Phys. Chem. C* **111,** 13794–13803 (2007).
17. Albrecht, M. G. & Creighton, J. A. Anomalously intense Raman spectra of pyridine at a silver electrode. *J. Am. Chem. Soc.* **99,** 5215–5217 (1977).
18. Stranahan, S. M. & Willets, K. a. Super-resolution optical imaging of single-molecule SERS hot spots. *Nano Lett.* **10,** 3777–3784 (2010).
19. Kasera, S., Biedermann, F., Baumberg, J. J., Scherman, O. a & Mahajan, S. Quantitative SERS Using the Sequestration of Small Molecules Inside Precise Plasmonic Nanoconstructs. *Nano Lett.* **12,** 5924–5928 (2012).
20. Kim, J. E., Kim, H. J. & Yoon, S. Influence of Surface Functionalities of Self-Assembled Monolayers on the Adsorption of Gold Nanoparticles. *Nature* **30,** 999–1000 (2009).
21. Singh, R. C. V. Raman and the Discovery of the Raman Effect. *Phys. Perspect.* **4,** 399–420 (2002).
22. M. Fleischmann, P. J. H. A. A. J. M. Raman Spectra Of Pyridine Adsorbed At A Silver Electrode. **26,** 2–5 (1974).
23. Severuhina, A. N. *et al.* Nanoplasmonic Chitosan Nanofibers as Effective SERS Substrate for Detection of Small Molecules. *ACS Appl. Mater. Interfaces* 15466−15473 (2015). doi:10.1021/acsami.5b03696
24. Nuntawong, N. *et al.* Surface-enhanced Raman scattering substrate of silver nanoparticles depositing on AAO template fabricated by magnetron sputtering. *Vacuum* **84,** 1415–1418 (2010).
25. Yang, M. *et al.* SERS-Active Gold Lace Nanoshells with Built-in Hotspots. *Nano Lett.* **10,** 4013–4019 (2010).
26. Jana, D., Matti, C., He, J. & Sagle, L. Capping Agent-Free Gold Nanostars Show Greatly Increased Versatility and Sensitivity for Biosensing. *Anal. Chem.* 150309113254008 (2015). doi:10.1021/acs.analchem.5b00014
27. Li, M., Kang, J. W., Dasari, R. R. & Barman, I. Shedding light on the extinction-enhancement duality in gold nanostar-enhanced Raman

spectroscopy. *Angew. Chem. Int. Ed. Engl.* **53,** 14115–9 (2014).
28. Ceja-Fdez, A. *et al.* Glucose Detection Using SERS with Multi-branched Gold Nanostructures in Aqueous Medium. *RSC Adv.* **4,** 59233–59241 (2014).
29. Munro, C. H., Smith, W. E., Garner, M., Clarkson, J. & White, P. C. Characterization of the surface of a citrate-reduced colloid optimized for use as a substrate for surface-enhanced resonance Raman scattering. *Langmuir* **11,** 3712–3720 (1995).
30. Faulds, K., Littleford, R. E., Graham, D., Dent, G. & Smith, W. E. Comparison of surface-enhanced resonance Raman scattering from unaggregated and aggregated nanoparticles. *Anal. Chem.* **76,** 592–598 (2004).
31. Polavarapu, L. & Liz-Marzán, L. M. Towards low-cost flexible substrates for nanoplasmonic sensing. *Phys. Chem. Chem. Phys.* **15,** 5288 (2013).
32. Wu, W. *et al.* Low-Cost, Disposable, Flexible and Highly Reproducible Screen Printed SERS Substrates for the Detection of Various Chemicals. *Sci. Rep.* **5,** 10208 (2015).
33. Su, Q., Ma, X., Dong, J., Jiang, C. & Qian, W. A reproducible SERS substrate based on electrostatically assisted aptes-functionalized surface-assembly of gold nanostars. *ACS Appl. Mater. Interfaces* **3,** 1873–1879 (2011).
34. Torul, H. *et al.* Glucose determination based on a two component self-assembled monolayer functionalized surface-enhanced Raman spectroscopy (SERS) probe. *Anal. Methods* **6,** 5097 (2014).
35. Park, W.-H., Ahn, S.-H. & Kim, Z. H. Surface-Enhanced Raman Scattering from a Single Nanoparticle-Plane Junction*. *ChemPhysChem* **9,** 2491–2494 (2008).
36. Radziuk, D. & Moehwald, H. Prospects for plasmonic hot spots in single molecule SERS towards the chemical imaging of live cells. *Phys. Chem. Chem. Phys.* **17,** 21072–21093 (2015).
37. Roncali, E, Tavitian, B, Texier, O. Peltie, P. *Nanoscience Nanobiotechnology and Nanobiology*. *Nanosci. Nanobiotechnology Nanobiology* (Springer Heidelberg Dordrecht London New York, 2010). doi:10.1007/978-3-540-88633-4
38. Zhang, Y. *et al.* One-pot green synthesis of Ag nanoparticles-graphene nanocomposites and their applications in SERS, H_2O_2, and Glucose sensing. *RSC Adv.* **2,** 538–545 (2012).
39. Mei, L.-P. *et al.* Simple electrodeposition of hierarchical gold-platinum nanothorns and their applications in electrocatalysis and SERS.

Electrochim. Acta **160,** 235–243 (2015).
40. Dong, J., Tao, Q., Guo, M., Yan, T. & Qian, W. Glucose-responsive multifunctional acupuncture needle: A universal SERS detection strategy of small biomolecules in vivo. *Anal. Methods* **4,** 3879–3883 (2012).
41. Theiss, J., Pavaskar, P., Echternach, P. M., Muller, R. E. & Cronin, S. B. Plasmonic Nanoparticle Arrays with Nanometer Separation for High-Performance SERS Substrates. *Nano Lett.* **10,** 2749–2754 (2010).
42. Torul, H. *et al.* Paper membrane-based SERS platform for the determination of Glucose in blood samples. *Anal. Bioanal. Chem.* 8243–8251 (2015). doi:10.1007/s00216-015-8966-x
43. Le Ru, E. C. & Etchegoin, P. G. Quantifying SERS enhancements. *MRS Bull.* **38,** 631–640 (2013).
44. Senthil Kumar, P., Pastoriza-Santos, I., Rodríguez-González, B., Javier García de Abajo, F. & Liz-Marzán, L. M. High-yield synthesis and optical response of gold nanostars. *Nanotechnology* **19,** 015606,1–6 (2008).
45. Srinivasan, U., Liepmann, D. & Howe, R. T. Microstructure to substrate self-assembly using capillary forces. *J. Microelectromechanical Syst.* **10,** 17–24 (2001).
46. Hou, X. *et al.* Self-assembly and Langmuir-Blodgett (LB) film of a novel hydrogen-bonded complex: A surface enhanced Raman scattering (SERS) study. *Colloids Surfaces A Physicochem. Eng. Asp.* **198-200,** 135–140 (2002).
47. Černiukė, I. *et al.* Formation of Metaloorganic Multilayer Structures by Langmuir-Blodgett Technique. *Mater. Sci.* **12,** 292–296 (2006).
48. Tao, A. R., Huang, J. & Yang, P. Langmuir - Blodgettry of Nanocrystals and Nanowires. *Acc. Chem. Res.* **41,** 1662–1673 (2008).
49. Canpean, V. & Astilean, S. Multifunctional plasmonic sensors on low-cost subwavelength metallic nanoholes arrays. *Lab Chip* **9,** 3574 (2009).
50. Denisyuk, A. I. *et al.* Emission hotspots in complex metal nanostructures. **44,** 8059 (2007).
51. Stiles, P. L., Dieringer, J. A., Shah, N. C. & Duyne, R. P. Van. Surface-Enhanced Raman Spectroscopy. (2008). doi:10.1146/annurev.anchem.1.031207.112814
52. Caldwell, J. D. *et al.* Large-area plasmonic hot-spot arrays: sub-2 nm interparticle separations with plasma-enhanced atomic layer deposition of Ag on periodic arrays of Si nanopillars. *Opt. Express* **19,**

26056 (2011).
53. Kumar, G. V. P. Plasmonic nano-architectures for surface enhanced Raman scattering : a review. doi:10.1117/1.JNP.6.064503
54. Hao, E. & Schatz, G. C. Electromagnetic fields around silver nanoparticles and dimers. **120,** 357–366 (2004).
55. Kim, H. C. & Cheng, X. SERS-active substrate based on gap surface plasmon polaritons. **17,** 17234–17241 (2009).
56. Wang, Z., Pan, S., Krauss, T. D., Du, H. & Rothberg, L. J. The structural basis for giant enhancement enabling single-molecule Raman scattering. **2003,** 1–6 (2003).
57. Ye, J. *et al.* Plasmonic nanoclusters: Near field properties of the Fano resonance interrogated with SERS. *Nano Lett.* **12,** 1660–1667 (2012).
58. Sahoo, G. P. *et al.* Colloids and Surfaces A : Physicochemical and Engineering Aspects Synthesis and photo physical properties of star shaped gold nanoparticles. *Colloids Surfaces A Physicochem. Eng. Asp.* **375,** 30–34 (2011).
59. Liao, P. F. & Wokaun, A. Lightning rod effect in surface enhanced Raman scattering. *J. Chem. Phys.* **751,** 1980–1982 (2013).
60. Gartia, M. R. *et al.* Rigorous surface enhanced Raman spectral characterization of large-area high-uniformity silver-coated tapered silica nanopillar arrays. **395701,** (2010).
61. Tan, E., Û, Ó. & À, L. G. Single-molecule surface-enhanced Raman scattering of R6G in aqueous environment under non-resonance conditions. **9,** 8–11 (2011).
62. Itoh, T. & Ozaki, Y. Detailed analysis of single-molecule surface-enhanced resonance Raman scattering spectra of Rhodamine 6G obtained from isolated nano-aggregates of colloidal silver ˘ si. 593–599 (2005). doi:10.1002/jrs.1329
63. Cho, D. J., Wang, F., Zhang, X. & Shen, Y. R. Contribution of the electric quadrupole resonance in optical metamaterials. 1–4 (2008). doi:10.1103/PhysRevB.78.121101
64. Norrod, K. L., Sudnik, L. E. O. M., Rousell, D., Rowlen, K. L. & Ag, T. Quantitative Comparison of Five SERS Substrates : Sensitivity and Limit of Detection. **51,** 994–1001 (1997).
65. Haynes, C. L., Yonzon, C. R., Zhang, X. & Duyne, R. P. Van. Surface-enhanced Raman sensors : early history and the development of sensors for quantitative biowarfare agent and Glucose detection. 471–484 (2005). doi:10.1002/jrs.1376
66. Fang, C., Agarwal, A., Ji, H., Karen, W. Y. & Yobas, L. Preparation of a SERS substrate and its sample-loading method for point-of-use.

405604, (2009).
67. Smorodin, T., Beierlein, U. & Kotthaus, P. Contacting gold nanoparticles with carbon nanotubes by self-assembly. **16,** 1123–1125 (2005).
68. Das, G. *et al.* Biosensors and Bioelectronics Nano-patterned SERS substrate : Application for protein analysis vs . temperature. **24,** 1693–1699 (2009).
69. Allaf, S. M. Optimizing the Direct Fabrication of Nanoparticles for Cancer Diagnostics. 4–5 (2008).
70. Ahamad, N. & Ianoul, A. Using Phospholipids To Control Interparticle Distance in SERS-Active Substrates. 3587–3594 (2011).
71. Enoch, S. & Quidant, R. Optical sensing based on plasmon coupling in nanoparticle arrays. **12,** 3422–3427 (2004).
72. Gopinath, A., Boriskina, S. V, Reinhard, B. M. & Negro, L. D. Deterministic aperiodic arrays of metal nanoparticles for surface-enhanced Raman scattering (SERS). **17,** 1102–1106 (2009).
73. Fang, J. *et al.* Gold Mesostructures with Tailored Surface Topography and Their Self-Assembly Arrays for Surface-Enhanced Raman Spectroscopy. 5006–5013 (2010). doi:10.1021/nl103161q
74. Yan, B., Thubagere, A., Premasiri, W. R., Ziegler, L. D. & Negro, D. Engineered SERS Substrates with Multiscale Signal Enhancement : Nanoparticle Cluster Arrays. **3,**
75. Javey, A., Qi, P., Wang, Q. & Dai, H. Ten- to 50-nm-long quasi-ballistic carbon nanotube devices obtained without complex lithography. **2004,** 4–6 (2004).
76. Jung, Y. M., Ahn, S. J., Kim, E. R. & Lee, H. Gold Nanoparticle Assemblies on a Functionalized Surface Patterned by AFM Lithography. **40,** 712–715 (2002).
77. Haynes, C. L., Haes, A. J. & Duyne, R. P. Van. Nanosphere Lithography: Synthesis and Application of Nanoparticles with Inherently Anisotropic Structures and Surface Chemistry Christy L. Haynes, Amanda J. Haes, and Richard P. Van Duyne.
78. Liu, G. L. & Lee, L. P. Nanowell surface enhanced Raman scattering arrays fabricated by soft-lithography for label-free biomolecular detections in integrated microfluidics. 1–3 (2005). doi:10.1063/1.2031935
79. Polavarapu, L., Porta, A. La, Novikov, S. M., Coronado-Puchau, M. & Liz-Marzán, L. M. Pen-on-Paper Approach Toward the Design of Universal Surface Enhanced Raman Scattering Substrates. *Small* **10,** 3065–3071 (2014).

80. Mu, C., Zhang, J. & Xu, D. Au nanoparticle arrays with tunable particle gaps by template-assisted electroless deposition for high performance surface-enhanced Raman scattering. **21,** 1–6 (2010).
81. Hossain, M. K. & Kitahama, Y. Surface-enhanced Raman scattering : realization of localized surface plasmon resonance using unique substrates and methods. 1747–1760 (2009). doi:10.1007/s00216-009-2762-4
82. Tripp, R. A., Dluhy, R. A. & Zhao, Y. Novel nanostructures for SERS biosensing recent progress in SERS biosensing is given in this article . **3,** 31–37 (2008).
83. Seol, M. *et al.* Multi-layer nanogap array for high-performance SERS substrate. **235303,** (2011).
84. Schatz, G. C., Young, M. A. & Duyne, R. P. Van. Electromagnetic Mechanism of SERS. **46,** 19–46 (2006).
85. Shao, K. & Yao, J. Preparation of silver nanoparticles via a non-template method. **60,** 3826–3829 (2006).
86. Fang, Y., Ren, Y. & Jiang, M. Co-effect of soft template and microwave irradiation on morphological control of gold nanobranches. 1769–1776 (2011). doi:10.1007/s00396-011-2493-x
87. Yang, L., Bao, Z. & Liu, J. Clean and reproducible SERS substrates for high sensitive detection by solid phase synthesis and fabrication of Ag-coated Fe 3 O 4 microspheres. 848–856 (2012). doi:10.1002/jrs.3106
88. Caswell, K. K. *et al.* Seedless , Surfactantless Wet Chemical Synthesis of Silver Nanowires. **35,** 3–5 (2003).
89. Dietrich, H. R. C. *et al.* Tethered particle motion mediated by scattering from gold nanoparticles and darkfield microscopy. **3,** 1–17 (2009).
90. Siekkinen, A. R., Mclellan, J. M., Chen, J. & Xia, Y. Rapid synthesis of small silver nanocubes by mediating polyol reduction with a trace amount of sodium sulfide or sodium hydrosulfide. **432,** 491–496 (2006).
91. Malvadkar, N., Kao, P., Wang, H., Allara, D. L. & Demirel, M. C. A SERS Substrate for Detection of.
92. Suk, Y., Aram, H. Æ. & David, J. C. Æ. Surface enhanced Raman spectroscopy and its application to molecular and cellular analysis. 285–297 (2009). doi:10.1007/s10404-008-0392-3
93. Potara, M., Baia, M., Farcau, C. & Astilean, S. Chitosan-coated anisotropic silver nanoparticles as a SERS substrate for single-molecule detection. **055501,** (2012).

94. Schatz, G. C. Using theory and computation to model nanoscale properties. (2007).
95. Katz, E. & Willner, I. Integrated Nanoparticle – Biomolecule Hybrid Systems : Synthesis , Properties , and Applications Angewandte. 6042–6108 (2004). doi:10.1002/anie.200400651
96. Cem, M. S. U. Surface Enhanced Raman Spectroscopy Christine J Hicks. (2001).
97. Therrien, J., Dindar, A. & Smith, D. AFM Studies of Nanoparticle Deposition via Electrospray Ionization. **533,** 530–533 (2007).
98. Nanowire, S. *et al.* Scalable Coating and Properties of. **XXX,** (2010).
99. Lin, X., Cui, Y., Xu, Y. & Ren, B. Surface-enhanced Raman spectroscopy : substrate-related issues. 1729–1745 (2009). doi:10.1007/s00216-009-2761-5
100. Schreiber, F. Structure and growth of self-assembling monolayers. **65,** (2000).
101. Technology, N. I. L. Surface Enhanced Raman Spectroscopy. 1–3 (2009).
102. Zeng, J. *et al.* Preparation and SERS study of triangular silver nanoparticle self-assembled films. 1673–1678 (2008). doi:10.1002/jrs
103. Kudelski, A., Michota, A. & Bukowska, J. SERS studies on the structure of thioglycolic acid monolayers on silver and gold. **535,** 227–232 (2003).
104. Kuncicky, D. M., Prevo, B. G. & Velev, O. D. Controlled assembly of SERS substrates templated by colloidal crystal films. 1207–1211 (2006). doi:10.1039/b512734c
105. Hasan, W., Lee, J., Henzie, J. & Odom, T. W. Selective Functionalization and Spectral Identification of Gold Nanopyramids. (2007).
106. Gonc, C., Martins, A. & Gama, F. M. Self-Assembled Nanoparticles of Dextrin Substituted with Hexadecanethiol. 392–398 (2007).
107. Viitala, T. Insoluble Monolayers : Preparation , Basic concepts in Langmuir and Langmuir-Blodgett technology Compression isotherm Compression isotherm.
108. Yang, P. & Kim, F. Langmuir-Blodgett assembly of one-dimensional nanostructures. *Chemphyschem* **3,** 503–506 (2002).
109. Reuter, S., Hofmann, A. M., Busse, K., Frey, H. & Kressler, J. Langmuir and Langmuir-Blodgett Films. *Society* **27,** 1978–89 (2011).
110. Acoustics, Q. & Langmuir-blodgett, T. LANGMUIR-BLODGETT LAYER AS CHEMOSENSITIVE ELEMENT. **27,** (2006).
111. Germer, L. H. & Storks, K. H. The Structure of Langmuir-Blodgett

Films of Stearic Acid. *Proc. Natl. Acad. …* **23,** 390–397 (1937).
112. Badia, A. Film Assemblies Molecular Self-Assembly and Supramolecular. *Презентация* 1–37 (2009).
113. Bernard, S. *et al.* Study of Langmuir-Blodgett phospholipidic films deposited on surface enhanced Raman scattering active gold nanoparticle monolayers. *Biopolym. - Biospectroscopy Sect.* **67,** 314–318 (2002).
114. Lin, Y., Liao, J. & Ju, Y. Focused ion beam-fabricated Au micro / nanostructures used as a surface enhanced Raman scattering-active substrate for trace detection of molecules. **185308,** (2011).
115. Goulet, P. J. G., Pieczonka, N. P. W. & Aroca, R. F. Mapping single-molecule SERRS from Langmuir – Blodgett monolayers on nanostructured silver island films. 574–580 (2005). doi:10.1002/jrs.1330
116. Cao, Y. *et al.* A technique for controlling the alignment of silver nanowires with an electric field. **17,** 2378–2380 (2006).
117. Jiang, S. Surface Enhanced Raman Scattering Spectroscopy. **4,** 1–16
118. Cho, W. J., Kim, Y. & Kim, J. K. Ultrahigh-Density Array of Silver Nanoclusters for SERS Substrate with High Sensitivity and Excellent Reproducibility. 249–255 (2012).
119. Aroca, R. Surface-Enhanced Resonance Raman Scattering and the Spectra of the Single Molecule. (2004).
120. Surovtsev, N. V, Adichtchev, S. V, Duda, T. A., Pokrovsky, L. D. & Sveshnikova, L. L. New Surface-Enhanced Raman Scattering Active Substrate Fabricated by Use of the Langmuir - Blodgett Technique. **3,** 4803–4807 (2010).
121. Genson, K. L. *et al.* Langmuir − Blodgett Monolayers of Gold Nanoparticles with Amphiphilic Shells from V-Shaped Binary Polymer Arms Langmuir-Blodgett Monolayers of Gold Nanoparticles with Amphiphilic Shells from V-Shaped Binary Polymer Arms. 7011–7015 (2006). doi:10.1021/la061163p
122. Dai, S., Zhang, X., Du, Z., Huang, Y. & Dang, H. Structural properties and Raman spectroscopy of lipid Langmuir monolayers at the air-water interface. *Colloids Surfaces B Biointerfaces* **42,** 21–28 (2005).
123. Liu, H. *et al.* Single molecule detection from a large-scale SERS-active Au 79 Ag 21 substrate. 1–5 (2011). doi:10.1038/srep00112
124. Qin, L. *et al.* Designing , fabricating , and imaging Raman hot spots. (2006).
125. Camden, J. P. *et al.* Probing the Structure of Single-Molecule Surface-Enhanced Raman Scattering Hot Spots Probing the Structure of

Single-Molecule Surface-Enhanced Raman. 1–3 (2008). doi:10.1021/ja8051427
126. Jackson, J. B. & Halas, N. J. Surface-enhanced Raman scattering on tunable plasmonic nanoparticle substrates. (2004).
127. Majimel, J., Bordeaux, U. & Schweitzer, A. Synthesis of nanoparticles. 195–207 (2008).
128. Vo-dinh, T. *et al.* Plasmonic Nanoparticles and Nanowires : Design , Fabrication and Application in Sensing †. 7480–7488 (2010).
129. Li, M., Zhang, Z. S., Zhang, X., Li, K. Y. & Yu, X. F. Optical properties of Au / Ag core / shell nanoshuttles. **16,** 2154–2157 (2008).
130. Rycenga, M. *et al.* Generation of Hot Spots with Silver Nanocubes for Single-Molecule Detection by Surface-Enhanced Raman Scattering **. 5473–5477 (2011). doi:10.1002/anie.201101632
131. Li, M., Cushing, S. K., Zhang, J. & Lankford, J. Shape-dependent surface-enhanced Raman scattering in gold – Raman- probe – silica sandwiched nanoparticles for biocompatible applications. **115501,** (2012).
132. Stiles, P. L., Dieringer, J. A., Shah, N. C. & Duyne, R. P. Van. Surface-Enhanced Raman Spectroscopy. 601–626 (2008). doi:10.1146/annurev.anchem.1.031207.112814
133. Smith, D. R. & Schultz, S. Plasmon resonances of silver nanowires with a nonregular cross section ¨. **64,** 1–10 (2001).
134. Khoury, C. G., Vo-dinh, T., V, D. U. & Carolina, N. Gold Nanostars For Surface-Enhanced Raman Scattering : Synthesis , Characterization and Optimization. 18849–18859 (2008).
135. Lu, Y., Liu, G. L. & Lee, L. P. High-Density Silver Nanoparticle Film with Temperature-Controllable Interparticle Spacing for a Tunable Surface Enhanced Raman Scattering Substrate. *Nano Lett.* **5,** 5–9 (2004).
136. Adato, R. *et al.* Ultra-sensitive vibrational spectroscopy of protein monolayers with plasmonic nanoantenna arrays. **106,** (2009).
137. Di, M. S. & Berkeley, L. LETTERS L a ngmu i r − B l odg e tt S ilve r N a now i r e Mono laye r s for Mo lec u la r S e n si ng U si ng Surf ace - E nh a n ce d R a m a n Sp ec tro sc op y. (2003).
138. Radziuk, D. & Moehwald, H. Highly effective hot spots for SERS signatures of live fibroblasts. *Nanoscale* **6,** 6115–26 (2014).
139. Smet, L. C. P. M. De. *Covalently Bound Organic Monolayers on Silicon Surfaces*. (2006).
140. Qin, G. & Cai, C. Oligo(ethylene glycol)-terminated monolayers on silicon surfaces and their nanopatterning with a conductive atomic

force microscope. *Sci. China Chem.* **53,** 36–44 (2010).
141. Tobergte, D. R. & Curtis, S. CHARACTERIZATION, FUNCTIONALIZATION AND APPLICATIONS OF ALKYL MONOLAYERS ON SILICON SURFACES. *J. Chem. Inf. Model.* **53,** 1689–1699 (2013).
142. Kokkoli, E. & Zukoski, C. Interaction Forces between Hydrophobic and Hydrophilic Self-Assembled Monolayers. *J. Colloid Interface Sci.* **230,** 176–180 (2000).
143. Zhao, Q., Qiu, Ã. J., Zhao, C., Hou, L. & Zhu, C. Synthesis and Formation Mechanism of Silver Nanowires by a Templateless and Seedless Method. **34,** 1–2 (2005).
144. Singh, P., Thuy, N. T. B., Aoki, Y., Mott, D. & Maenosono, S. Intensification of surface enhanced Raman scattering of thiol-containing molecules using Ag @ Au core @ shell nanoparticles. **094301,** 1–7 (2011).
145. Wang, J., Neogi, P. & Forciniti, D. On one-dimensional self-assembly of surfactant-coated nanoparticles. 1–6 (2006). doi:10.1063/1.2375091
146. MCGOVERN, M. E. & THOMPSON, M. Self-assembled silanes and the thiol functionalization of surfaces. *Anal. Commun.* **35,** 391–393 (1998).
147. Yuan, H., Khoury, C. G. & Hwang, H. Gold nanostars : surfactant-free synthesis , 3D modelling , and two-photon photoluminescence imaging. **075102,** (2012).
148. Kah, J. C. Y. Synthesis of gold nanoshells based on the deposition-precipitation process. 23–36 (2008).
149. Tang, J. *et al.* Sensitive enzymatic Glucose detection by TiO_2 nanowire photoelectrochemical biosensors. *J. Mater. Chem. A* **2,** 6153–6157 (2014).
150. Martin, M. N., Basham, J. I., Chando, P. & Eah, S. Charged Gold Nanoparticles in Non-Polar Solvents : 10-min Synthesis and. **26,** 7410–7417 (2010).
151. Radhakumary, C. & Sreenivasan, K. Naked Eye Detection of Glucose in Urine Using Glucose Oxidase Immobilized Gold Nanoparticles. *Anal. Chem.* **83,** 2829–2833 (2011).
152. Jr, D. D. E. & Chumanov, G. Synthesis and Optical Properties of Silver Nanoparticles and Arrays. **29634,** 1221–1231 (2005).
153. Chalmers, J. M. & Mackenzie, M. W. FT-IR Spectroscopy in an Industrial Laboratory*. *Appl. Spectrosc.* **38,** 763–773 (1984).
154. Camino, F. E. *et al.* transparent electrical contacts for organic transform methods. *J. Mod. Opt.* **61:21,** 1735–1742 (2014).

155. Ko, H., Singamaneni, S. & Tsukruk, V. V. Nanostructured surfaces and assemblies as SERS media. *Small* **4,** 1576–1599 (2008).
156. Pérez-mayen, L., Oliva, J. & Torres-castro, A. SERS substrates fabricated with star-like gold nanoparticles for zeptomole detection of analytes. *Nanoscale* **7,** 10249–10258 (2015).
157. Ayenimo, J. G. & Adeloju, S. B. Improved potentiometric Glucose detection with ultra-thin polypyrrole-Glucose oxidase films. *Anal. Methods* **6,** 8996–9006 (2014).
158. Freckmann, G. *et al.* Continuous Glucose profiles in healthy subjects under everyday life conditions and after different meals. *J. diabetes Sci. Technol.* **1,** 695–703 (2007).
159. Benjamin, E. M. Self-Monitoring of Blood Glucose: The Basics. *Clin. Diabetes* **20,** 45–47 (2002).
160. Diabetes, D. O. F. Diagnosis and Classification of Diabetes Mellitus. *Diabetes Care* **31,** S55–S60 (2008).
161. Kottmann, J., Grob, U., Rey, J. & Sigrist, M. Mid-Infrared Fiber-Coupled Photoacoustic Sensor for Biomedical Applications. *Sensors* **13,** 535–549 (2013).
162. Yang, X. *et al.* Direct molecule-specific Glucose detection by Raman spectroscopy based on photonic crystal fiber. *Anal. Bioanal. Chem.* **402,** 687–691 (2012).
163. Shao, J. *et al.* In Vivo Blood Glucose Quantification Using Raman Spectroscopy. *PLoS One* **7,** e48127, 1–10 (2012).
164. Soderholm, S., Roos, Y. H., Meinander, N. & Hotokka, M. Raman spectra of fructose and Glucose in the amorphous and crystalline states. *J. Raman Spectrosc.* **30,** 1009–1018 (1999).
165. Cocinero, E. J., Carcabal, P., Vaden, T. D., Simons, J. P. & Davis, B. G. Sensing the anomeric effect in a solvent-free environment. *Nature* **469,** 76–79 (2011).
166. Roohk, H. V. & Zaidi, A. R. A Review of Glycated Albumin as an Intermediate Glycation Index for Controlling Diabetes. *J. diabetes Sci. Technol.* **2,** 1114–1121 (2008).
167. Zhang, Q. *et al.* NIH Public Access. *J. Proteome Res.* **10,** 3076–3088 (2011).
168. Grdadolnik, J. & Maréchal, Y. Bovine serum albumin observed by infrared spectrometry. I. Methodology, structural investigation, and water uptake. *Biopolymers* **62,** 40–53 (2001).
169. Murayama, K. & Tomida, M. Heat-induced secondary structure and conformation change of bovine serum albumin investigated by Fourier transform infrared spectroscopy. *Biochemistry* **43,** 11526–11532

(2004).
170. Baggio, L. L., Huang, Q., Brown, T. J. & Drucker, D. J. Peptidergic Activation of GLP-1 Receptor – Dependent. *Diabetes* **53,** 2492–2500 (2004).
171. Gonçalves, M. R., Enderle, F. & Marti, O. Surface-enhanced Raman spectroscopy of dye and thiol molecules adsorbed on triangular silver nanostructures: A study of near-field enhancement, localization of hot-spots, and passivation of adsorbed carbonaceous species. *J. Nanotechnol.* **2012,** (2012).
172. Note, T. Application of Raman Spectroscopy and Surface-Enhanced Raman Scattering to the Analysis of Synthetic Dyes Found in Ballpoint Pen Inks *. **54,** 947–952 (2009).
173. Us, C. A., Plante, P. J. & Llp, F. *SENSOR FOR IN VITRO DETERMINATION*. **2,** (2012).
174. Perez-mayen, L., Oliva, J., Salas, P. & Rosa, E. De. Nanomolar detection of Glucose using SERS substrates fabricated with albumin coated. 11862–11869 (2016). doi:10.1039/c6nr00163g

A n n e x e s

A.1 scientific publications made during the thesis project

“Nanomolar detection of Glucose using SERS substrates fabricated with albumin coated gold nanoparticles”; *Nanoscale* IF 7.76 Leonardo Perez-Mayen, Jorge Oliva, P. Salas and Elder De la Rosa**,** 2016, 8, 11862–11869.

“SERS substrates fabricated with star-like gold nanoparticles for zeptomole detection of analytes”; *Nanoscale* IF 7.76, Leonardo Pérez-Mayen, Jorge Oliva, Alejandro Torres-Castro and Elder De la Rosa, 2015, 7, 10249–10258.

“SERS and integrative imaging upon internalization of quantum dots into human oral epithelial cells”; *Biophotonics* IF 4.44, Elisa Cepeda-Pérez, Tzarara López Luke, Germán Plascencia Villa, Leonardo Perez-Mayen, Andrea Ceja Fdez, Arturo Ponce, Juan Vivero Escoto, and Elder de la Rosa, 2016 1–11.

“Effect of TEA on the blue emission of ZnO quantum dots with high quantum yield”;***Optical Materials Express*** **IF 2.65,** Jorge Oliva , Luis Diaz-Torres , Alejandro Torres-Castro , Pedro Salas , Leonardo Perez-Mayen and Elder De la Rosa, 1110.

“Tunable white light from photo and electroluminescence of ZnO nanoparticles”*; J. Phys. D*: *Appl. Phys* IF 2.77, Jorge Oliva, Leonardo Perez Mayen, Alejandro Torres Castro, Luis A. Diaz Torres, Pedro Salas, and Elder De la Rosa Cruz, 015104,6pp.

A.2 Enhancement factor (EF) example error calculation.

For the Enhancement error was use the next formula, applied to the each data base.

$$error = \frac{value - average\ value}{average\ value} x100$$

Applied to each set, the maximum value and the minimum value are not taking in count, the average is obtained by 8 values that remain, this calculus give an error of ±12.45% for the EF between sets of samples using the same solution of rodhamine B (1x10-^{14} M).

For samples using glucose the error was ±20.9% using the same solution of glucose (1x10-^{9} M).

EF Samples made with RB 1x10^{-14} M (same solution)										
25mN set 1	25mN set 2	25mN set 3	25mN set 4	25mN set 5	25mN set 6	25mN set 7	25mN set 8	25mN set 9	25mN set 10	
4,05E+11	1,62E+12	1,90E+12	2,05E+12	1,86E+12	6,68E+11	4,26E+11	7,95E+11	3,07E+12	6,05E+12	1
4,08E+11	1,67E+12	1,90E+12	2,06E+12	1,97E+12	6,69E+11	4,49E+11	8,01E+11	3,27E+12	6,05E+12	2
4,12E+11	1,75E+12	1,91E+12	2,08E+12	1,98E+12	6,92E+11	4,69E+11	8,23E+11	3,34E+12	6,09E+12	3
4,17E+11	1,77E+12	1,93E+12	2,09E+12	2,02E+12	7,56E+11	4,82E+11	8,64E+11	3,35E+12	6,10E+12	4
4,19E+11	1,84E+12	1,94E+12	2,09E+12	2,03E+12	7,61E+11	5,44E+11	8,75E+11	3,38E+12	6,11E+12	5
4,33E+11	1,91E+12	1,94E+12	2,09E+12	2,04E+12	8,78E+11	5,71E+11	9,39E+11	3,39E+12	6,14E+12	6

4,35E+11	1,95E+12	1,94E+12	2,10E+12	2,10E+12	9,66E+11	6,38E+11	9,74E+11	3,45E+12	6,20E+12	7
4,61E+11	1,95E+12	1,95E+12	2,12E+12	2,11E+12	1,00E+12	6,92E+11	1,02E+12	3,46E+12	6,22E+12	8
4,63E+11	1,96E+12	1,96E+12	2,12E+12	2,11E+12	1,16E+12	8,03E+11	1,14E+12	3,49E+12	6,25E+12	9
4,85E+11	1,96E+12	1,98E+12	2,13E+12	2,13E+12	1,21E+12	8,60E+11	1,16E+12	3,54E+12	6,29E+12	10
4,93E+11	1,98E+12	1,99E+12	2,13E+12	2,14E+12	1,35E+12	9,80E+11	1,28E+12	3,58E+12	6,32E+12	11
4,95E+11	2,02E+12	1,99E+12	2,13E+12	2,15E+12	1,37E+12	1,00E+12	1,30E+12	3,59E+12	6,35E+12	12
5,12E+11	2,03E+12	2,00E+12	2,13E+12	2,16E+12	1,57E+12	1,14E+12	1,37E+12	3,63E+12	6,37E+12	13
5,45E+11	2,05E+12	2,01E+12	2,14E+12	2,16E+12	1,61E+12	1,17E+12	1,39E+12	3,63E+12	6,64E+12	14
5,59E+11	2,08E+12	2,02E+12	2,15E+12	2,19E+12	1,70E+12	1,29E+12	1,41E+12	3,66E+12	6,64E+12	15
5,81E+11	2,08E+12	2,02E+12	2,16E+12	2,19E+12	1,72E+12	1,32E+12	1,42E+12	3,68E+12	6,64E+12	16
5,84E+11	2,08E+12	2,02E+12	2,16E+12	2,21E+12	1,76E+12	1,36E+12	1,42E+12	3,68E+12	6,67E+12	17
5,98E+11	2,09E+12	2,02E+12	2,17E+12	2,22E+12	1,76E+12	1,45E+12	1,45E+12	3,69E+12	6,68E+12	18
6,02E+11	2,09E+12	2,04E+12	2,18E+12	2,24E+12	1,77E+12	1,52E+12	1,45E+12	3,71E+12	6,72E+12	19
6,09E+11	2,09E+12	2,04E+12	2,18E+12	2,24E+12	1,84E+12	1,55E+12	1,45E+12	3,74E+12	6,74E+12	20
6,10E+11	2,09E+12	2,04E+12	2,18E+12	2,24E+12	1,91E+12	1,56E+12	1,46E+12	3,79E+12	6,75E+12	21
6,15E+11	2,10E+12	2,05E+12	2,19E+12	2,26E+12	1,91E+12	1,59E+12	1,50E+12	3,86E+12	6,78E+12	22
6,15E+11	2,10E+12	2,06E+12	2,19E+12	2,27E+12	1,91E+12	1,61E+12	1,52E+12	3,86E+12	6,78E+12	23
6,16E+11	2,10E+12	2,07E+12	2,20E+12	2,27E+12	1,92E+12	1,65E+12	1,54E+12	3,87E+12	6,79E+12	24
6,18E+11	2,10E+12	2,08E+12	2,20E+12	2,28E+12	1,94E+12	1,66E+12	1,54E+12	3,87E+12	6,80E+12	25
6,20E+11	2,10E+12	2,09E+12	2,21E+12	2,31E+12	1,95E+12	1,67E+12	1,58E+12	3,89E+12	6,80E+12	26
6,22E+11	2,10E+12	2,09E+12	2,22E+12	2,32E+12	1,95E+12	1,69E+12	1,61E+12	3,93E+12	6,82E+12	27
6,25E+11	2,11E+12	2,09E+12	2,23E+12	2,33E+12	2,00E+12	1,69E+12	1,62E+12	3,96E+12	6,84E+12	28
6,26E+11	2,12E+12	2,10E+12	2,23E+12	2,33E+12	2,01E+12	1,72E+12	1,68E+12	4,00E+12	6,87E+12	29
6,30E+11	2,12E+12	2,10E+12	2,23E+12	2,33E+12	2,01E+12	1,72E+12	1,69E+12	4,00E+12	6,92E+12	30
6,52E+11	2,12E+12	2,11E+12	2,23E+12	2,34E+12	2,02E+12	1,72E+12	1,71E+12	4,01E+12	6,95E+12	31
6,68E+11	2,13E+12	2,11E+12	2,24E+12	2,34E+12	2,02E+12	1,75E+12	1,74E+12	4,08E+12	6,96E+12	32
6,73E+11	2,13E+12	2,11E+12	2,24E+12	2,34E+12	2,02E+12	1,77E+12	1,74E+12	4,10E+12	6,99E+12	33
6,86E+11	2,14E+12	2,11E+12	2,24E+12	2,34E+12	2,02E+12	1,78E+12	1,76E+12	4,10E+12	7,04E+12	34
7,36E+11	2,14E+12	2,11E+12	2,25E+12	2,36E+12	2,03E+12	1,80E+12	1,77E+12	4,11E+12	7,11E+12	35
7,59E+11	2,15E+12	2,15E+12	2,25E+12	2,37E+12	2,04E+12	1,81E+12	1,82E+12	4,13E+12	7,24E+12	36
7,94E+11	2,15E+12	2,15E+12	2,25E+12	2,37E+12	2,04E+12	1,82E+12	1,82E+12	4,16E+12	7,26E+12	37
8,82E+11	2,15E+12	2,15E+12	2,26E+12	2,38E+12	2,05E+12	1,86E+12	1,84E+12	4,17E+12	7,27E+12	38
9,16E+11	2,16E+12	2,16E+12	2,26E+12	2,39E+12	2,06E+12	1,87E+12	1,84E+12	4,17E+12	7,29E+12	39
9,77E+11	2,17E+12	2,16E+12	2,27E+12	2,39E+12	2,06E+12	1,88E+12	1,86E+12	4,18E+12	7,32E+12	40
1,01E+12	2,17E+12	2,16E+12	2,27E+12	2,39E+12	2,07E+12	1,89E+12	1,87E+12	4,22E+12	7,34E+12	41
1,01E+12	2,20E+12	2,17E+12	2,27E+12	2,39E+12	2,09E+12	1,90E+12	1,87E+12	4,22E+12	7,35E+12	42
1,02E+12	2,20E+12	2,20E+12	2,28E+12	2,40E+12	2,09E+12	1,91E+12	1,87E+12	4,22E+12	7,36E+12	43
1,03E+12	2,21E+12	2,20E+12	2,28E+12	2,40E+12	2,10E+12	1,94E+12	1,88E+12	4,23E+12	7,52E+12	44

d

1,06E+12	2,22E+12	2,21E+12	2,28E+12	2,40E+12	2,11E+12	1,94E+12	1,90E+12	4,23E+12	7,65E+12	45
1,07E+12	2,23E+12	2,21E+12	2,28E+12	2,40E+12	2,11E+12	1,95E+12	1,92E+12	4,26E+12	7,69E+12	46
1,10E+12	2,23E+12	2,21E+12	2,29E+12	2,41E+12	2,12E+12	1,99E+12	1,93E+12	4,31E+12	7,72E+12	47
1,10E+12	2,24E+12	2,22E+12	2,29E+12	2,41E+12	2,13E+12	2,00E+12	1,94E+12	4,34E+12	7,81E+12	48
1,12E+12	2,24E+12	2,23E+12	2,31E+12	2,42E+12	2,14E+12	2,01E+12	1,94E+12	4,34E+12	7,84E+12	49
1,12E+12	2,24E+12	2,24E+12	2,31E+12	2,42E+12	2,16E+12	2,02E+12	1,97E+12	4,37E+12	7,87E+12	50
1,16E+12	2,25E+12	2,24E+12	2,31E+12	2,43E+12	2,16E+12	2,02E+12	1,99E+12	4,38E+12	7,98E+12	51
1,17E+12	2,25E+12	2,24E+12	2,31E+12	2,43E+12	2,16E+12	2,02E+12	2,01E+12	4,43E+12	8,00E+12	52
1,20E+12	2,25E+12	2,25E+12	2,31E+12	2,44E+12	2,17E+12	2,03E+12	2,01E+12	4,43E+12	8,03E+12	53
1,20E+12	2,25E+12	2,26E+12	2,32E+12	2,45E+12	2,18E+12	2,03E+12	2,02E+12	4,43E+12	8,11E+12	54
1,21E+12	2,26E+12	2,26E+12	2,33E+12	2,46E+12	2,19E+12	2,05E+12	2,04E+12	4,50E+12	8,15E+12	55
1,24E+12	2,26E+12	2,26E+12	2,33E+12	2,47E+12	2,24E+12	2,05E+12	2,04E+12	4,55E+12	8,15E+12	56
1,24E+12	2,26E+12	2,26E+12	2,33E+12	2,47E+12	2,27E+12	2,10E+12	2,05E+12	4,75E+12	8,19E+12	57
1,25E+12	2,27E+12	2,28E+12	2,34E+12	2,47E+12	2,29E+12	2,11E+12	2,06E+12	4,75E+12	8,29E+12	58
1,25E+12	2,27E+12	2,28E+12	2,34E+12	2,48E+12	2,30E+12	2,11E+12	2,06E+12	4,76E+12	8,32E+12	59
1,27E+12	2,28E+12	2,28E+12	2,34E+12	2,48E+12	2,30E+12	2,12E+12	2,08E+12	4,82E+12	8,32E+12	60
1,28E+12	2,28E+12	2,29E+12	2,34E+12	2,49E+12	2,31E+12	2,13E+12	2,09E+12	4,85E+12	8,36E+12	61
1,29E+12	2,29E+12	2,29E+12	2,35E+12	2,49E+12	2,33E+12	2,14E+12	2,11E+12	4,85E+12	8,39E+12	62
1,32E+12	2,30E+12	2,30E+12	2,35E+12	2,49E+12	2,33E+12	2,15E+12	2,12E+12	4,85E+12	8,41E+12	63
1,32E+12	2,31E+12	2,31E+12	2,35E+12	2,50E+12	2,35E+12	2,15E+12	2,13E+12	4,88E+12	8,46E+12	64
1,33E+12	2,32E+12	2,31E+12	2,37E+12	2,50E+12	2,36E+12	2,15E+12	2,13E+12	4,90E+12	8,49E+12	65
1,33E+12	2,32E+12	2,32E+12	2,37E+12	2,50E+12	2,36E+12	2,16E+12	2,13E+12	4,90E+12	8,55E+12	66
1,38E+12	2,32E+12	2,32E+12	2,38E+12	2,51E+12	2,37E+12	2,16E+12	2,20E+12	4,93E+12	8,57E+12	67
1,40E+12	2,32E+12	2,33E+12	2,38E+12	2,51E+12	2,38E+12	2,16E+12	2,21E+12	4,97E+12	8,59E+12	68
1,40E+12	2,32E+12	2,36E+12	2,38E+12	2,51E+12	2,39E+12	2,17E+12	2,22E+12	4,97E+12	8,66E+12	69
1,44E+12	2,33E+12	2,36E+12	2,38E+12	2,51E+12	2,39E+12	2,18E+12	2,23E+12	5,04E+12	8,67E+12	70
1,46E+12	2,33E+12	2,36E+12	2,38E+12	2,52E+12	2,40E+12	2,18E+12	2,24E+12	5,13E+12	8,81E+12	71
1,47E+12	2,33E+12	2,37E+12	2,39E+12	2,52E+12	2,41E+12	2,18E+12	2,24E+12	5,17E+12	8,90E+12	72
1,47E+12	2,34E+12	2,40E+12	2,41E+12	2,53E+12	2,42E+12	2,19E+12	2,24E+12	5,20E+12	8,94E+12	73
1,47E+12	2,34E+12	2,40E+12	2,41E+12	2,54E+12	2,42E+12	2,19E+12	2,25E+12	5,20E+12	8,96E+12	74
1,47E+12	2,36E+12	2,41E+12	2,43E+12	2,54E+12	2,42E+12	2,19E+12	2,27E+12	5,21E+12	9,12E+12	75
1,48E+12	2,36E+12	2,46E+12	2,44E+12	2,54E+12	2,43E+12	2,19E+12	2,31E+12	5,25E+12	9,13E+12	76
1,49E+12	2,37E+12	2,46E+12	2,46E+12	2,55E+12	2,43E+12	2,19E+12	2,31E+12	5,27E+12	9,15E+12	77
1,49E+12	2,37E+12	2,46E+12	2,47E+12	2,56E+12	2,43E+12	2,20E+12	2,32E+12	5,28E+12	9,19E+12	78
1,50E+12	2,41E+12	2,46E+12	2,49E+12	2,56E+12	2,44E+12	2,20E+12	2,32E+12	5,30E+12	9,19E+12	79
1,50E+12	2,43E+12	2,50E+12	2,49E+12	2,57E+12	2,45E+12	2,21E+12	2,32E+12	5,36E+12	9,23E+12	80
1,50E+12	2,52E+12	2,56E+12	2,54E+12	2,57E+12	2,45E+12	2,21E+12	2,34E+12	5,37E+12	9,25E+12	81
1,51E+12	2,53E+12	2,69E+12	2,55E+12	2,59E+12	2,46E+12	2,21E+12	2,40E+12	5,42E+12	9,29E+12	82

1,51E+12	2,56E+12	2,75E+12	2,56E+12	2,60E+12	2,46E+12	2,22E+12	2,46E+12	5,42E+12	9,36E+12	83
1,52E+12	2,66E+12	2,90E+12	2,63E+12	2,60E+12	2,46E+12	2,23E+12	2,49E+12	5,45E+12	9,38E+12	84
1,52E+12	2,67E+12	2,92E+12	2,64E+12	2,61E+12	2,47E+12	2,24E+12	2,51E+12	5,49E+12	9,46E+12	85
1,52E+12	2,79E+12	3,13E+12	2,64E+12	2,61E+12	2,47E+12	2,25E+12	2,52E+12	5,49E+12	9,49E+12	86
1,52E+12	2,79E+12	3,16E+12	2,70E+12	2,65E+12	2,49E+12	2,27E+12	2,53E+12	5,50E+12	9,50E+12	87
1,53E+12	2,84E+12	3,65E+12	2,70E+12	2,67E+12	2,49E+12	2,29E+12	2,54E+12	5,53E+12	9,58E+12	88
1,53E+12	2,85E+12	3,66E+12	2,75E+12	2,68E+12	2,50E+12	2,29E+12	2,58E+12	5,54E+12	9,65E+12	89
1,53E+12	2,88E+12	4,56E+12	2,78E+12	2,68E+12	2,50E+12	2,30E+12	2,58E+12	5,57E+12	9,69E+12	90
1,54E+12	2,88E+12	4,69E+12	2,79E+12	2,68E+12	2,50E+12	2,30E+12	2,64E+12	5,57E+12	9,74E+12	91
1,54E+12	2,89E+12	6,69E+12	2,81E+12	2,81E+12	2,50E+12	2,33E+12	2,64E+12	5,59E+12	9,76E+12	92
1,55E+12	2,89E+12	7,19E+12	2,88E+12	2,82E+12	2,52E+12	2,33E+12	2,64E+12	5,60E+12	9,78E+12	93
1,56E+12	2,92E+12	1,15E+13	2,90E+12	2,86E+12	2,53E+12	2,33E+12	2,67E+12	5,61E+12	9,88E+12	94
1,57E+12	2,93E+12	1,29E+13	2,90E+12	2,92E+12	2,54E+12	2,34E+12	2,68E+12	5,71E+12	1,00E+13	95
1,58E+12	2,95E+12	1,93E+13	2,95E+12	2,93E+12	2,55E+12	2,37E+12	2,69E+12	5,78E+12	1,01E+13	96
1,59E+12	2,96E+12	2,33E+13	2,96E+12	2,95E+12	2,55E+12	2,41E+12	2,76E+12	5,83E+12	1,03E+13	97
1,60E+12	3,00E+12	2,74E+13	2,97E+12	2,97E+12	2,55E+12	2,43E+12	2,80E+12	5,88E+12	1,03E+13	98
1,60E+12	3,00E+12	2,99E+13	2,98E+12	3,00E+12	2,57E+12	2,45E+12	2,95E+12	5,95E+12	1,03E+13	99
1,64E+12	3,01E+12	1,29E+13	3,03E+12	3,00E+12	2,58E+12	2,48E+12	3,01E+12	6,01E+12	1,04E+13	100

EF of Samples made with glucose $1x10^{-9}$ M (same solution)										
set 1	set 2	set 3	set 4	set 5	set 6	set 7	set 8	set 9	set 10	
3,95E+11	4,32E+11	4,19E+11	5,42E+11	3,20E+11	3,20E+11	3,21E+11	3,21E+11	2,75E+11	3,44E+11	1
4,06E+11	4,32E+11	4,28E+11	5,34E+11	3,20E+11	3,20E+11	3,21E+11	3,21E+11	2,75E+11	3,44E+11	2
4,07E+11	4,32E+11	4,22E+11	5,20E+11	3,20E+11	3,20E+11	3,21E+11	3,21E+11	2,75E+11	3,44E+11	3
3,99E+11	4,32E+11	4,24E+11	5,07E+11	3,20E+11	3,20E+11	3,21E+11	3,21E+11	2,75E+11	3,44E+11	4
4,01E+11	4,32E+11	4,21E+11	4,91E+11	3,20E+11	3,20E+11	3,21E+11	3,21E+11	2,75E+11	3,44E+11	5
4,12E+11	4,32E+11	4,21E+11	4,86E+11	3,20E+11	3,20E+11	3,21E+11	3,21E+11	2,75E+11	3,44E+11	6
3,96E+11	4,32E+11	4,16E+11	4,60E+11	3,20E+11	3,20E+11	3,21E+11	3,21E+11	2,75E+11	3,44E+11	7
4,55E+11	4,32E+11	4,09E+11	4,65E+11	3,20E+11	3,20E+11	3,21E+11	3,21E+11	2,75E+11	3,44E+11	8
4,35E+11	4,32E+11	4,18E+11	4,57E+11	3,20E+11	3,20E+11	3,21E+11	3,21E+11	2,75E+11	3,44E+11	9
3,97E+11	4,32E+11	4,23E+11	4,51E+11	3,20E+11	3,20E+11	3,21E+11	3,21E+11	2,75E+11	3,44E+11	10
3,59E+11	4,32E+11	4,18E+11	4,39E+11	3,20E+11	3,20E+11	3,21E+11	3,21E+11	2,75E+11	3,44E+11	11
3,45E+11	5,51E+11	4,27E+11	4,27E+11	3,20E+11	3,20E+11	3,21E+11	3,21E+11	2,75E+11	3,44E+11	12
3,89E+11	5,75E+11	4,32E+11	4,25E+11	3,20E+11	3,20E+11	3,21E+11	3,21E+11	2,75E+11	3,44E+11	13
4,55E+11	5,89E+11	4,15E+11	4,27E+11	3,20E+11	3,20E+11	3,21E+11	3,21E+11	2,75E+11	3,44E+11	14
4,13E+11	5,97E+11	4,17E+11	4,23E+11	3,20E+11	3,20E+11	3,21E+11	3,21E+11	2,75E+11	3,44E+11	15
4,29E+11	6,08E+11	4,25E+11	4,20E+11	3,20E+11	3,20E+11	3,21E+11	3,21E+11	2,75E+11	3,44E+11	16

4,22E+11	6,16E+11	4,21E+11	4,25E+11	3,20E+11	3,20E+11	3,21E+11	2,34E+11	2,75E+11	3,44E+11	17
3,99E+11	6,23E+11	4,17E+11	4,33E+11	3,20E+11	3,20E+11	3,21E+11	2,25E+11	2,75E+11	3,44E+11	18
4,08E+11	6,24E+11	4,26E+11	4,38E+11	3,20E+11	3,20E+11	3,21E+11	2,15E+11	2,75E+11	3,44E+11	19
4,61E+11	6,32E+11	4,22E+11	4,32E+11	3,20E+11	3,20E+11	3,21E+11	2,13E+11	2,75E+11	3,44E+11	20
4,19E+11	6,34E+11	4,23E+11	4,37E+11	3,20E+11	3,20E+11	3,21E+11	2,20E+11	2,75E+11	3,44E+11	21
4,18E+11	6,35E+11	4,21E+11	4,28E+11	3,20E+11	3,20E+11	3,21E+11	2,26E+11	2,75E+11	3,44E+11	22
4,19E+11	6,29E+11	4,19E+11	4,25E+11	3,20E+11	3,20E+11	3,21E+11	2,35E+11	2,75E+11	3,44E+11	23
4,14E+11	6,18E+11	4,20E+11	4,40E+11	3,20E+11	3,20E+11	3,21E+11	2,48E+11	2,75E+11	3,44E+11	24
4,10E+11	6,18E+11	4,11E+11	4,51E+11	3,20E+11	3,20E+11	3,21E+11	2,62E+11	2,75E+11	3,44E+11	25
4,15E+11	5,98E+11	3,98E+11	4,61E+11	3,20E+11	3,20E+11	3,21E+11	2,75E+11	2,75E+11	3,44E+11	26
4,12E+11	5,91E+11	4,01E+11	4,63E+11	3,20E+11	3,20E+11	3,21E+11	2,78E+11	2,75E+11	3,44E+11	27
4,06E+11	5,72E+11	4,15E+11	4,66E+11	3,20E+11	3,20E+11	3,21E+11	2,95E+11	2,75E+11	3,44E+11	28
4,18E+11	5,70E+11	4,09E+11	4,83E+11	3,20E+11	3,20E+11	3,21E+11	2,98E+11	2,75E+11	3,44E+11	29
4,13E+11	5,55E+11	4,06E+11	4,99E+11	3,20E+11	3,20E+11	3,21E+11	2,88E+11	2,75E+11	3,44E+11	30
4,09E+11	5,29E+11	4,28E+11	5,09E+11	3,20E+11	3,20E+11	3,21E+11	3,14E+11	2,75E+11	3,44E+11	31
4,15E+11	5,10E+11	4,27E+11	5,29E+11	3,20E+11	3,20E+11	3,21E+11	3,03E+11	2,75E+11	3,44E+11	32
4,23E+11	4,96E+11	4,43E+11	5,44E+11	3,20E+11	3,20E+11	3,21E+11	3,07E+11	2,75E+11	3,44E+11	33
4,37E+11	4,93E+11	4,63E+11	5,47E+11	3,20E+11	3,20E+11	3,21E+11	3,10E+11	2,75E+11	3,44E+11	34
4,50E+11	4,81E+11	4,84E+11	5,57E+11	3,20E+11	3,20E+11	3,21E+11	3,06E+11	2,75E+11	3,44E+11	35
4,59E+11	4,74E+11	5,42E+11	5,96E+11	3,20E+11	3,20E+11	3,21E+11	3,19E+11	2,75E+11	3,44E+11	36
4,71E+11	4,62E+11	6,34E+11	5,94E+11	3,20E+11	3,20E+11	3,21E+11	3,17E+11	2,75E+11	3,44E+11	37
4,83E+11	4,55E+11	7,06E+11	6,11E+11	3,20E+11	3,20E+11	3,21E+11	3,20E+11	2,75E+11	3,44E+11	38
4,89E+11	4,55E+11	7,08E+11	6,36E+11	3,20E+11	3,20E+11	3,21E+11	3,11E+11	2,75E+11	3,44E+11	39
5,02E+11	4,53E+11	6,02E+11	6,36E+11	3,20E+11	3,20E+11	3,21E+11	2,97E+11	2,75E+11	3,44E+11	40
5,10E+11	4,46E+11	5,25E+11	6,17E+11	3,20E+11	3,20E+11	3,21E+11	2,95E+11	2,75E+11	3,44E+11	41
5,18E+11	4,42E+11	4,71E+11	6,14E+11	3,20E+11	3,20E+11	3,21E+11	2,91E+11	2,75E+11	3,44E+11	42
5,14E+11	4,44E+11	4,54E+11	6,07E+11	3,20E+11	3,20E+11	3,21E+11	2,62E+11	2,75E+11	3,44E+11	43
5,06E+11	4,38E+11	4,47E+11	5,88E+11	3,20E+11	3,20E+11	3,21E+11	2,49E+11	2,75E+11	3,44E+11	44
4,98E+11	4,34E+11	4,43E+11	5,70E+11	3,20E+11	3,20E+11	3,21E+11	2,43E+11	2,75E+11	3,44E+11	45
4,78E+11	4,35E+11	4,34E+11	5,57E+11	3,20E+11	3,20E+11	3,21E+11	2,44E+11	2,75E+11	3,44E+11	46
4,51E+11	4,31E+11	4,23E+11	5,46E+11	3,20E+11	3,20E+11	3,21E+11	2,57E+11	2,75E+11	3,44E+11	47
4,17E+11	4,20E+11	4,23E+11	5,20E+11	3,20E+11	3,20E+11	3,21E+11	2,68E+11	2,75E+11	3,44E+11	48
3,84E+11	4,19E+11	4,18E+11	4,97E+11	3,20E+11	3,20E+11	3,21E+11	2,88E+11	2,75E+11	3,44E+11	49
3,52E+11	4,22E+11	3,97E+11	5,10E+11	3,20E+11	3,20E+11	3,21E+11	3,17E+11	2,75E+11	3,44E+11	50
3,22E+11	4,08E+11	3,94E+11	5,17E+11	3,20E+11	3,20E+11	3,21E+11	3,32E+11	2,75E+11	3,44E+11	51
2,94E+11	4,14E+11	3,81E+11	5,02E+11	3,20E+11	3,20E+11	3,21E+11	3,34E+11	2,75E+11	3,44E+11	52
2,65E+11	4,12E+11	3,68E+11	4,76E+11	3,20E+11	3,20E+11	3,21E+11	3,25E+11	2,75E+11	3,44E+11	53
2,49E+11	4,08E+11	3,60E+11	4,80E+11	3,20E+11	3,20E+11	3,21E+11	3,17E+11	2,75E+11	3,44E+11	54

2,32E+11	4,10E+11	3,63E+11	4,80E+11	3,20E+11	3,20E+11	3,21E+11	2,93E+11	2,75E+11	3,44E+11	55
2,19E+11	4,16E+11	3,57E+11	4,79E+11	3,20E+11	3,20E+11	3,21E+11	2,64E+11	2,75E+11	3,44E+11	56
2,11E+11	4,21E+11	3,48E+11	4,83E+11	3,20E+11	3,20E+11	3,21E+11	2,40E+11	2,75E+11	3,44E+11	57
2,11E+11	4,39E+11	3,49E+11	4,70E+11	3,20E+11	3,20E+11	3,21E+11	2,25E+11	2,75E+11	3,44E+11	58
2,16E+11	4,33E+11	3,52E+11	4,65E+11	3,20E+11	3,20E+11	3,21E+11	2,05E+11	2,75E+11	3,44E+11	59
2,18E+11	4,35E+11	3,45E+11	4,74E+11	3,20E+11	3,20E+11	3,21E+11	2,02E+11	2,75E+11	3,44E+11	60
2,30E+11	4,40E+11	3,58E+11	4,72E+11	3,20E+11	3,20E+11	3,21E+11	2,01E+11	2,75E+11	3,44E+11	61
2,42E+11	4,44E+11	3,66E+11	4,69E+11	3,20E+11	3,20E+11	3,21E+11	2,05E+11	2,75E+11	3,44E+11	62
2,59E+11	4,44E+11	3,90E+11	4,61E+11	3,20E+11	3,20E+11	3,21E+11	2,11E+11	2,75E+11	3,44E+11	63
2,79E+11	4,43E+11	3,78E+11	4,60E+11	3,20E+11	3,20E+11	3,21E+11	2,17E+11	2,75E+11	3,44E+11	64
2,97E+11	4,44E+11	3,80E+11	4,67E+11	3,20E+11	3,20E+11	3,21E+11	2,21E+11	2,75E+11	3,44E+11	65
3,12E+11	4,42E+11	3,83E+11	4,71E+11	3,20E+11	3,20E+11	3,21E+11	2,34E+11	2,75E+11	3,44E+11	66
3,34E+11	4,47E+11	3,84E+11	4,67E+11	3,20E+11	3,20E+11	3,21E+11	2,46E+11	2,75E+11	3,44E+11	67
3,46E+11	4,51E+11	3,86E+11	4,66E+11	3,20E+11	3,20E+11	3,21E+11	2,61E+11	2,75E+11	3,44E+11	68
3,59E+11	4,46E+11	3,91E+11	4,80E+11	3,20E+11	3,20E+11	3,21E+11	2,72E+11	2,75E+11	3,44E+11	69
3,80E+11	4,47E+11	3,97E+11	4,79E+11	3,20E+11	3,20E+11	3,21E+11	2,75E+11	2,75E+11	3,44E+11	70
3,98E+11	4,55E+11	3,97E+11	4,79E+11	3,20E+11	3,20E+11	3,21E+11	2,70E+11	2,75E+11	3,44E+11	71
4,07E+11	4,59E+11	3,92E+11	4,70E+11	3,20E+11	3,20E+11	3,21E+11	2,56E+11	2,75E+11	3,44E+11	72
4,15E+11	4,53E+11	3,99E+11	4,80E+11	3,20E+11	3,20E+11	3,21E+11	2,47E+11	2,75E+11	3,44E+11	73
4,29E+11	4,48E+11	4,05E+11	4,74E+11	3,20E+11	3,20E+11	3,21E+11	2,46E+11	2,75E+11	3,44E+11	74
4,41E+11	4,51E+11	4,04E+11	4,63E+11	3,20E+11	3,20E+11	3,21E+11	2,27E+11	2,75E+11	3,44E+11	75
4,41E+11	4,42E+11	4,02E+11	4,69E+11	3,20E+11	3,20E+11	3,21E+11	2,00E+11	2,75E+11	3,44E+11	76
4,45E+11	4,30E+11	3,97E+11	4,67E+11	3,20E+11	3,20E+11	3,21E+11	1,80E+11	2,75E+11	3,44E+11	77
4,53E+11	4,30E+11	3,90E+11	4,50E+11	3,20E+11	3,20E+11	3,21E+11	1,59E+11	2,75E+11	3,44E+11	78
4,60E+11	4,31E+11	3,93E+11	4,41E+11	3,20E+11	3,20E+11	3,21E+11	1,46E+11	2,75E+11	3,44E+11	79
4,61E+11	4,30E+11	3,96E+11	4,31E+11	3,20E+11	3,20E+11	3,21E+11	1,26E+11	2,75E+11	3,44E+11	80
4,60E+11	4,28E+11	3,88E+11	4,29E+11	3,20E+11	3,20E+11	3,21E+11	1,10E+11	2,75E+11	3,44E+11	81
4,62E+11	4,25E+11	3,79E+11	4,23E+11	3,20E+11	3,20E+11	3,21E+11	1,00E+11	2,75E+11	3,44E+11	82
4,67E+11	4,22E+11	3,71E+11	4,19E+11	3,20E+11	3,20E+11	3,21E+11	9,13E+10	2,75E+11	3,44E+11	83
4,62E+11	4,18E+11	3,73E+11	4,17E+11	3,20E+11	3,20E+11	3,21E+11	8,37E+10	2,75E+11	3,44E+11	84
4,54E+11	4,04E+11	3,70E+11	4,25E+11	3,20E+11	3,20E+11	3,21E+11	7,82E+10	2,75E+11	3,44E+11	85
4,51E+11	3,98E+11	3,76E+11	4,15E+11	3,20E+11	3,20E+11	3,21E+11	7,85E+10	2,75E+11	3,44E+11	86
4,49E+11	3,92E+11	3,84E+11	4,02E+11	3,20E+11	3,20E+11	3,21E+11	7,60E+10	2,75E+11	3,44E+11	87
4,44E+11	3,85E+11	3,87E+11	4,10E+11	3,20E+11	3,20E+11	3,21E+11	8,21E+10	2,75E+11	3,44E+11	88
4,46E+11	3,88E+11	3,89E+11	4,10E+11	3,20E+11	3,20E+11	3,21E+11	8,36E+10	2,75E+11	3,44E+11	89
4,48E+11	3,90E+11	4,04E+11	4,02E+11	3,20E+11	3,20E+11	3,21E+11	9,46E+10	2,75E+11	3,44E+11	90
4,40E+11	3,79E+11	4,15E+11	4,05E+11	3,20E+11	3,20E+11	3,21E+11	1,02E+11	2,75E+11	3,44E+11	91
4,39E+11	3,72E+11	4,22E+11	4,11E+11	3,20E+11	3,20E+11	3,21E+11	1,19E+11	2,75E+11	3,44E+11	92

h

4,39E+11	3,86E+11	4,47E+11	4,16E+11	3,20E+11	3,20E+11	3,21E+11	1,42E+11	2,75E+11	3,44E+11	93
4,33E+11	3,89E+11	4,79E+11	4,19E+11	3,20E+11	3,20E+11	3,21E+11	1,59E+11	2,75E+11	3,44E+11	94
4,35E+11	3,85E+11	4,73E+11	4,23E+11	3,20E+11	3,20E+11	3,21E+11	1,77E+11	2,75E+11	3,44E+11	95
4,21E+11	4,03E+11	4,88E+11	4,23E+11	3,20E+11	3,20E+11	3,21E+11	1,94E+11	2,75E+11	3,44E+11	96
4,29E+11	4,08E+11	5,06E+11	4,21E+11	3,20E+11	3,20E+11	3,21E+11	2,19E+11	2,75E+11	3,44E+11	97
4,29E+11	4,07E+11	5,02E+11	4,33E+11	3,20E+11	3,20E+11	3,21E+11	2,29E+11	2,75E+11	3,44E+11	98
4,26E+11	4,12E+11	5,10E+11	4,46E+11	3,20E+11	3,20E+11	3,21E+11	2,40E+11	2,75E+11	3,44E+11	99
4,26E+11	4,19E+11	5,18E+11	4,35E+11	3,20E+11	3,20E+11	3,21E+11	2,51E+11	2,75E+11	3,44E+11	100

A.3 Atomic force microscopy (AFM) and scanning electron microscope (SEM) characterization of substrates.

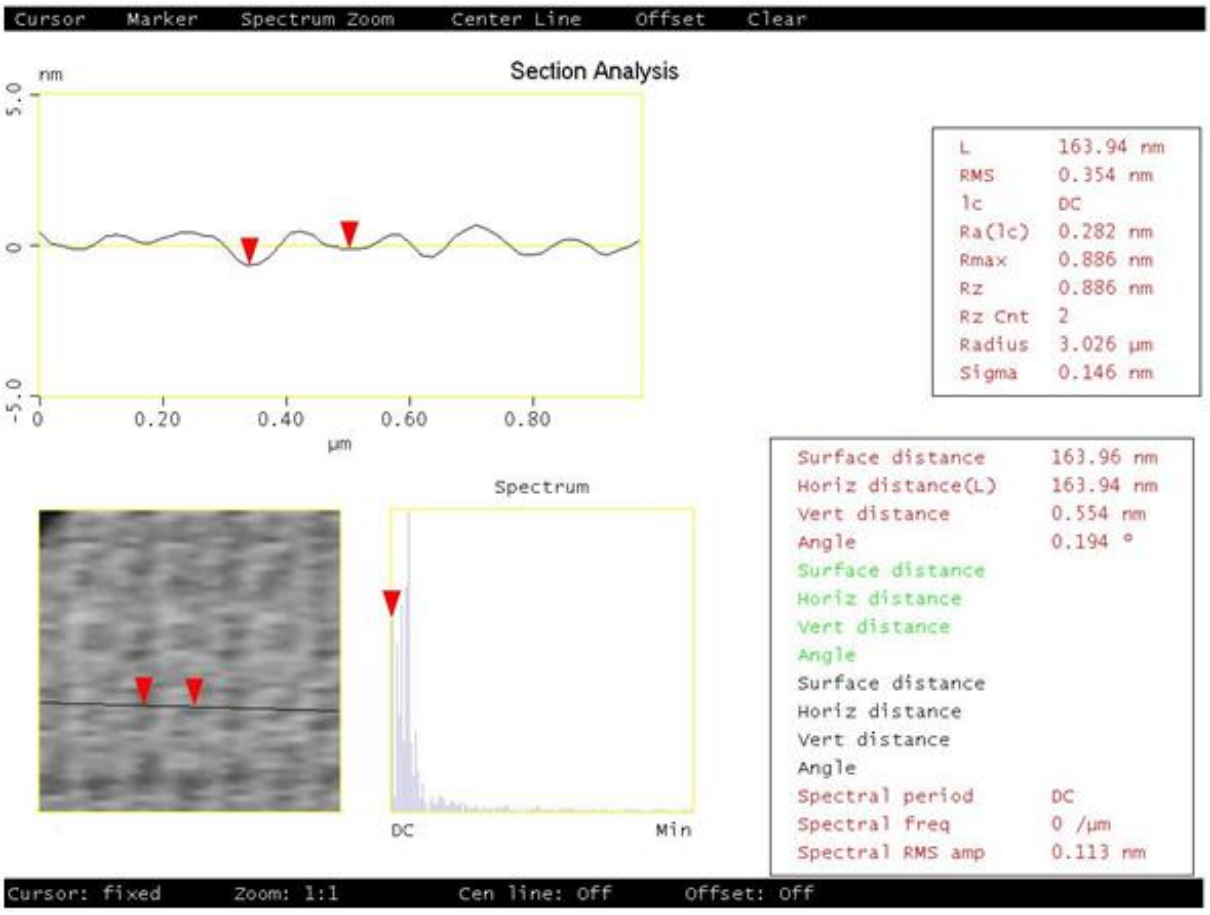

Sample R1 spacing study by AFM

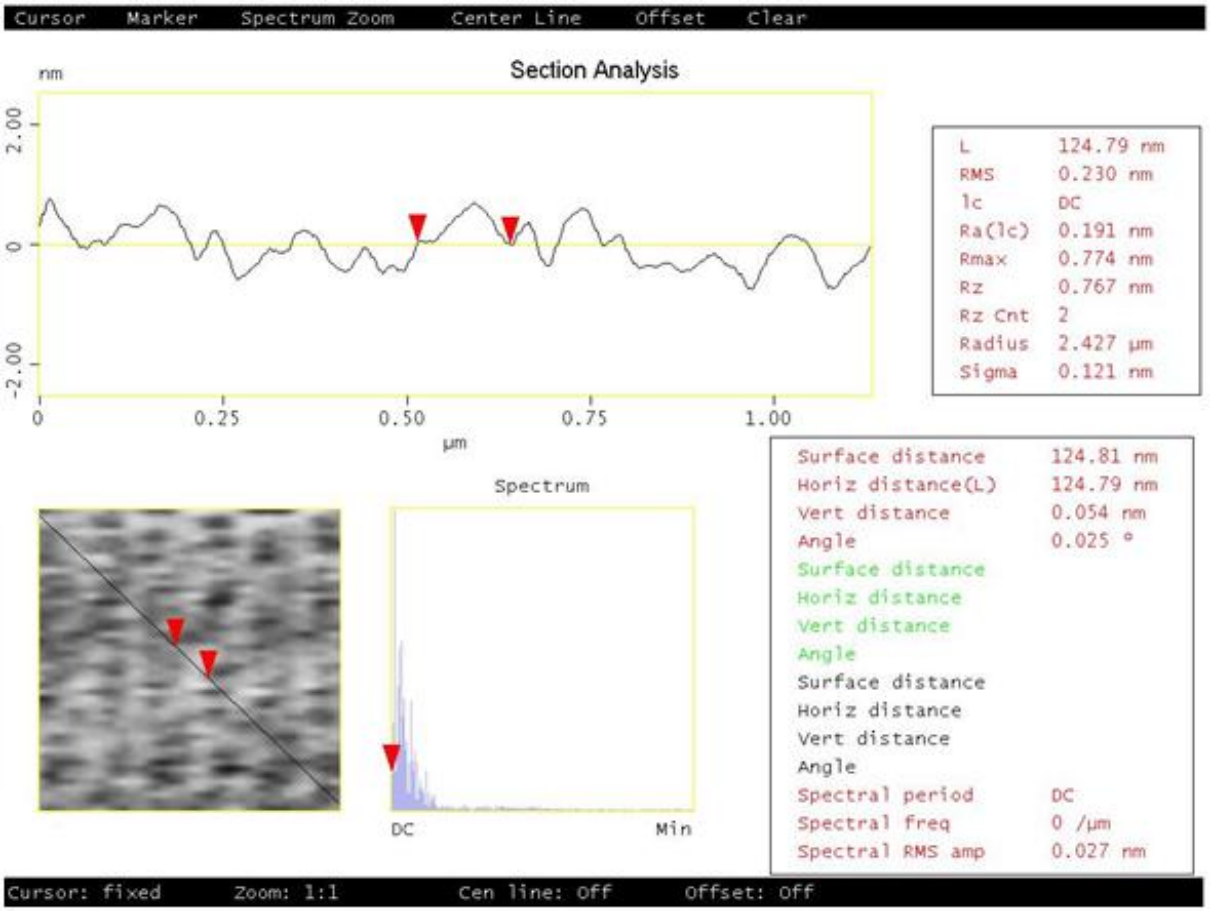

Sample R2 spacing study by AFM

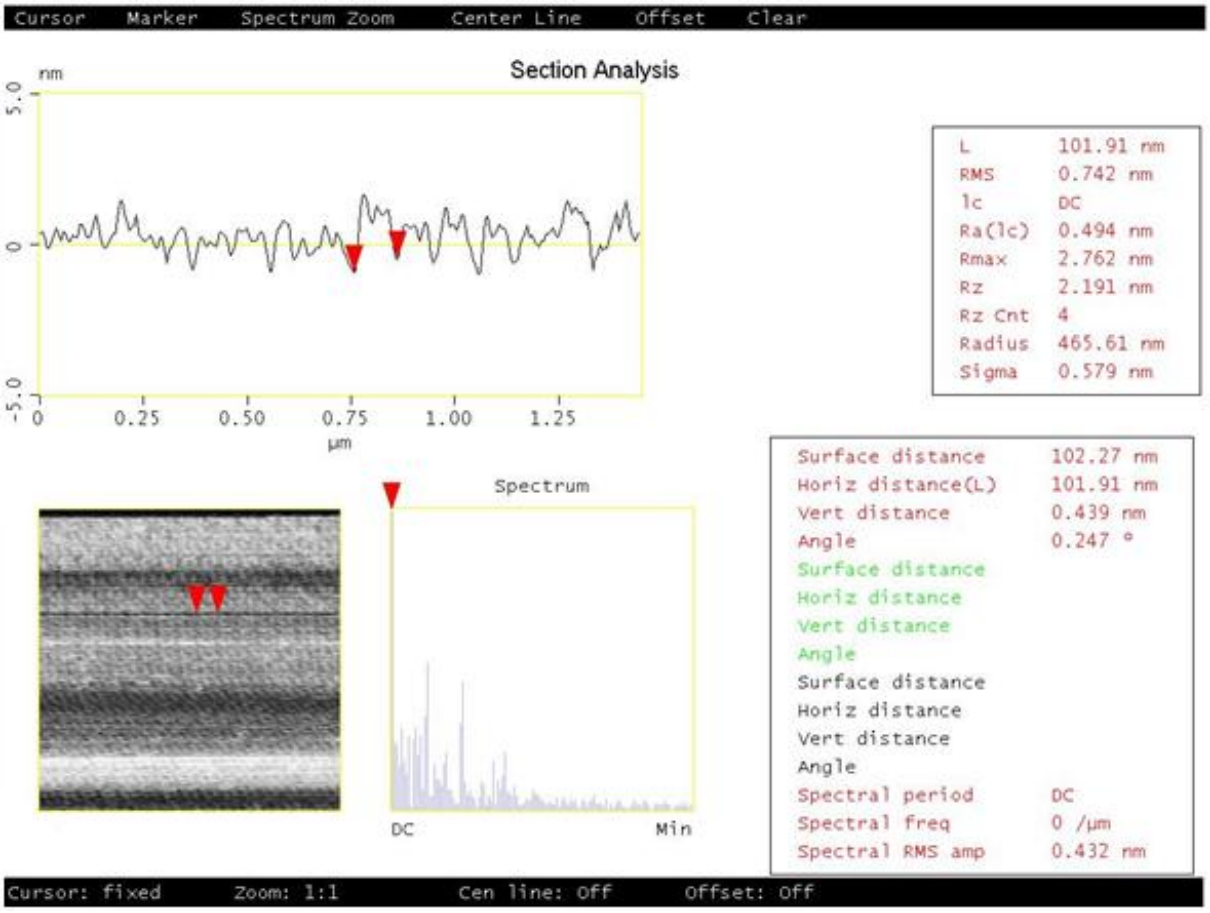

Sample R3 spacing study by AFM

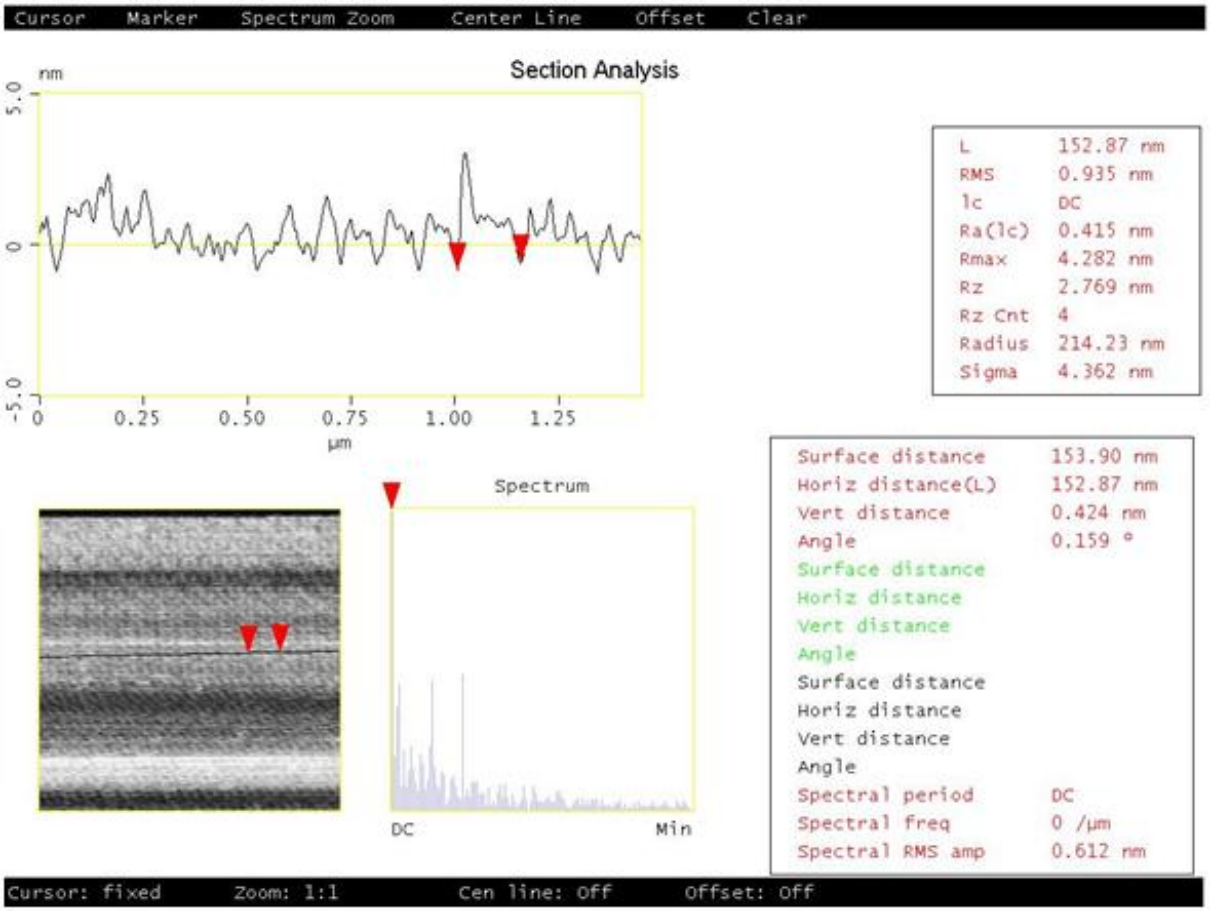

Sample R4 spacing study by AFM

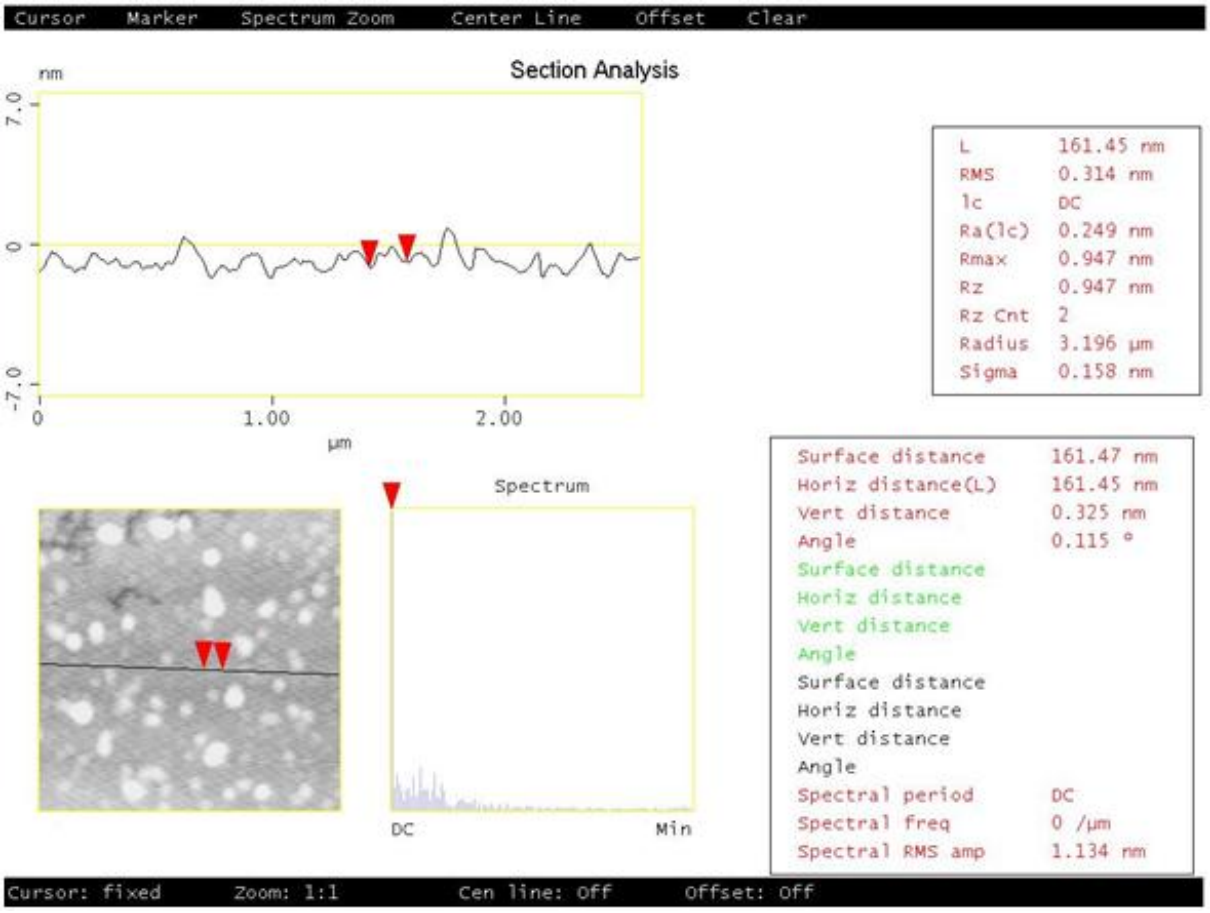

Sample R5 spacing study by AFM[6]

[6] because the spacing measured by AFM and SEM in some parts the particles are nearest as spacing molecule this fact confirm the "hot spot" formation.

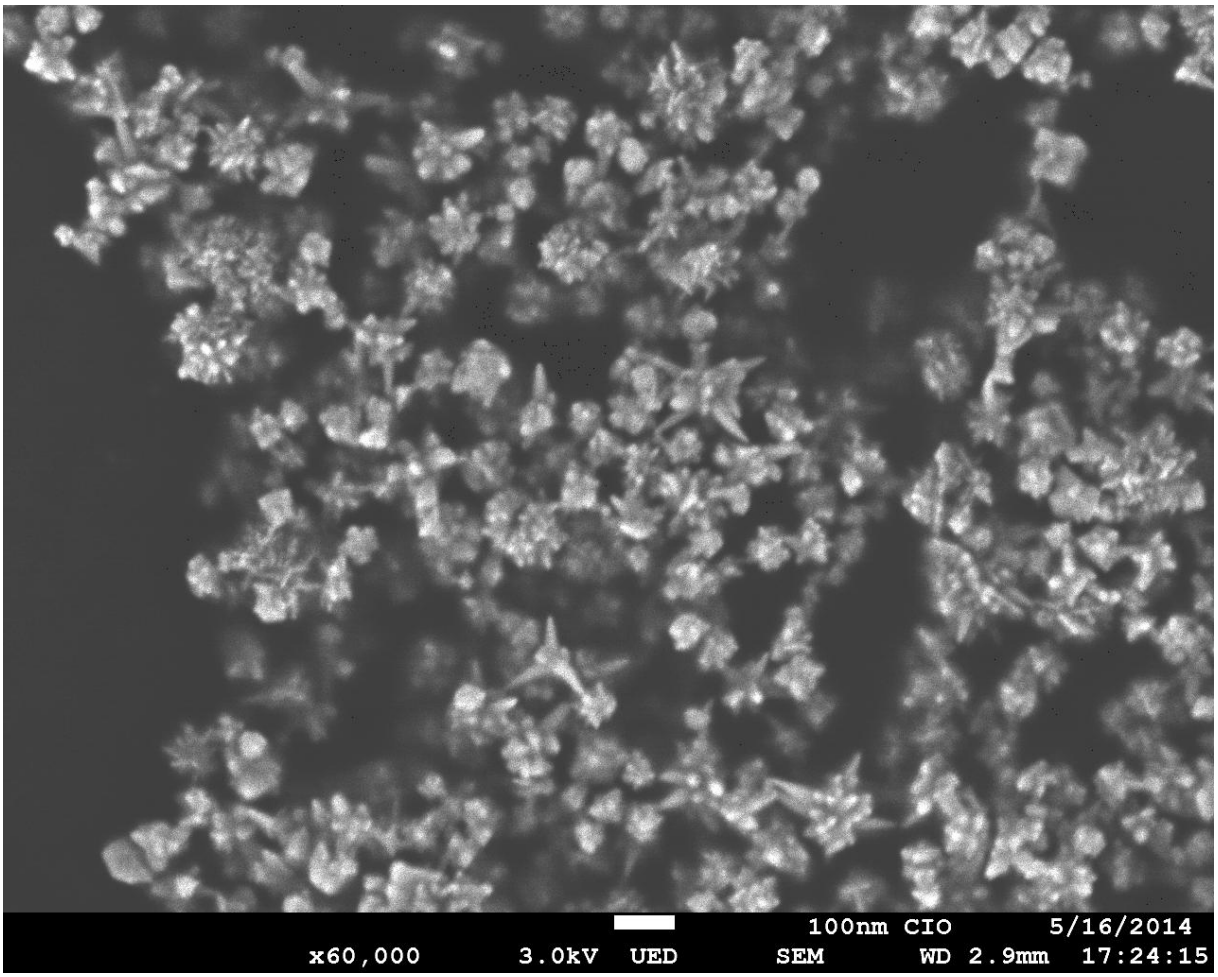

Sample R5 spacing study by SEM 60,000X

o

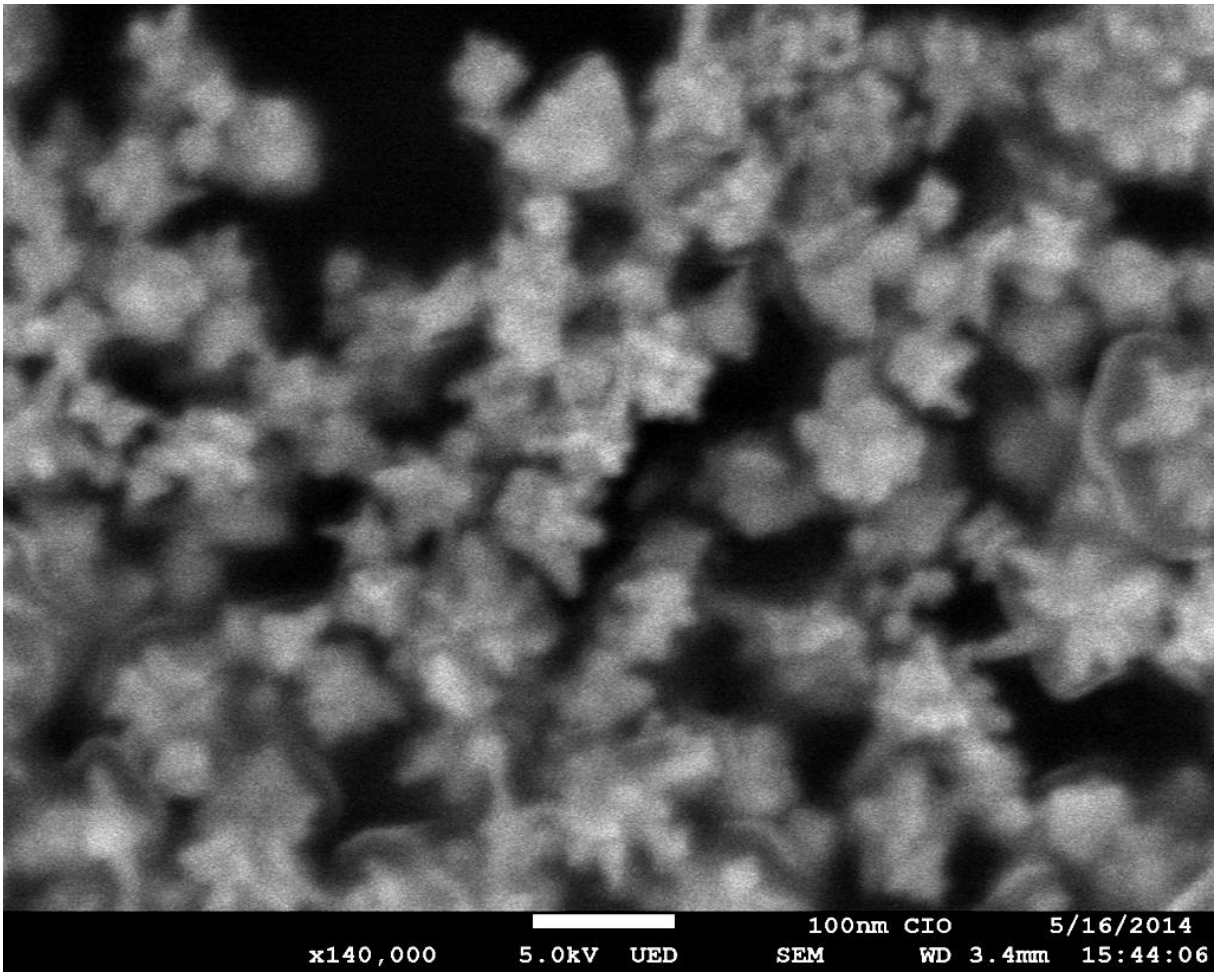

Sample R5 spacing study by SEM 140,000X

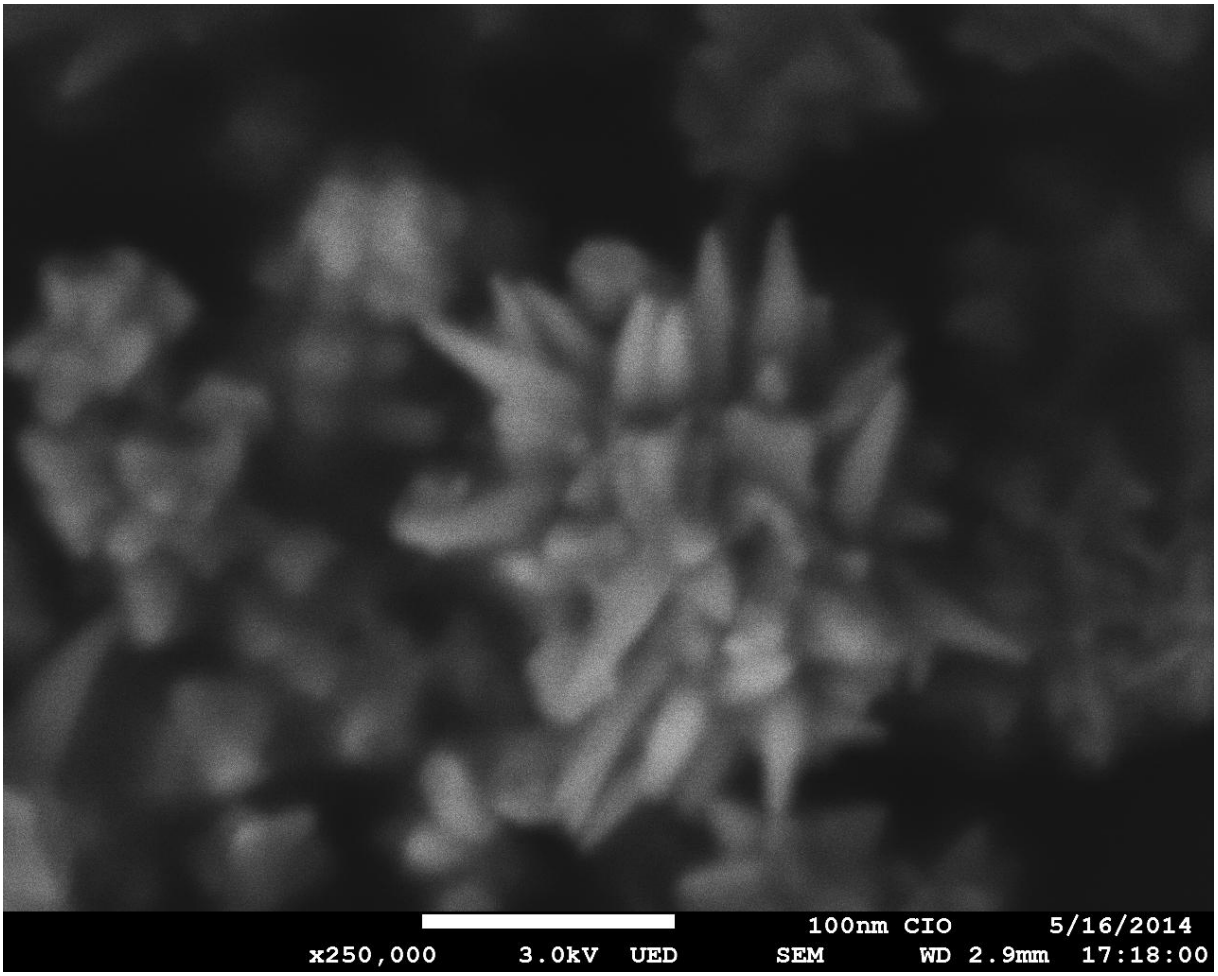

Sample R5 spacing study by SEM 250,000X[7]

[7] Because the spacing measured by AFM and SEM in some parts the particles are nearest as spacing molecule this fact confirm the "hot spot" formation.

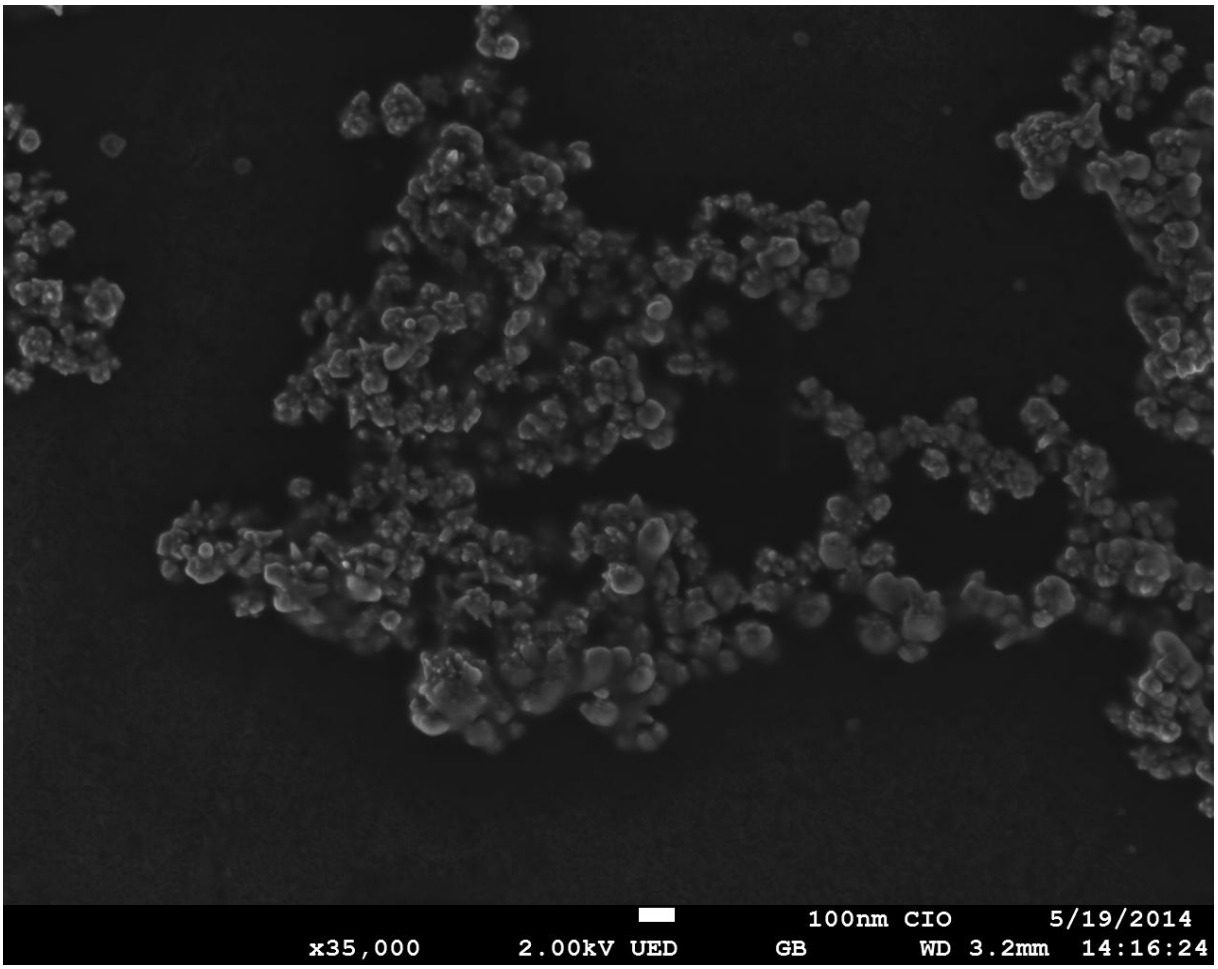

Sample M5 spacing study by SEM 35,000X, before albumin deposition

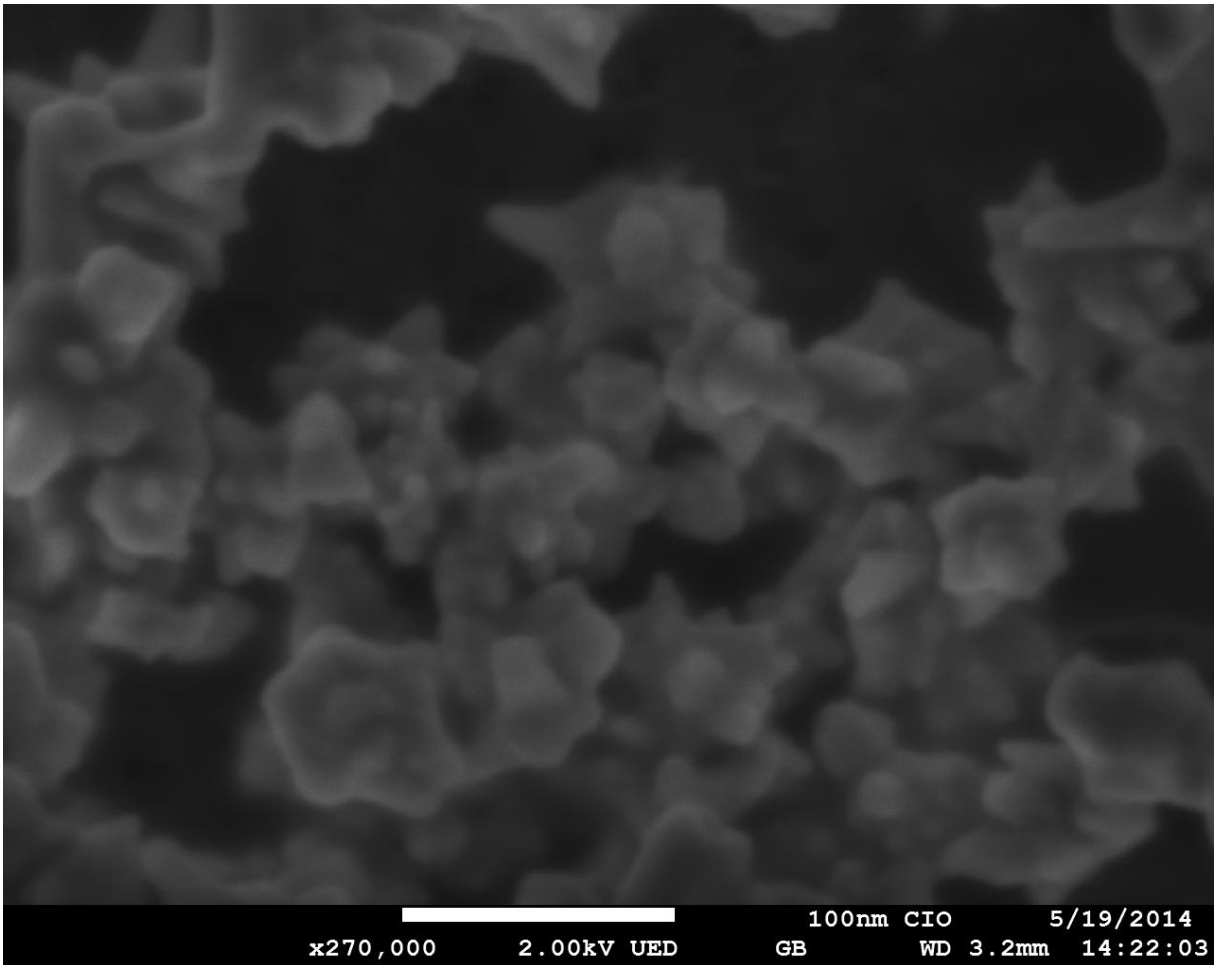

Sample M5 spacing study by SEM 270,000X, before albumin deposition

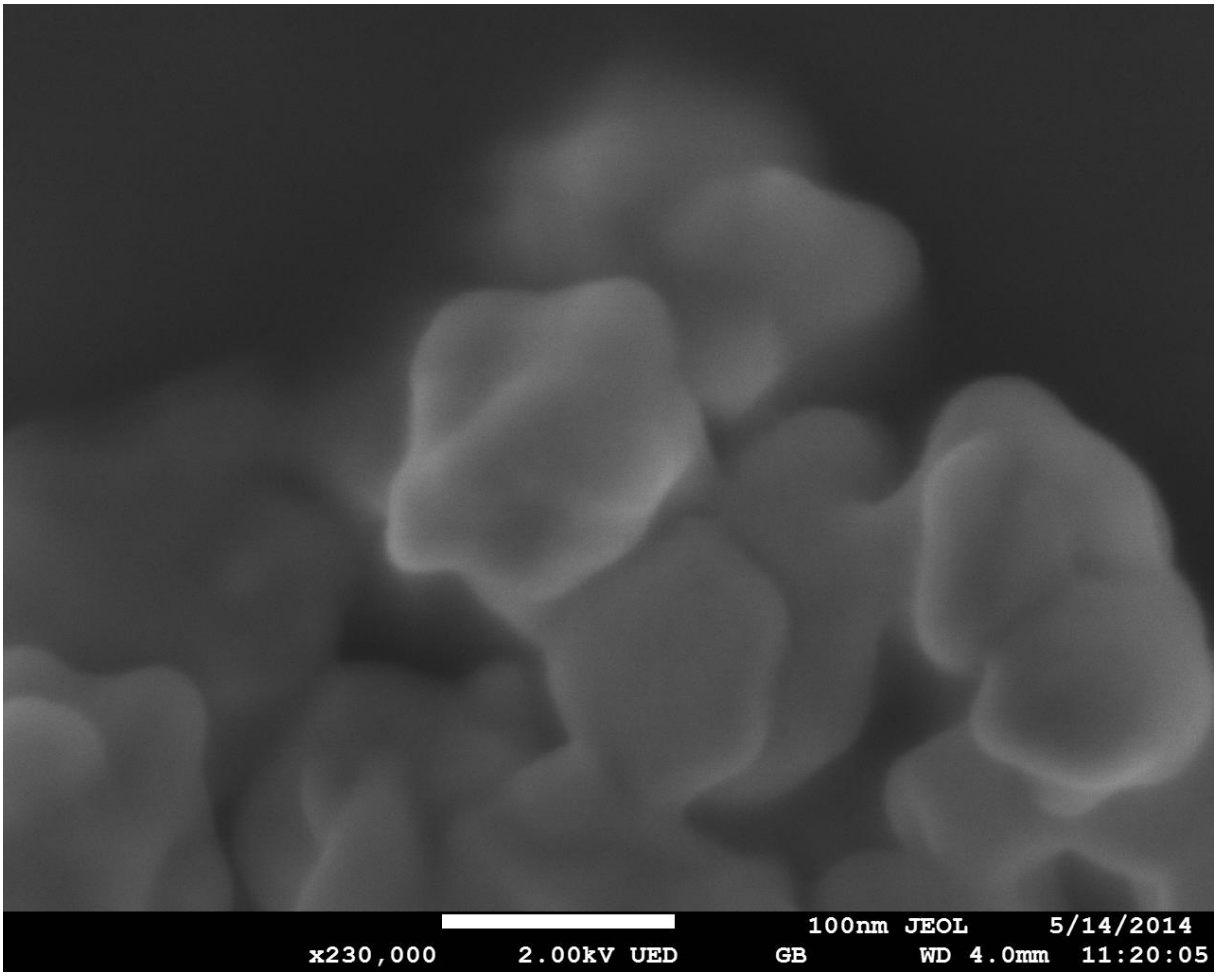

Sample M5 spacing study by SEM 230,000X, after albumin deposition

t